Yb-based femtosecond oscillators for high-power amplification

Cristtel Yoloxochitl Ramírez Corral

A dissertation submitted for the degree of Doctor of Philosophy

Heriot-Watt University

School of Engineering and Physical Sciences

May 2014

Abstract

Motivated by the industrial requirement for multi-100-W sub-ps pulses, this thesis describes the development of a high-average-power master-oscillator power-amplifier (MOPA) based on seeding an Yb:YAG planar waveguide amplifier using an Yb-based modelocked oscillator operating at 1030 nm. The scope of the research presented includes both the development of the seed oscillators and of the high-power amplifier.

Two end pumped Yb:KYW oscillators were demonstrated, one with Brewster-Brewster crystal geometry and another with a novel plane-Brewster crystal, permitting a simple pumping arrangement and which provided superior efficiency than Brewster-Brewster geometry. In both oscillators, one or more Gires-Tournois interferometer (GTI) mirrors were used in the cavity to compensate for the large amount of positive dispersion from the crystal. Both systems were modelocked using semiconductor saturable absorber mirrors. The oscillators demonstrated here produced amongst the highest average powers reported from end-pumped systems to date, generating up to 4.5 W in the near-infra-red region in the form of 500-fs pulses, with a repetition frequency of 53 MHz.

The study of oscillator performance was extended to include a comparison between Yb:KYW and Yb:YAG lasers constructed in similar configurations, both based on plane-Brewster crystal geometries and dispersion compensated using GTI mirrors. The Yb:YAG system provided 700-fs pulses, compared to 500-fs pulses obtained using Yb:KYW, with the average power produced being 2.88 W for Yb:YAG, and 2.42 W for Yb:KYW, despite significantly better CW performance being observed with Yb:YAG. Due to their near-infrared wavelengths, high average powers and sub-ps pulse durations, both systems showed potential as seed lasers for high-power Yb:YAG amplifiers.

A MOPA system was developed around an Yb:YAG planar waveguide amplifier seeded by the Yb:KYW femtosecond laser based on a Brewster-Brewster crystal geometry and operating at 53 MHz repetition frequency. With single-sided pumping and five passes of the gain waveguide, the Yb:YAG amplifier provided 700-fs pulses with average powers of 50 W at 1030 nm. With the extension to double-sided pumping and the use of toroidal mirrors to achieve seven passes, the amplifier produced 780-fs pulses with average powers of 255 W. A numerical simulation of the amplifier identified gain-narrowing as the dominant pulse-shaping mechanism.

To my family and friends

Acknowledgements

First I would like to thank my supervisor Prof. Derryck T. Reid for all the support and the big amount of knowledge in laser development that he gave me during all my PhD. Also my second supervisor Prof. Howard Baker who provided all the knowledge about amplifiers in this thesis. I also want to thank Dr. Christopher Leburn for the great help that he offered me in the lab during all these years and the nice conversations that we had about a range of different topics.

I also want to thank my parents Irma and Luis who has been always a main support for me in the good and the bad moments in my life and have cared for me every day since I was born. Also my brother Alberto and my sisters Jannet, Charlotte and Michelle who shared with me all the adventures that lead to this point of my life.

I would like to thank Rose Mary who shared all the great moments with me during all my PhD, inside and outside the university, starting from the unforgettable summer school SUSSP66 in which we meet for the first time. Additionally all the members of the ultrafast optics group (UFO) at Heriot Watt University, Tobi, Euan, Teresa, Richard, Thomas, Karolis, Marius, Carl, Xinhua, Zhaowei and Oguzhan who teach me and shared so many things at the lab and the office. Of course I can't forget to mention all my friends who were a great company during different stages of my PhD: Yingying, Ying, Ximing, Arun, Xiaohui, Shraddha, Anusha, Rishad, Nitin, Jamie, Adel, Gillian, David, Jhon, and many more who are not mentioned but are very important to me and I am so grateful.

Finally I would like to thank Heriot Watt University for opportunity to get this knowledge through my PhD and the great experiences that they provided through all the events and services that they offer for all the students at the Chaplaincy and the Sports Centre which made my studies more enjoyable, and allowed me to meet a lot of my friends in Edinburgh.

Table of Contents

Lists of Figures

List of Tables

List of Publications

Journal Publications

1. Leburn, C. G., Ramirez-Corral, C. Y., Thomson, I. J., Hall, D. R, Baker, H. J, Reid, D. T., "Femtosecond pulses at 50-W average power from an Yb:YAG planar waveguide amplifier seeded by an Yb:KYW oscillator," Optics Express **20**, 17367-17373, (2012)

Conference publications

1. C. Ramirez, I. Thomson, C. Leburn, D. Hall, D. Reid, H. Baker, "High power femtosecond pulsed amplifier combining Ytterbium-doped KYW-YAG materials in a MOPA configuration," Photon'12 (Durham, UK)

2. C. Y. Ramirez-Corral, I. J. Thomson, C. G. Leburn, D. R. Hall, D. T. Reid, H. J. Baker, "Femtosecond pulses at 50-W average power from an Yb:YAG planar waveguide amplifier seeded by an Yb:KYW oscillator," XVIIIth International Conference on Ultrafast Phenomena **41**, (2013)

3. C. Y. Ramirez-Corral, I. J. Thomson, C. G. Leburn, D. R. Hall, D. T. Reid, and H. J. Baker, "Amplification of Femtosecond Pulses from an Yb:KYW Oscillator in a High-power Yb:YAG Planar Waveguide Amplifier," in *Lasers, Sources, and Related Photonic Devices*, OSA Technical Digest (CD) (Optical Society of America, 2012), paper AT3A.5.

Chapter 1

Introduction

1.1 Motivation

Since the first reported laser in 1960 [1], the reach of laser technology has been increasing every year into greater number of applications, from the most common ones within CD/DVD and bar code readers, to communications, industrial processing, and nuclear science [2, 3]. For these applications it is necessary to tailor each laser's characteristics to optimise it for a given purpose. Critical aspects include compactness, wavelength coverage, pulse duration, and output power. The application of modelocked lasers in material processing is the context of this thesis research, specifically the development of systems offering multi-100-Watt average powers.

To obtain higher peak powers, the pulse energy coming out of a laser has to be increased or delivered in shorter periods of time [2]. Different techniques were developed in order to obtain such pulses such as Q-switching technique in 1961 [4] and modelocking in 1964 [5], which allows the generation of shorter pulses and is the method used in this thesis.

Because laser operation depends on the stimulated emission of photons in a certain gain material, the quest for higher powers from modelocked lasers has led also to testing different gain materials (solid, liquid and gas [3]). Crystalline materials, have been used widely for room-temperature femtosecond pulse generation since the first Ti:sapphire laser in 1990 [6]. Notably a range of different Yb-doped materials has since been used to achieve pulse durations of the order of picoseconds (10^{-12} s) to femtoseconds (10^{-15} s) generating up to hundreds of watts [7]. Figure 1.1 shows the power generated with these materials.

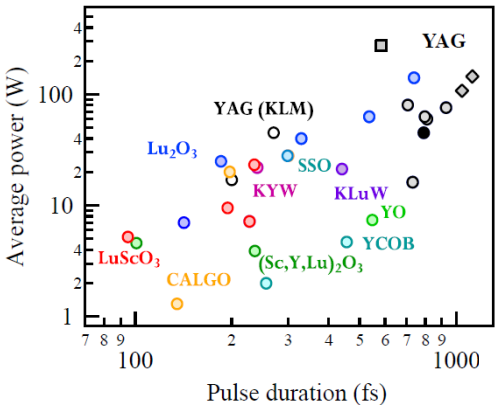

Figure 1.1 Power obtained for different pulse durations using a range of Yb-doped gain materials [7].

The use of rare earth metal ions such as Yb^{3+} as a doping in crystalline hosts such as those in Figure 1.1 made it possible to obtain high peak powers, high efficiencies and broad gain bandwidths, facilitating femtosecond pulse generation. After the development of diode lasers in the 1980s [8], the improvement in high power laser technology improved the suitability of these lasers for pumping rare-earth doped crystals. With these lasers it was possible to build end-pumped cavities and be able to spatially match the modes of the pump beam with the generated beam. These also made it possible to achieve better system efficiency, improvements in beam quality and lower thermal loading [8, 9]. In addition to these characteristics, these configurations have become more compact and suitable for low threshold oscillator applications.

1.2 High Power Yb-based MOPAs

In the case of industrial applications such as welding, cutting and marking, where high power is required, the use of rare earth doped materials provide an important route to high peak-power/high energy pulses. A new way of achieving higher power was developed using pulsed oscillators as a seed beam which is amplified through a high-power gain material. This device is known as a master oscillator power amplifier (MOPA), where the high-power gain material works as an amplifier and not as an oscillator. This can be extended to a chain of amplifiers, which can go as far as pettawatt level [10] as shown in Figure 1.2.

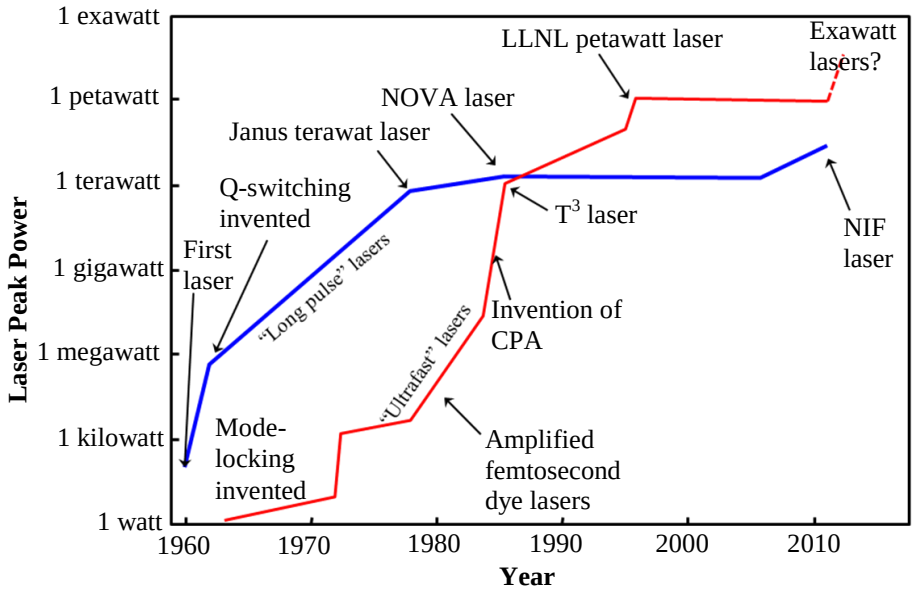

Figure 1.2 Peak power increment through the years since the first laser built [2].

For industrial applications, which are the main interest of this thesis, the output peak power required goes from a couple of watts to megawatts [11]. Usually lasers of CO_2 and Yb:YAG are the most common to achieve such power.

1.3 Generation and Control of Ultrashort Pulses

Ultrashort pulses are a form of electromagnetic wave packet. For this reason a pulse can be characterized by variables related only to electric field. These pulses can be used in a wide range of applications, which is why different techniques have been developed to generate even shorter pulses. One of the most successful techniques for the generation of ultrashort pulses (pico/femtosecond range), is called modelocking.

Modelocking is achieved by locking a number of longitudinal modes so that they are in phase with each other [13]. When the sum of electromagnetic wave modes at different frequencies is made a distribution function is obtained, which is the average of the electric field on the time domain, and the square of the field would give the variation in time of the intensity. When these frequencies are also in phase, their sum describes the total electric field and intensity of a pulse. Therefore this technique has become a very useful method to generate ultrashort pulses.

In a standing-wave cavity, the distance between longitudinal modes is defined by: $\Delta\nu = c/2L$, where L is the optical path length of the cavity, since the medium of index n does not normally fill the cavity. If the gain bandwidth is bigger than the separation

between modes, it is possible for more than one longitudinal mode to be oscillating at the same time.

To have all the modes in phase it is necessary to introduce some kind of modulation; then if the pulse contains *N* modes the total amplitude will be given by [14],

$$E(t) = \sum_n E_n e^{i(\omega_0 + n\Delta\omega)t + i(\varphi_n)} \tag{1.1}$$

where ω_0 is the central frequency, $\Delta\omega$ is the frequency separation and φ_n is the phase of the *n*th mode. Taking the gain to be uniform across the entire emission bandwidth, and taking $E_n = 1$ and $\varphi_n = 0$, then the field can be written as:

$$E(t) = \sum_{-(N-1)/2}^{(N-1)/2} e^{i(\omega_0 + n\omega t)} = e^{i\omega_0 t} \frac{\sin\left[\frac{N\omega t}{2}\right]}{\sin\frac{\omega t}{2}} \tag{1.2}$$

Then the amplitude of the pulse will be proportional to *N*. In a modelocked laser system a sequence of pulses is formed with a time separation between them of

$$\Delta T_{sep} = \frac{2L}{c} = \frac{2\pi}{\omega} = \frac{1}{\Delta\nu} \tag{1.3}$$

where *L* is the optical single-pass length of the cavity. This is the time that the pulse takes to make one roundtrip inside the cavity. The pulse width, defined as the full-width half-maximum (FWHM) of the pulse intensity, is given by [13, 14]:

$$\Delta\tau_p = \frac{\Delta T_{sep}}{N} = \frac{1}{N\Delta\nu} \tag{1.4}$$

where $N\Delta\nu$ is the gain bandwidth. Therefore when the gain bandwidth increases, the number of modes will be greater and the pulses will be shorter.

There are two main ways to produce pulses by modelocking; which are described in the following sub sections [14].

1.3.1 Active Modelocking

When the modulation is introduced by an external source it is called active modelocking. In this case the modulation frequency is a multiple of the repetition frequency of the pulses in such a way that every time the pulse passes through the modulator, the gain is a maximum. Some examples of active modelocking are amplitude modulation, frequency-modulation modelocking, and modulation of the gain. Most common devices for this technique are the electro-optic and acousto-optic modulators.

1.3.2 Passive Modelocking

When the element that produces the modelocking is working internally with the use of some nonlinear process, it is called passive modelocking. In this case the main types of modelocking are the fast and slow saturable absorber modelocking, Kerr lens modelocking and additive pulse modelocking. With passive modelocking it is possible to get shorter pulses than with the active technique. Using a nonlinear element with losses dependent on the intensity it is possible to increase the gain experienced by wavepackets with higher intensities [15, 16, 17].

In a laser cavity, the intensity increases until it saturates the gain, that is to say until it matches the unsaturable losses. When an absorber is used in the cavity the oscillation in the laser continues to increase in intensity until it starts to saturate the losses in the absorber. At this moment a spike appears which runs through the cavity, and the losses in this spike decrease each time it reaches the saturable absorber, then its intensity grows more than any other components in the cavity for which the losses remains unsaturated. Such a spike can then transform into a very short pulse travelling inside the cavity. Saturable absorbers can be made with different materials, the most common being semiconductor saturable absorber mirrors (SESAM), which are structures formed by a Bragg mirror and a quantum well absorber layer. Some properties that describe the operation of a good saturable absorber are the absorption cross section of the absorber, the stimulated emission cross section at the gain medium, the saturation fluence, its modulation depth and relaxation time. These devices are divided into different classes

depending on their recovery time. Fast saturable absorbers are characterised by having a recovery time comparable to or shorter than the pulse duration, while slow saturable absorbers have a recovery time much longer than the pulse duration.

For the lasers described in this thesis the modelocking was achieved by using SESAM devices, like the ones used previously [15-17], which are approximately fast saturable absorbers.

1.4 Group Delay Dispersion

In modelocked lasers usually one or more dispersive intracavity elements are present. Stable pulse generation requires near-zero or net negative group delay dispersion (GDD) in order to achieve soliton-like pulse shaping. Generally the gain material and some other elements have a normal dispersion which gives a positive value of GDD [18, 19], so to get the shortest pulses the dispersion of these elements has to be compensated with other elements contributing negative GDD.

In the case of ultrashort pulses, due to the generation of a broad gain bandwidth, dispersion management becomes important. To understand this process the behaviour of the waves as they travel has to be studied.

When two or more phase-coherent waves of different frequencies travelling in the same direction are added, the result is a modulated wave or pulse (Figure 1.3).

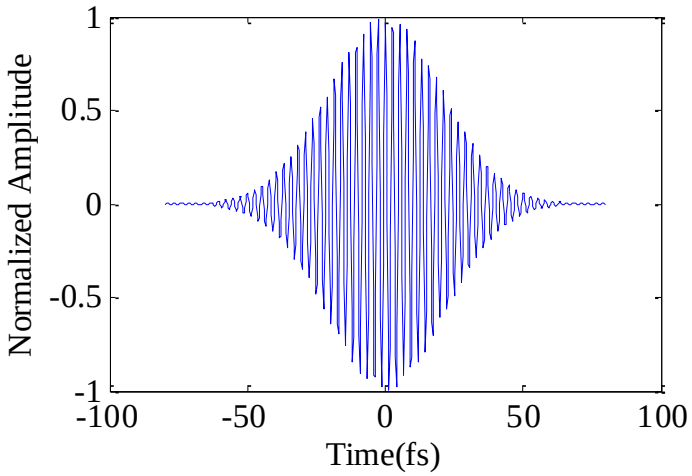

Figure 1.3 Electric field of a pulse, the blue line corresponds to the total electric field and the surrounding shape is the modulation envelope.

The total field is of the form,

$$E(x,t) = E_0(x,t)\cos\left(kx - \omega t\right) \tag{1.5}$$

The wave obtained takes the form of a carrier wave travelling at an average angular frequency ω and wave number k modulated in amplitude by a component $E_0(x,t)$, where the modulation envelope is the curve that encloses the carrier wave. The velocity at which the envelope travels is known as the group velocity v_g. The velocity of a wave travelling in a non-dispersive material is given by $v = \omega/k$, known as the phase velocity v_p, but in a dispersive material the velocity of propagation depends on its frequency. For a pulse formed by waves with different frequencies the velocity of the modulation envelope would be different from the carrier wave velocity. The group velocity can be smaller, bigger or equal to the phase velocity depending on the type of dispersion; for normal dispersion $v_p > v_g$, for anomalous dispersion $v_p < v_g$, and for non dispersive media $v_p = v_g$.

The group velocity is given in terms of the variation of the frequency and the wave number of the waves forming the pulse as $v_g = \Delta\omega/\Delta k$. If the frequency variation is given by the dispersion relation as $\omega = \omega(k)$, then for small changes in the frequency the group velocity can be written as [20]:

$$v_g = \left(\frac{d\omega}{dk}\right)_{\omega_0} \tag{1.6}$$

where ω_0 is the center frequency of the pulse. When a pulse travels through a dispersive medium it will have a time delay τ_g depending on the group velocity and the length of the material l known as the group delay,

$$\tau_g = \frac{l}{v_g} = l\left(\frac{dk}{d\omega}\right)_{\omega_0} \tag{1.7}$$

If $\phi = (kx - \omega t)$ is the phase of the pulse, then the group delay time has the form $\tau_g = \phi'(\omega_0)$ [20]. In the case of ultrashort pulses where the bandwidth is large enough,

different spectral components inside the pulse travel at different velocities generating a broadening of the pulse, then the pulse broadens as a function of the difference in group delay between the fastest and slowest spectral components of the pulse. The pulse broadening is then given as,

$$\Delta\tau_d \cong \left|\varphi''(\omega_0)\right|\Delta\omega \cong l\left(\frac{d^2k}{d\omega^2}\right)_{\omega_0}\Delta\omega \tag{1.8}$$

where $\phi''(\omega_0)$ defines the GDD of the medium, and the second derivative of the wave number is known as the group velocity dispersion (GVD) at a frequency ω_0, which gives the pulse broadening per unit bandwidth of a pulse. In some cases it is easier to use GDD to estimate the pulse broadening.

1.4.1 Techniques for managing group-delay dispersion

To compensate for the positive dispersion generated by optical elements of the laser [18, 19], an arrangement of gratings, prisms or other elements that have negative GDD is used. In the case of prisms, a set of them (a two or four prism sequence [19]) is placed at the minimum deviation angle and cut at Brewster angle, utilizing angular dispersion to control the path length of the pulses and thus generate a negative dispersion that can be varied by changing the distance between the prisms.

Prisms can be used over a wide wavelength range, however in some cases the elements that introduce the negative dispersion can depend more critically on the wavelength of the laser. Such elements include chirped dielectric-stack mirrors or Gires-Tournois interferometer (GTI) mirrors. Chirped mirrors use a multilayer coated structure of high refractive index ratio between the materials on the layers [21, 22], with the ones best suited to the near-infrared region being TiO_2 and SiO_2. The layers of the materials in these mirrors have to be a quarter of the wavelength thickness of the required wavelength, then the period of the layers is increased to generate a group delay that increases with wavelength. Therefore these mirrors can generate a nearly constant GDD over a larger bandwidth, however their absolute dispersion is limited to a few hundred femtosecond squared.

The GTI mirror structure offers much greater GDD (as high as 20000 fs^2) and consists of a partially reflecting mirror (R<100%), a resonant cavity (forming an etalon-like structure), and a high reflector at the end (R=100%). In this case, in common with chirped mirrors, the high reflector consists of a multi-layer arrangement of high and low index of refraction materials, whilst the partially reflective material corresponds to a high refractive index material and the spacer cavity to a low refractive index material. These mirrors provide GDD compensation with intrinsic low intracavity loss. The only inconvenience using such mirrors is that sometimes the amount of negative dispersion is limited, so for greater values of negative dispersion it is necessary to make an arrangement with many reflections of the mirrors inside the cavity [23]. GTI mirrors have been used successfully to compensate for dispersion in oscillators to obtain femtosecond pulses [23-25].

Some of the devices mentioned above have been used in this thesis research to compensate the positive dispersion introduced by the gain material as well as other elements in the cavity. It will be seen later that such elements are of great importance to get the best performance from our laser. Figure 1.4 shows an example of the GDD for GTI mirrors in the near-infrared region.

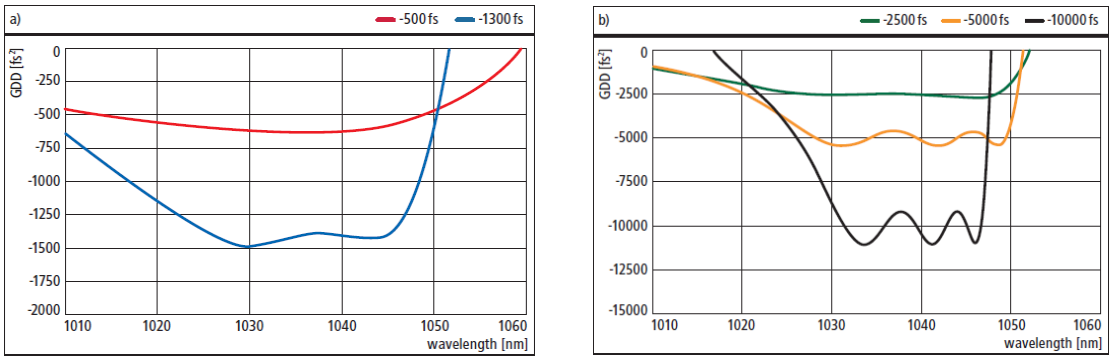

Figure 1.4 GDD spectra of GTI-mirrors for 1030 nm with different GDD values [26].

1.5 Standard Optical Pulse Diagnostics

Due to its short duration in time it is complicated to get an exact value for the duration of a femtosecond or picosecond pulse. A number of different techniques have been developed to measure the pulse duration, the most commonly used (because of their reliability and the information about the pulse that can be provided) being second-harmonic generation (SHG) autocorrelation, frequency-resolved optical grating (FROG)

and the spectral phase interferometry for direct electric field reconstruction (SPIDER) [12].

1.5.1 Autocorrelation

Depending on the pulse duration and the accuracy required, different measurement techniques are chosen. For ultrashort pulses, in the range of picoseconds to femtoseconds, the most commonly used technique is second harmonic generation (SHG) autocorrelation. With this technique a device based on a Michelson interferometer is used to split the signal pulse into two equal pulses travelling different paths. This produces a delay in time for one of the pulses, and then the two pulses are focused into a second harmonic crystal to produce an autocorrelation signal on the detector. The autocorrelation obtained in this way gives only an intensity measurement of the signal which is used at the same time as a reference, that is why it is called intensity autocorrelation. An example of an autocorrelator of this type is shown in Figure 1.5 (FR-103XL Femtochrome autocorrelator), which is the one used in this thesis research to obtain the intensity autocorrelations of the pulses. In this instrument, when the parallel mirrors are rotated the delay between the pulses changes as a function of the rotation, repeating consecutively on each rotation and producing an autocorrelation function of the pulses that can be seen on an oscilloscope synchronized to the rotation. To obtain a measurement of the pulse duration, the FWHM has to be calculated from the autocorrelation signal and this must be divided by a correction factor, depending on the pulse shape. Nevertheless, this technique is not able to obtain detailed information about the pulse shape, because differently shaped pulses can have the same intensity; thus this cannot be used to know about the phase or other characteristics of the pulse [20].

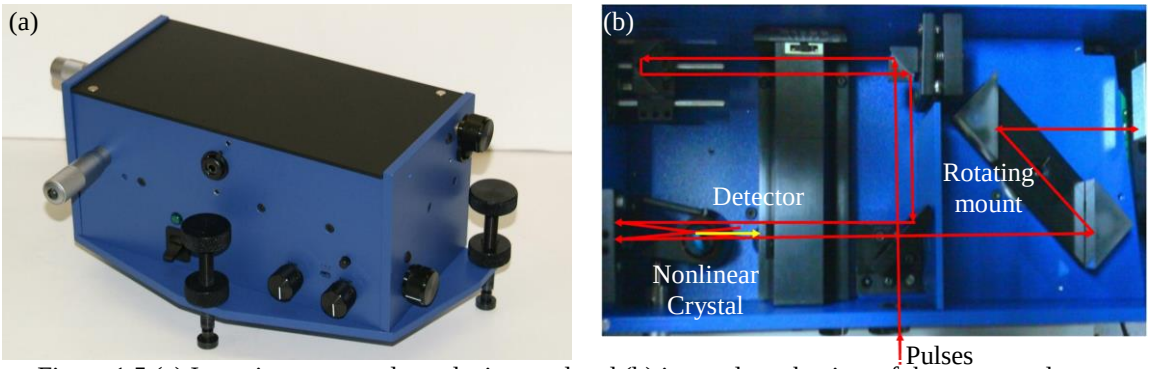

Figure 1.5 (a) Intensity autocorrelator device used and (b) internal mechanism of the autocorrelator.

Pulse duration is usually defined as the full-width at half-maximum (FWHM) of the pulse intensity as in Figure 1.6, though when inferring a duration from an autocorrelation measurement it is necessary to consider the shape of the pulse. The pulse duration is given by the FWHM of the autocorrelation trace divided by a factor depending on the pulse shape. For Gaussian pulses $\Delta\tau_p = \Delta\tau_{ac}/1.414$, and for sech^2 pulses $\Delta\tau_p = \Delta\tau_{ac}/1.543$.

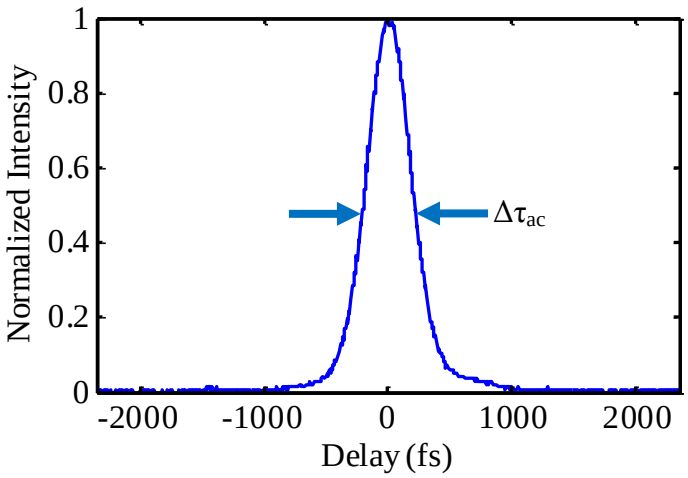

Figure 1.6 Example of an intensity autocorrelation measurement.

The product of the pulse duration and the pulse spectral bandwidth gives another property of the pulses known as the duration-bandwidth product, which also depends on the shape of the pulse, and has an exact value for transform-limited pulses. For Gaussian pulses $\Delta\nu\Delta\tau = 0.44$, and for sech^2 pulses $\Delta\nu\Delta\tau = 0.315$, where the spectral bandwidth relation between wavelength and frequency is $|\Delta\nu| = c\Delta\lambda/\lambda^2$.

Another form of autocorrelation, also used in this thesis, can be implemented through two-photon absorption and allows the measurement of interferometric autocorrelation. This technique has the advantage of being inexpensive as the autocorrelator can be home made. The autocorrelator in this case is built as a Michelson interferometer in which the input pulses are divided into two paths using a beam splitter coated for the required wavelength. Then one of the pulses is reflected by a high reflector mounted on a translation stage, and the other pulse is reflected by a high reflector mounted on a speaker which allows the mirror to oscillate at the required frequency. When the mirror is oscillating, the pulses can be scanned through each other as they are focused onto the detector. The detector used in this case is typically a photodiode which responds nonlinearly if the photon energy is less than the semiconductor bandgap energy but

greater than half the bandgap, or $E_g > E_{photon} > E_g/2$ [27]. Figure 1.7 shows a home built autocorrelator made by members of the Ultrafast Optics Group at Heriot-Watt University using a silicon diode to measure near-infrared pulses.

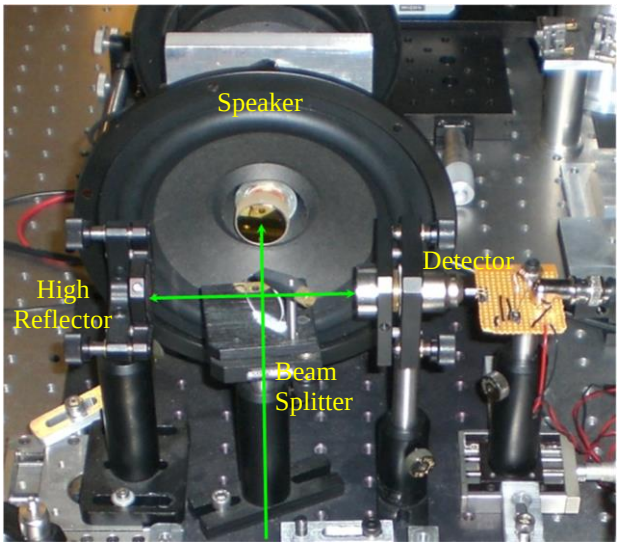

Figure 1.7 Home built interferometric autocorrelator.

The interferometric autocorrelation makes possible to scan the fringes of the pulse created by the beam splitter [27]. This is due to the variation of the speed in the mirror mounted on the speaker. Then this technique can provide also information about the phase variations on the pulse [20], and also give some information about the chirp of the pulses. Furthermore, the two-photon process does not depend on the polarization, unlike in the case of SHG crystals. In this type of autocorrelation the fringes exhibit a peak to background ratio of 8 to 1, as illustrated in Figure 1.8.

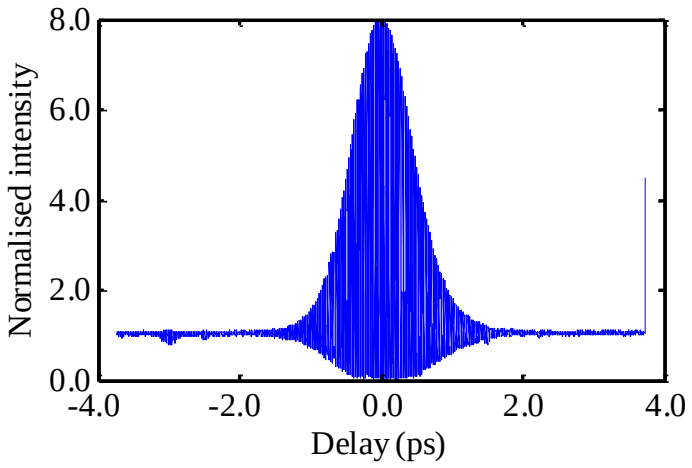

Figure 1.8 Scan of an interferometric autocorrelation.

In Figure 1.8 an example is presented on autocorrelation used to measure the pulse durations from a Yb:KYW laser described later in this thesis. When more information of the pulses is required it is necessary to use more advanced FROG or SPIDER techniques.

1.5.2 Spectral measurements

The autocorrelation measurements discussed in Section 1.5.1 are related directly to the pulse shape [20]. Complementary information about the pulses is provided by measuring the spectrum of the laser. The spectrum of the pulse gives information about the relative energy for each wavelength contained in the pulse. This is always presented as the intensity as a function of wavelength (Figure 1.9). In combination with the autocorrelation, the pulse spectrum and its FWHM bandwidth, lead to the quantity known as the duration bandwidth product ($\Delta\omega\Delta\tau$) which has a specific value for each pulse shape. For $sech^2(t)$ shaped pulses $\Delta\omega\Delta\tau = 1.98$ and for Gaussian shaped pulses $\Delta\omega\Delta\tau = 2.77$. These values can be used to know if the measured pulsed are chirped or not, depending on how much they approximate to the ideal values mentioned [20].

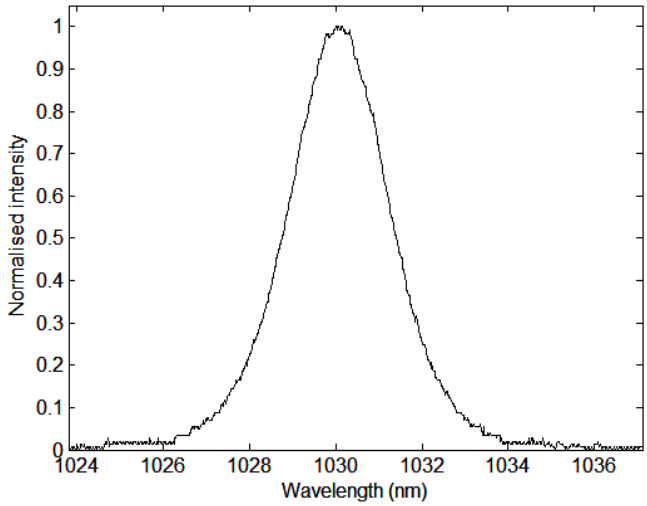

Figure 1.9 Pulse spectral intensity

1.5.3 Power measurements

Laser power is defined as the energy delivered per unit of time. Various detectors can measure from very low powers (nW), to higher power beams (kW) by the use of radiation pressure, pyroelectric, thermal and photodetector sensors [28]. The type of detector depends on the amount of power to be measured and also on the type of beam

(CW or ML). Nevertheless for higher powers, the use of attenuators or other type of power conditioning methods are required [29]. For modelocked lasers, the pulse energy must be inferred from an average power measurement.

1.5.4 Radio frequency measurements

Photodiodes are useful for measuring the modelocking stability of a pulsed laser by acquiring its radio frequency spectrum, which also provides direct information about the repetition frequency of the laser. If the pulse sequence is directed onto a fast photodetector, then the signal detected will show a series of harmonics equally spaced at the pulse repetition frequency, as shown in Figure 1.10. Fluctuations in this signal indicate phase noise which is the variation in the temporal position of the pulses. This noise is undesirable for applications requiring the synchronization of one or more laser sources.

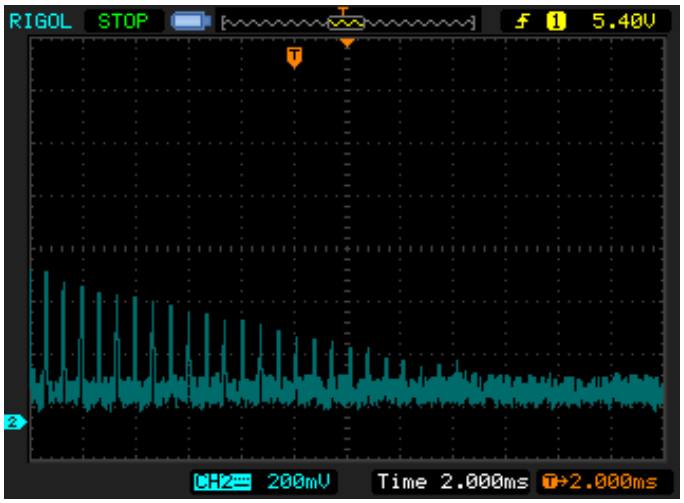

Figure 1.10 Harmonics of the repetition frequency, where the x axis shows the frequency (150 MHz per division) and the y axis is the amplitude (10 dBm per division).

1.5.5 Beam waist and M^2 measurements

Spatial beam measurements are used in this thesis research to evaluate the quality and focusing properties of the beams produced by Yb-doped lasers/amplifiers and their pump sources.

Considering a Gaussian beam it is possible to define the beam waist and the M^2 value of the beam. The intensity for a transverse mode (TEM_{00}) of the beam is given by [13]:

$$I(r) = I_o e^{-ar^2} = I_o e^{-2r^2/w^2} \tag{1.9}$$

where the parameter w is the radius of the beam at which its intensity falls to $1/e^2$ (13.6%) of its maximum intensity, I_o. When focused, this beam will form a waist of radius w_o.

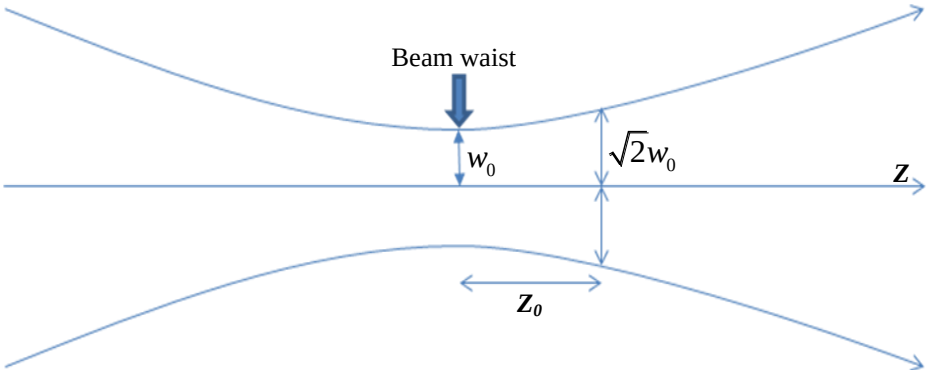

Figure 1.11 Beam waist.

The beam radius diverges from its minimum radius with respect to the propagation distance z as,

$$w(z) = w_0 \left(1 + \frac{z^2}{z_0^2}\right)^{1/2} \tag{1.10}$$

If n is the index of the propagation medium and λ is the free space propagation wavelength then

$$z_0 = \frac{n\pi w_0^2}{\lambda} \tag{1.11}$$

The value z_0 is the distance at which the beam radius expands by a factor of $\sqrt{2}$ and is known as the *Rayleigh range*. To understand how the beam is diffracted as it travels a certain distance it is necessary to introduce the angular spread of the beam in the far-field, given as the full angle of divergence of the beam,

$$\theta = \frac{2\lambda}{\pi w_0 n} \tag{1.12}$$

A real beam can be compared to a Gaussian beam by considering a multiple of the diffraction limited beam taken as M. If the divergence for an actual beam is given by

$\Theta = M\theta$ and the minimum beam waist by $W_0 = Mw_0$ then the product of those quantities will be [13]:

$$\Theta W_0 = M^2 \frac{2\lambda}{\pi} \tag{1.13}$$

where M^2 describes the difference between the real beam and the Gaussian beam. For a Gaussian beam $M^2=1$. Correspondingly, a real beam of wavelength λ and beam quality parameter M^2 diffracts into a divergence angle equal to that of a Gaussian beam of wavelength $M^2\lambda$. This method was used to assess the beam quality of the pump source by using a knife edge and a power meter, and for the second oscillator a beam profiler.

1.6 Conclusions and thesis structure

This thesis addresses the construction of two different configurations of Yb:KYW femtosecond oscillators and a similar configuration using Yb:YAG, ultimately drawing a comparison between them. These oscillators were built using passive modelocking configurations enabled by the use of a SESAM. Dispersion compensation was included in by the insertion of GTI mirrors. Besides these oscillators this thesis also deals with the construction of a MOPA system which provides high average power for industrial applications. This introductory chapter has outlined the context of this research, together with characterization techniques applied to these systems and providing measurements of the pulse duration, spectrum, power, beam quality and beam parameters.

This thesis is focused on the development of diode pumped Yb doped oscillators and their application in high-power amplifiers. Chapter 2 presents the construction of an Yb:KYW oscillator in a Z-fold cavity configuration. Chapter 5 discusses the development of an Yb:KYW oscillator using a more compact and robust v-folded cavity configuration. Chapter 6 describes the construction of an Yb:YAG oscillator in a similar V-folded cavity and a comparison between two similar oscillators using Yb:KYW and Yb:YAG as their gain materials. Also a MOPA system is described in Chapter 3 which was built using the Yb:KYW system described in Chapter 2 as a master oscillator and Yb:YAG as the gain material for the amplifier. Finally, in Chapter 4, some improvements of the amplifier are described making it possible to obtain the higher power from the system.

1.7 References

[1] T. H. Maiman, “Stimulated optical radiation in ruby” Nature **187**, 493-494 (1960).

[2] T. Ditmire, "High-power Lasers," American Scientist **98**, 394–401 (2010).

[3] P. M. W. French, "The generation of ultrashort laser pulses," Reports on Progress in Physics **58**, 169–267 (1995).

[4] R. W. Hellwarth, *Advances in Quantum Electronics* (Columbia University Press, 1961).

[5] L. E. Hargrove, R. L. Fork, and M. A. Pollack, "Locking of He-Ne laser modes induced by synchronous intracavity modulation" Applied Physics Letters **5**, 4–5 (1964).

[6] D. E. Spence, P. N. Kean, and W. Sibbett, “Sub-100fs Pulse Generation from a Self-Modelocked Titanium:Sapphire Laser” in Conference on Lasers and Electro-optics, CLEO, Techical Digest Series 619-620 (1990).

[7] C. Saraceno, C. Schriber, F. Emaury, O. Heckl, C. Baer, M. Hoffmann, K. Beil, C. Kränkel, M. Golling, T. Südmeyer, and U. Keller, "Cutting-Edge High-Power Ultrafast Thin Disk Oscillators," Applied Sciences **3**, 355–395 (2013).

[8] W. F. Krupke, "Ytterbium solid-state lasers. The first decade," IEEE Journal of Selected Topics in Quantum Electronics **6**, 1287–1296 (2000).

[9] C. Hönninger, R. Paschotta, M. Graf, G. Zhang, M. Moser, S. Biswal, J. Nees, and A. Braun, "Ultrafast ytterbium-doped bulk lasers and laser amplifiers," Applied Physics B: Lasers and Optics **17**, 3–17 (1999).

[10] M. D. Perry and G. Mourou, "Terawatt to petawatt subpicosecond lasers," Science **264**, 917–924 (1994).

[11] J. T. Luxon, D. E. Parker, *Industrial Lasers and their Applications* (Prentice-Hall Inc., 1985).

[12] Iain G. Cormack, “Rapid techniques for ultrashort optical pulse characterisation” Thesis, University of St. Andrews, (2001).

[13] W. T. Silfvast, *Laser Fundamentals* (Cambridge University Press, 2004).

[14] A. Yariv, *Quantum Electronics* (John Wiley & Sons, 1988).

[15] A. A. Lagatsky, F. Bain, C. T. A. Brown, W. Sibbett, D. A. Livshits, G. Erbert, and E. U. Rafailov, "Diode-pumped femtosecond Yb:KYW laser incorporating a quantum-dot saturable absorber," 2007 Conference on Lasers and ElectroOptics CLEO 472–473 (2007).

[16] A. A. Lagatsky, F. M. Bain, C. T. A. Brown, W. Sibbett, D. A. Livshits, G. Erbert, and E. U. Rafailov, "Low-loss quantum-dot-based saturable absorber for efficient femtosecond pulse generation," Applied Physics Letters **91**, 231111–1–23111–3 (2007).

[17] E. U. Rafailov, S. J. White, A. A. Lagatsky, A. Miller, W. Sibbett, D. A. Livshits, A. E. Zhukov, and V. M. Ustinov, "Fast Quantum-Dot Saturable Absorber for Passive Mode-Locking of Solid-State Lasers," IEEE Photonics Technology Letters **16**, 2439–2441 (2004).

[18] S. A. Meyer, J. A. Squier, and S. A. Diddams, "Diode-pumped Yb:KYW femtosecond laser frequency comb with stabilized carrier-envelope offset frequency," The European Physical Journal D **48**, 19–26 (2008).

[19] P. Wiewior, "Group velocity dispersion compensation in femtosecond Ti:sapphire laser," Proceedings SPIE 2208, Refractometry **11**, (1995).

[20] J. C. Diels, W. Rudolph, *Ultrafast Laser Pulse Phenomena* (Academic Press, 2006).

[21] W. Koechner, *Solid-State Laser Engineering* (Springer, 2006).

[22] R. Szipocs, "Invited paper Theory and design of chirped dielectric laser mirrors," Applied Physics B: Lasers and Optics **135**, 115–135 (1997).

[23] G. R. Holtom, "Mode-locked Yb:KGW laser longitudinally pumped by polarization-coupled diode bars.," Optics letters **31**, 2719–2721 (2006).

[24] D. Kopf, G. Zhang, R. Fluck, M. Moser, and U. Keller, "All-in-one dispersion-compensating saturable absorber mirror for compact femtosecond laser sources.," Optics letters **21**, 486–488 (1996).

[25] I. T. Sorokina, E. Sorokin, E. Wintner, A. Cassanho, H. P. Jenssen, and R. Szipöcs, "Prismless passively mode-locked femtosecond Cr:LiSGaF laser.," Optics letters **21**, 1165–1167 (1996).

[26] http://www.layertec.de/en/home/index (accessed on November of 2012)

[27] C. G Leburn, "Femtosecond Lasers for Datacommunications Applications" Thesis, University of St. Andrews, (2005).

[28] P. A. Williams, J. A. Hadler, R. Lee, F. C. Maring, and J. H. Lehman, "Use of radiation pressure for measurement of high-power laser emission," Optics letters **38**, 4248–4251 (2013).

[29] H. G. Heard, *Laser Parameter Measurements Handbook* (John Wiley & Sons Inc., 1968).

Chapter 2

Yb:KYW laser – initial design, construction and characterisation

2.1 Introduction

This chapter presents the development of an Yb:KYW based solid state laser oscillator, detailing the construction from the initial design to the most optimized form at a first stage. Each element of the cavity has been characterized and analysed in order to get a better performance and understanding of the system. On the basis of the results obtained, some modifications to the first cavity configuration are made to deliver a final improved oscillator with the necessary features to become a master oscillator suitable for Yb:YAG amplifier seeding.

2.2 The Yb:KYW Gain Medium

2.2.1 Crystal Structure

Potassium Yttrium Tungstate ($KY(WO_4)_2$) is a monoclinic crystal that can be easily doped with rare earth dopants such as ytterbium ions. It can be doped with a high concentration of ions without significant quenching, where Yb^{3+} ions substitute for the Y^{3+} (stoichiometric doping) [1]. Figure 2.1 illustrates the monoclinic structure of KYW, whose space group *C2/c* produces birefringence of a form which avoids thermally induced polarization rotation [2]. Its unit cell parameters are a = 8.05 Å, b = 10.35 Å, c = 7.54 Å, β = 94° and Z = 4. Yb:KYW is one of the most efficient vibronic crystals that can be pumped longitudinally by diode lasers due to its strong absorption bands that are closely matched to the wavelengths of commercially available diodes. It also has a very high emission cross section compared to other solid state gain media, which gives higher gain bandwidth for shorter pulses. The Yb:KYW material exhibits a low quantum defect (≅5%) and heat generation, allowing for very high power efficiencies. For these reasons in this project a Yb:KYW crystal was chosen as the gain material of the laser.

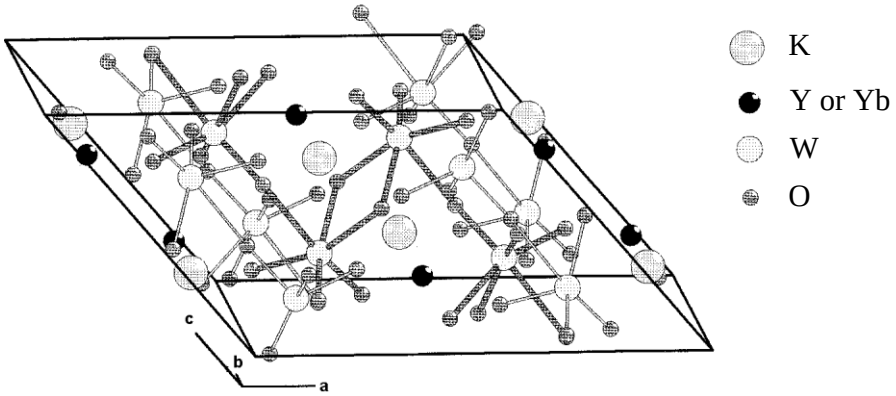

Figure 2.1 Yb:KYW crystal structure [1].

The Yb:KYW crystal has three principal crystallo-optic axes, which are N_g, N_m and N_p. Figure 2.2 shows the optical indicatrix formed by these axes with respect to the crystallographic axes a, b and c. N_p is parallel to the C2 axis of symmetry due to its monoclinic structure. This axis also coincides with the b axis, and therefore the other two axes lie rotated on the a-c plane [2].

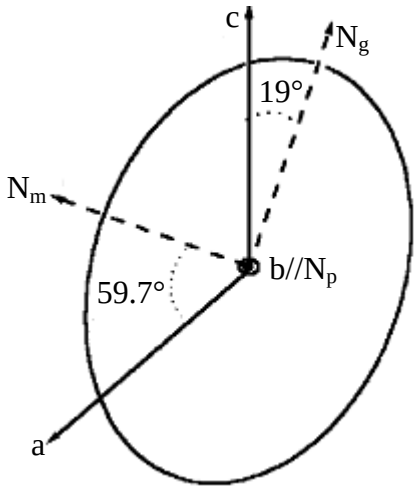

Figure 2.2 Optical indicatrix of Yb:KYW crystal [2].

2.2.2 Optical Properties

Femtosecond laser technology has over the last decade adopted new laser materials such as highly efficient Yb-doped crystals. Due to the properties of the Yb^{3+} ion as a dopant in laser materials, it is now used for high power diode-pumped solid state lasers operating in the near IR region of the spectrum. One of the advantages of using the Yb^{3+} ion in laser host media is its basic energy level scheme, in which the $^2F_{7/2}$ ground state and the $^2F_{5/2}$ excited state are split by the crystal field through the Stark effect [3]. This splitting leads to a quasi-three level energy manifold which can give rise to a population inversion. Lasing transitions for the Yb:KYW crystal are shown in Figure 2.3.

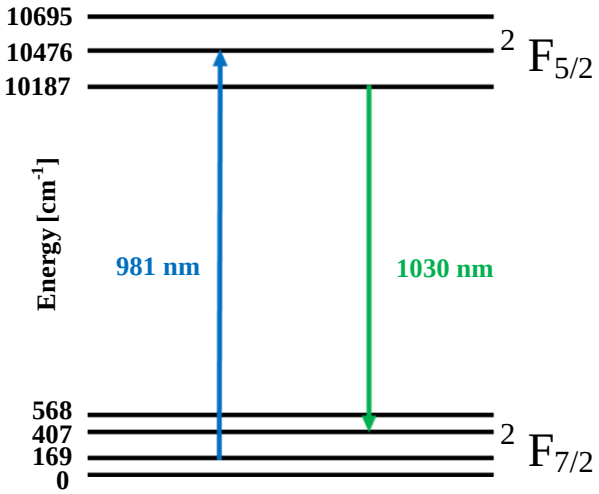

Figure 2.3 Energy levels and transitions of the Yb:KYW crystal with lasing between 1025 and 1045 nm [4, 5, 6].

The quasi-three level scheme of the trivalent Yb^{3+} ion leads to relatively low parasitic process, like excited-state absorption, up-conversion, cross-relaxation and quenching [7]; however the quasi-three level system does require very good mode overlap between the laser mode and high brightness diffraction-limited pump beams [2].

Transmission characteristics

The typical transmission of a Yb:KYW crystal with 0.2 mm thickness is shown in Figure 2.4 for a sample at room temperature being illuminated by unpolarized light. The crystal is transparent from 300-5300 nm approximately, except for a small gap at 981 nm where absorption occurs [2].

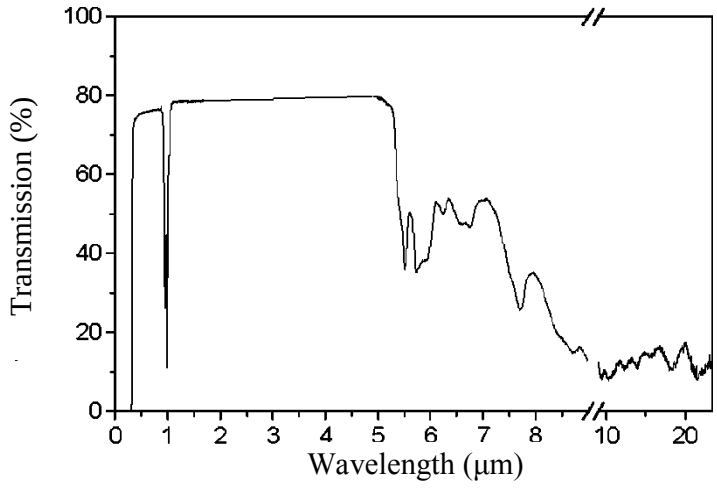

Figure 2.4 Optical window of Yb:KYW crystal at room temperature [2].

Refractive Index

The refractive index can be calculated for each direction of the crystallographic axis with the Sellmeier equation which, for this crystal, has the form [2]:

$$n^2 = A + \frac{B}{\left[1 - C/\lambda\right]^2} - D\lambda^2 \tag{2.1}$$

and using the parameters for the Sellmeier coefficients in Table 2.1.

Table 2.1 Room-temperature Sellmeier coeficients of Yb:KYW [2].

Principal Refractive Index	A	B	C μm	D μm^{-2}
n_g	3.28412	0.9921	0.25426	0.01936
n_m	3.17884	0.91624	0.25087	0.00485
n_p	3.06172	0.88655	0.23858	0.02286

Emission and Absorption Properties

The emission bandwidth that can be supported via the laser transitions of Yb:KYW is large enough for the generation of ultrashort pulses. Other advantages of these crystals include their absorption band at 981 nm where high brightness diodes can be implemented to pump the gain system [8]. High emission cross sections are also a good characteristic of KYW lasers which are essential for passive modelocking.

For an anisotropic crystal like KYW, it is necessary to measure the polarized absorption and emission spectra along the three principal crystallo-optic axes [9].

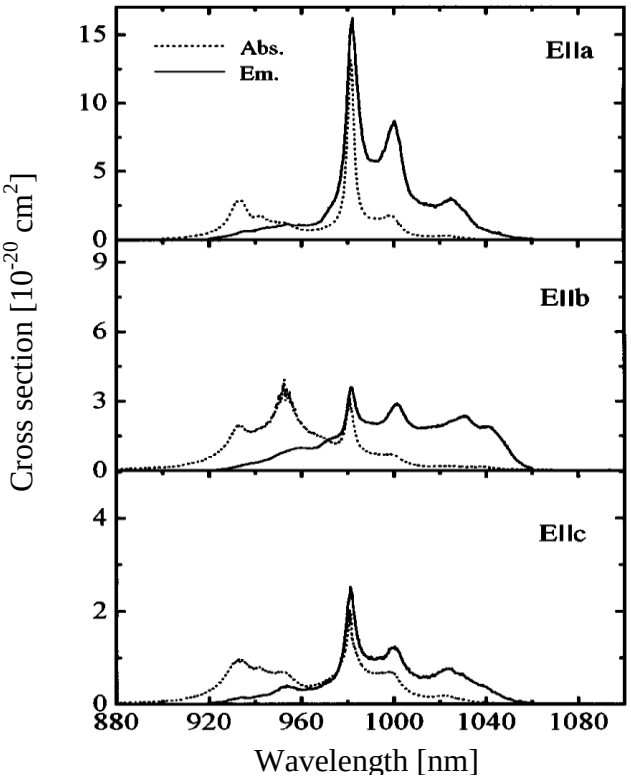

Figure 2.5 Polarized absorption and emission spectra of Yb^{3+}:KYW at room temperature [4].

Figure 2.5 shows that the strongest absorption cross section peak is observed at 981 nm along E||a polarization. The absorption cross section for Yb:KYW has been measured for E||a polarization to be of the order of $\sigma_{abs} \approx 1.33\times10^{-19}\,\mathrm{cm}^2$ at 981.2 nm[4], and $\sigma_e \approx 3\times10^{-20}\,\mathrm{cm}^2$ at 1025 nm[4, 10] for the emission cross section.

Many tungstate lasers employ absorption and emission cross sections polarized parallel to the crystal *a* axis [10, 11, 12], because the *b* axis has smaller absorption, but at 1030 nm the absorption of both axes is comparable and *b* has a broader bandwidth and lower absorption losses [13]. Consequently the polarization choice is important because it can provide a maximum emission and amplification. Compared to Yb:YAG lasers the quantum defect is smaller and the emission linewidth is broader in Yb:KYW lasers [2]. In almost all the configurations a Yb:KYW crystal cut for Brewster incidence is used, but a plane-Brewster cut has also been used [14], along the N_m direction. A tunability of ~80 nm has been demonstrated across the wavelength range between ~1000 nm to ~1080 nm [8, 15, 16].

2.3 Review of Yb:KYW Lasers

Due to the favourable characteristics of Yb:KYW, described above, a number of lasers have been developed for different applications using this gain material. Table 2.2 presents the characteristics for several laser configurations using this crystal. In these configurations different pump sources have been used, nevertheless—due to their commercial availability for the required absorption wavelength in tungstates—diode lasers have become the most common option for pumping Yb:KYW.

One of the first reported Ytterbium tungstate lasers [17] generated a power of 120 mW with a slope efficiency of 37% using a pump at 940 nm and a 10 at. % doped crystal. Later configurations demonstrated output powers > 10 W [13, 18, 19], and high slope efficiencies up to 80% [10, 14, 8]. Although KYW crystals can be doped with high concentrations of Ytterbium (up to 100%), it is most common to work at lower doping concentrations from 1.5 at.% to 10 at.% due to undesirable thermal effects associated with using larger concentrations. Pulses from ~6 ps [15] to 71 fs [17] have been achieved so far using these gain materials, with repetition frequencies ranging from 45 MHz [13] to a few GHz [20, 21].

To avoid undesirable effects like thermal lensing or the introduction of excessive amounts of GDD, small crystal dimensions have been employed, between 1-3 mm in length. In some cases larger crystals of 3.5 mm thickness [22] and 10 mm length [13] have been used successfully. With these conditions the quality of the output beam obtained has had values that range from M^2 = 1 [23] to M^2 = 1.8 [24] in the sagittal plane and M^2 = 1.05 [25] to M^2 = 5 [24] in the tangential plane.

From Table 2.2 it can be assumed that to generate high power femtosecond pulses at 1030 nm, it is better to use a 981-nm diode laser as a pump laser, and doping concentrations of the Yb:KYW crystal between 1.5-10 at.% with a Brewster cut, and thickness of a few mm [13, 18, 19].

Due to the ability to vary the doping concentration of Yb:KYW, laser systems based on this material can be used for several applications [6, 11, 26]. In industry some applications include micromachining, drilling, ablation and cutting of different materials [27].

Table 2.2 Parameters for different configurations of the Yb:KYW oscillator.

Ref.	Pump Laser	Pump Power (mW)	Output Power (mW)	Yb^{3+} at% Doping	Pump λ (nm)	Laser λ (nm)	Laser Mode	Slope Efficiency (%)	Pulse Width (fs)
[2]	Homemade Ti:Sapphire	3000	16	5	963	1074	Pulsed	41	350
[6]	Thomson model TH-C5712-F4	12000	70	10	978.3		Pulsed	34	
[8]	Narrow-stripe InGaAs	308	163	10	980	1047	Pulsed	73	123
[10]	Ti:Sapphire	940	400	5	930	1025	CW	78	-
[10]	InGaAs Diode Laser	1000	43	5	965	1025	CW	10	-
[11]	Fiber Coupled InGaAs	650	60	5	980	1042	CW	52	-
[12]	Yb:glass laser oscillator	60000		10	981	1030	Pulsed		300
[13]	Apollo ModS14-981-1	23000	10000	1.5	981	1039	Pulsed		290
[14]	Coupled fiber InGaAs	430	227	10	980.5	1056	Pulsed	80	107
[15]	Fiber coupled laser diode	440	90		980	1048	Pulsed		6.8ps
[16]	Fiber Coupled Laser Diode	410	87			1029	Pulsed		400
[17]	Single stripe diode lasers	1600	120	10	940	1057	Pulsed	37	71
[18]	Fiber coupled laser diode	22000	10700	10	981	1025	CW	54	-
[19]	Fiber coupled laser diode	30000	14600	5	981	1044	Pulsed	51	450
[20]	Fiber coupled InGaAs Diode laser	325	33	3		1040		34	170ns
[21]	Fiber coupled laser diode	485	115	10	980	1040	Pulsed	36	200
[22]	InGaAs Uniphase	970	360	10	980.5	1048	Pulsed		114
[23]	InGaAs Laser Diode	4000	1100	5	980	1037	Pulsed	57	176
[24]	Diode bar (Limo GmbH)	19300	4700	5	980	1029.6	CW	45	-
[25]		25000	2700	5	980		Pulsed		264
[26]	Multimode diode laser	240		5	980		CW	66	-
[28]	InGaAs Tapered	3500	500	10	980	1035	Pulsed		114
[29]	InGaAs Tapered	3000	500	10	980	1040	Pulsed		114
[31]	Tapered Diode Laser	1100	100	5		1046	Pulsed	14	101
[32]	Fiber coupled laser diode	4150	92	5	981	1039	Pulsed		106.5
[33]	Ti:Sapphire	57	16		971	1074	Pulsed	41	350μs
[34]	Ti:Sapphire			20	940		Pulsed		670
[35]	Laser diode	3200	550	10	981	1003.4	CW		
[36]	Free space diode bar	19100	3600	5	982	997.77	CW	40	
[37]	Multimode diode laser	550	26	10	980	1026	Pulsed	23	2ns

2.4 Pump Laser Characterisation

The first step of this project involved understanding the behaviour of the pump laser (Figure 2.6). The pump laser used for this system consisted of a collimated beam laser diode stack, from Apollo (model # C32-981-0). This pump provided 32 W of linearly polarized light at 981 nm. The output of this laser diode stack was reshaped to produce a 8 x 8 mm^2 beam with 4-mrad divergence. The system was cooled via a recirculating water cooling system and a peltier heat pump that maintained a temperature of 18^{0}C.

Figure 2.6 Laser diode stack head.

The head of the pump laser was mounted on a metallic base which was connected to the chiller via a water-cooled brass module located in the middle of the mount, and employed a thermoelectric device (RS peltier 490-1373) for temperature stabilization on the top part of the mount as shown in Figure 2.7. The working height for the system was 84 mm. Plastic washers were used between the water cooling module and the base to avoid thermal contact.

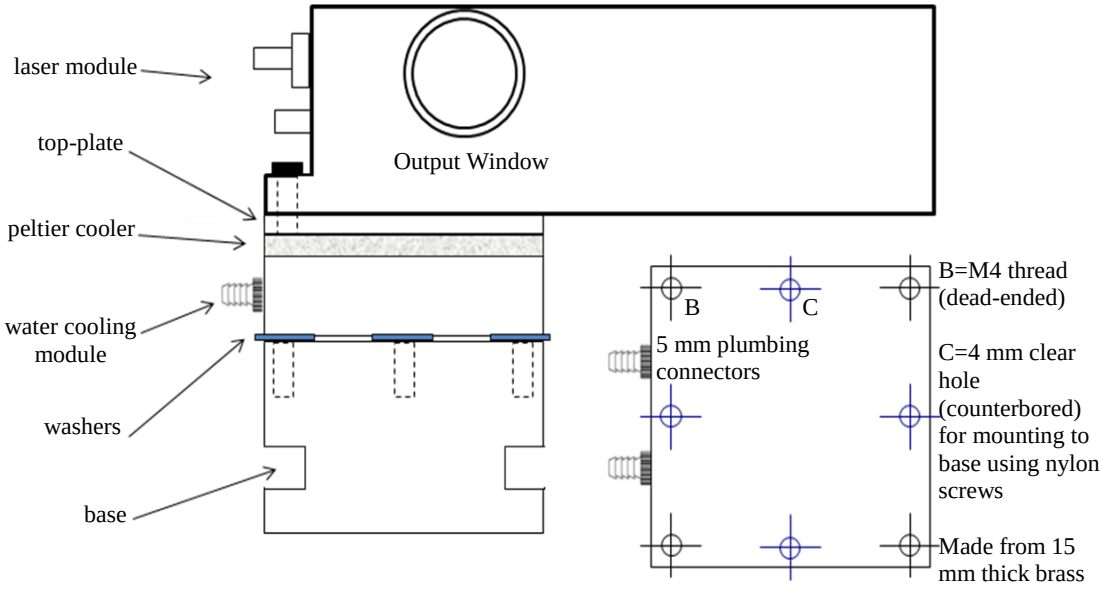

Figure 2.7 Mount for the Apollo laser and peltier.

2.4.1 Beam Quality Measurement

A knife-edge experiment was carried out to better understand the beam quality of the pump source, as explained in Chapter 1. A 75-mm focal lens was placed in the beam and the power was measured at a distance of twice the focal length. Positioning a knife-edge on a translation stage at different distances, moving the knife-edge from 10-150 mm after the lens, and introducing this edge in the beam path, in steps of 0.01 mm perpendicular to the beam (Figure 2.9 (a), (b) and (c)), the beam planes were sampled at the distances measured. Representative results are presented in Figure 2.8 (d) and illustrate that the beam had $M^2 = 16$ and could generate a beam waist of radius $w_0 = 160$ μm.

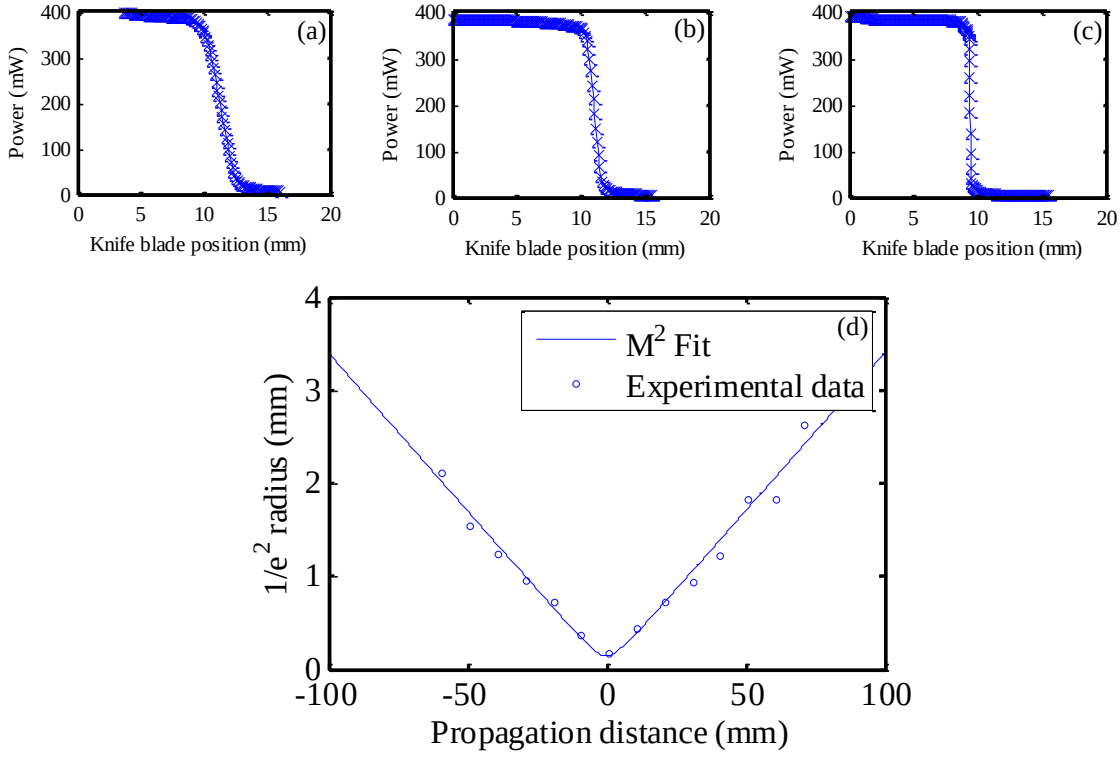

Figure 2.8 Output power as the knife-edge was scanned at positions a) -60 mm, b) -30 mm, and c) 0 mm from the focus; d)beam radius fitted to experimental data assuming $M^2 = 16$.

2.4.2 Slope Efficiency and Temperature Tuning

A complete characterisation of the pump laser was carried out to understand what the optimal drive parameters needed to be for pumping the Yb:KYW crystal. Figure 2.10 shows the output power of the pump laser as a function of the current applied by the driver of the Apollo, showing a maximum output power of 26.5W at 40A for a temperature of 25°C. The data in Figure 2.9 imply a slope efficiency of 0.8 W/A, with no indication of roll-off for the available current.

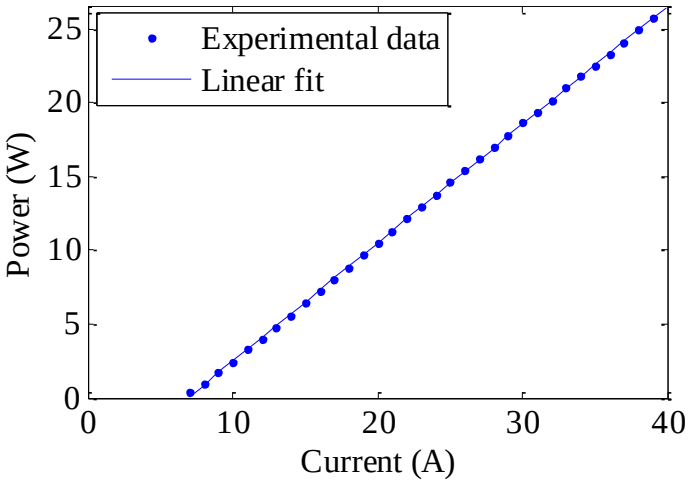

Figure 2.9 Output power as a function of driver current of the pump laser.

The temperature of the pump was controlled by a SkyTronic thermoelectric cooler. The variation of the diode temperature generated a change in the wavelength that varied also with different drive currents (Figure 2.10). In this case, to match the narrow (~3 nm) absorption line of Yb:KYW at 981.2 nm the current had to be increased to 40 A and the temperature of the diode raised to 27°C, approximately the maximum permitted for safe operation.

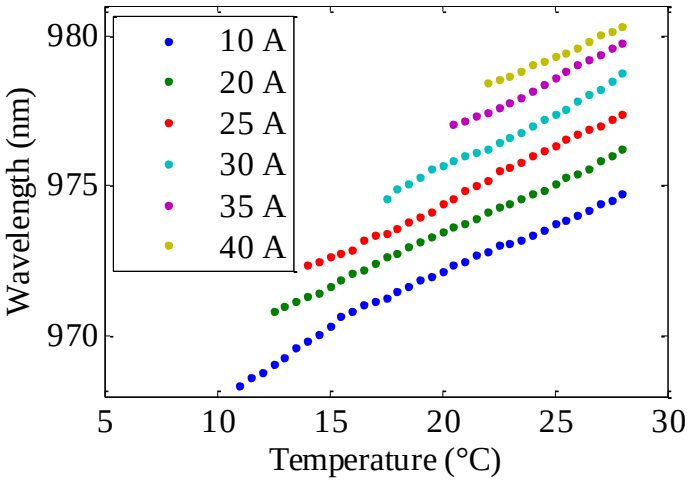

Figure 2.10 Variation of the wavelength as a function of the temperarure for different drive currents.

2.5 The Yb:KYW Laser

2.5.1 Yb:KYW Crystal Design

With the knowledge of the parameters of the pump required, it was possible to build the cavity for optimum performance.

The crystal used for this cavity was a Yb:KYW crystal with a 1.5 at.% doping. The crystal dimensions were 10×8×1.5 mm as shown in Figure 2.11, and Brewster-Brewster cut such that the p-polarization at 981 nm and 1030 nm was incident along the N_m axis. The crystal was placed between two water cooled plates (to remove heat), and set on a rotation/translation mount to allow for optimal positioning of the crystal within the cavity. This allowed the Brewster angle to be achieved with greater precision.

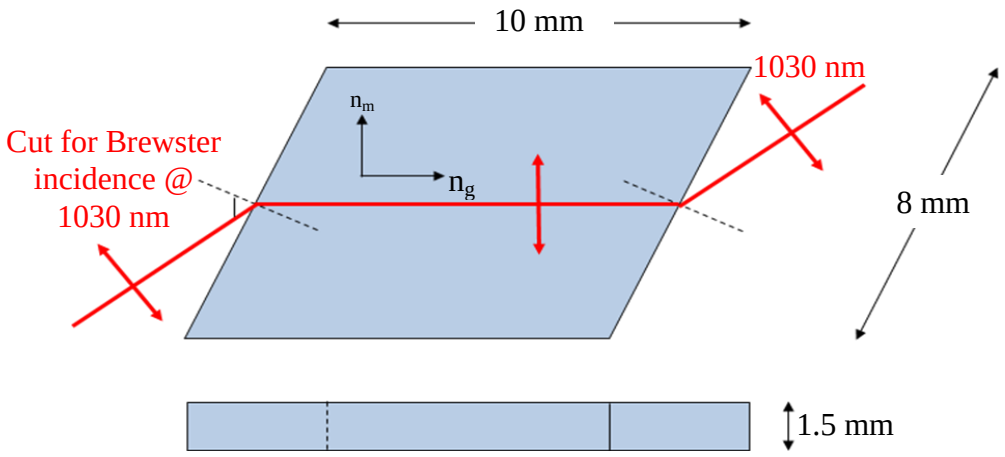

Figure 2.11 Yb:KYW crystal geometry.

The crystal was surrounded with indium foil on its top and bottom for better thermal contact with the mount. This mount also allowed levelling of the crystal to the breadboard for better alignment (Figure 2.12).

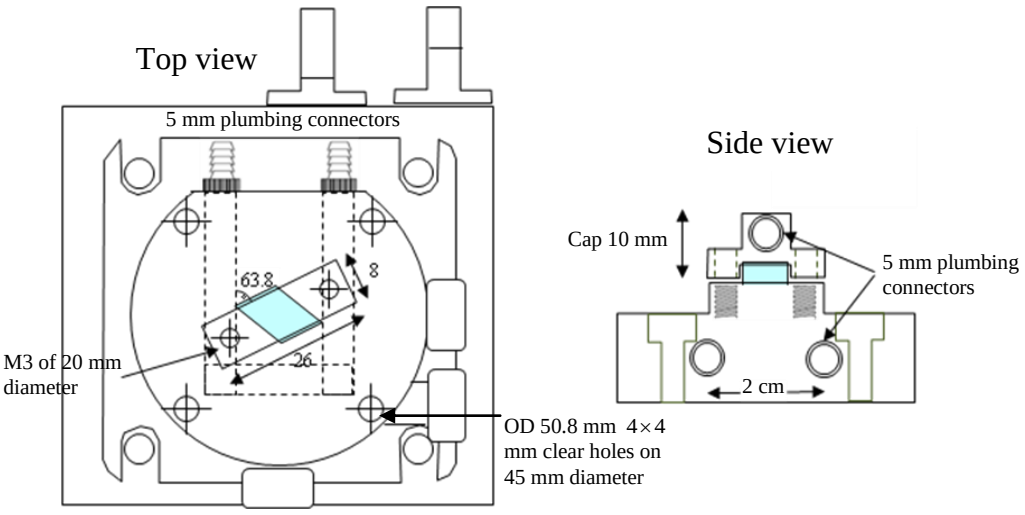

Figure 2.12 Crystal mount.

To assess the amount of pump light absorbed by the Yb:KYW crystal a beam splitter and a half wave plate were inserted between the pump laser and the lens. With these elements it was possible to control the power that would be incident on the Yb:KYW crystal. After the pump beam travelled through the KYW crystal, the total transmitted

pump power was measured to be ~1% of the total input pump power as shown in Figure 2.13, which means that 99% of the pump was absorbed by the 10 mm long crystal. This substantial absorption may have led to later parts of the crystal being weakly pumped and so unable to contribute gain, or even act as an absorber for the laser light.

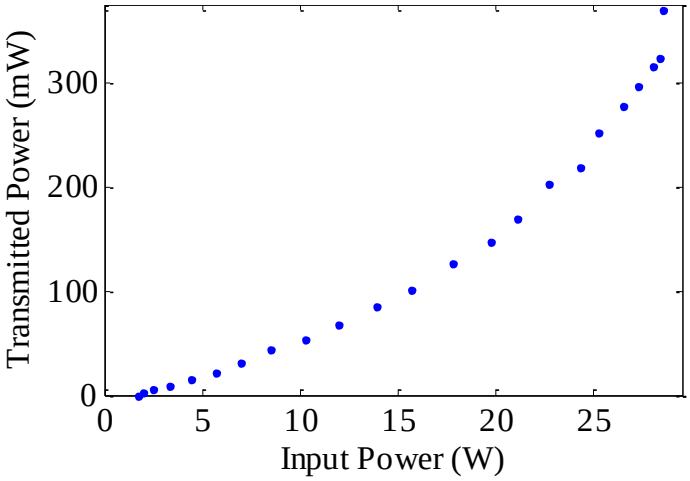

Figure 2.13 Transmitted pump power through the crystal.

2.5.2 Cavity Design

A laser cavity design package based on ABCD matrix multiplication was used to calculate the correct positions and angles of the mirrors and the laser crystal [38]. The package, known as LCAV, was used to calculate the stability regions and the beam size in each part of the cavity for an astigmatcally-compensating configuration (Figure 2.14). Introducing the data of the elements used, the distances and angles between each element were found for the desired folded *z*-cavity to get the best performance.

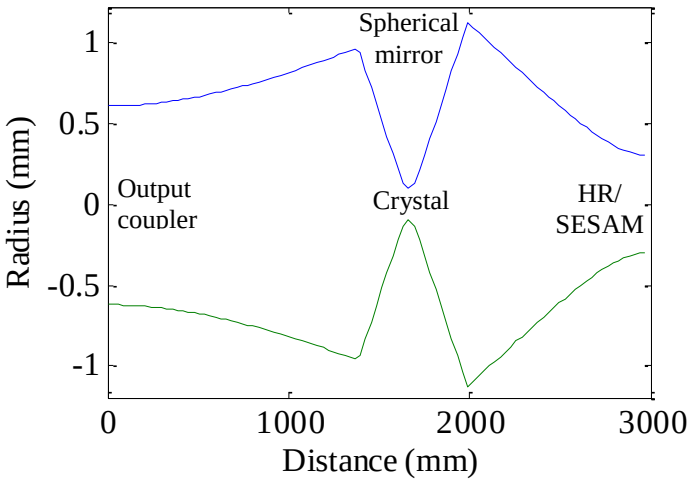

Figure 2.14 Beam size though different positions in the cavity, with the blue line showing the tangential beam radius and the green line the sagittal beam radius.

Using the data obtained from the program, the first configuration was built. In this configuration (Figure 2.15) the oscillator was pumped at 981 nm, with a pump power of 26 W. The pump beam was focused by a 75-mm lens into the Yb:KYW crystal. The cavity was designed so the spot radius in the crystal was 160 μm (that is the smallest radius that can be achieved with the pump beam used), to mode-match the size of the pump mode in the crystal. One arm of the cavity was terminated by a SESAM (which for the CW operation was replaced with a high reflector (HR) mirror), and the other arm by an output coupler.

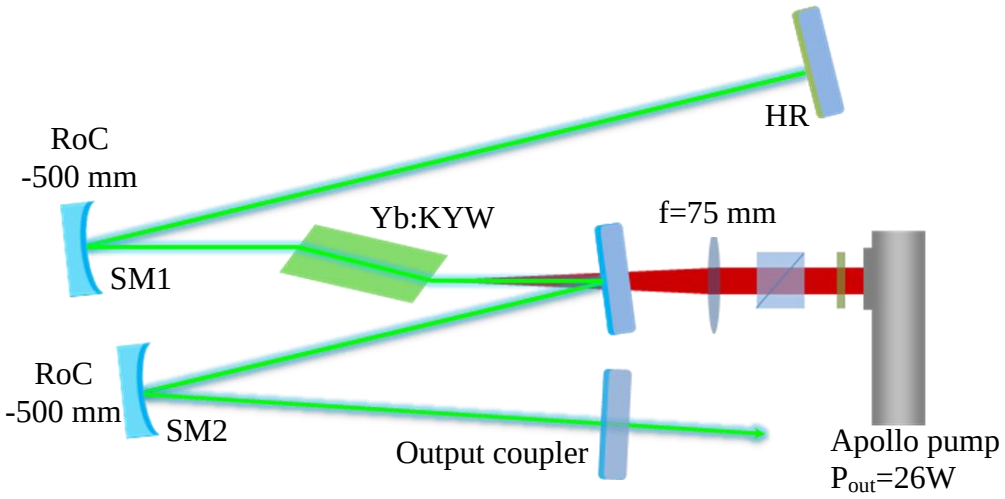

Figure 2.15 First cavity configuration.

For the first configuration the distances between each element calculated with LCAV were 1000 mm between the high reflector and the first spherical mirror (SM1), which had a radius of curvature −500 mm. A distance of 250 mm was used between the spherical mirror and the crystal. From the crystal to the folding mirror (a plane HR mirror), the distance was 35 mm. From the HR mirror to the second spherical mirror (SM2) was 215 mm, with the same radius as the first one, and 305 mm to the end of the cavity. With angles of 6° on the SM1, 10° on the HR and 16° on SM2. All HR mirrors were coated for >95% transmittance from 979-983 nm and ≥99.9% reflectance at 1035 nm. Using an output coupler with 2.5% transmission a laser average output power of 1 W was obtained. Once the laser was optimized for this configuration, a measurement of the M^2 value of the output beam was made with a 200 mm focal length lens. The laser produced a beam waist of w_o = 0.0911 mm, and a M^2 = 1.12 (Figure 2.16).

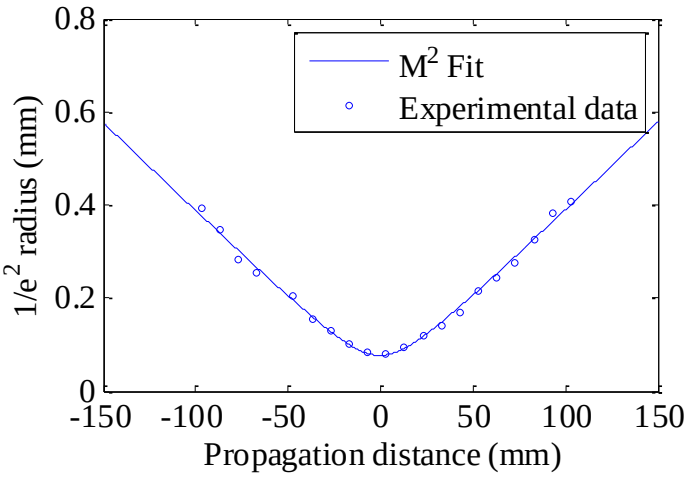

Figure 2.16 Beam waist for the KYW laser output, where the line represents the M^2 fit.

2.5.3 CW Operation of the Yb:KYW Laser

Individual output couplers (2%, 2.5%, 5%, 8% and 15% transmittance), and combinations of them, were used to perform an analysis of input and output powers for a total transmittance between 2.5% and 23% (Figure 2.17). Powers of up to 4.03 W for a 5% output coupler and slope efficiencies from 16% to 26% were obtained. The results for the measurements using each output coupler are shown in Table 2.3. The best performance, producing an output of 4.03 W was achieved at λ = 1041 nm with an output coupler of 5%.

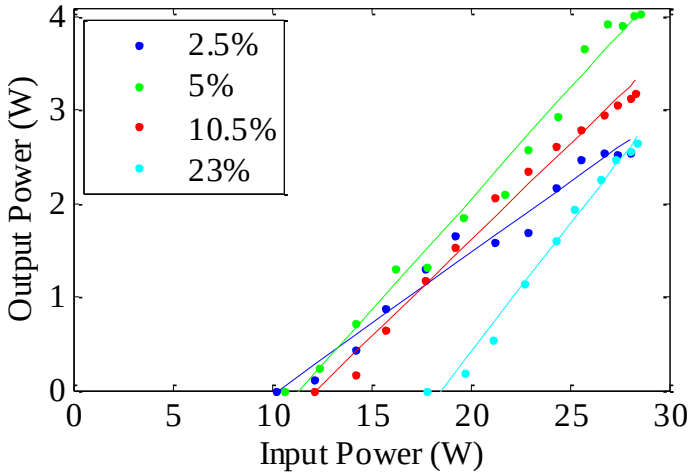

Figure 2.17 Output power as a function of the input power for different output couplers with slope efficiencies of 16%, 24%, 23% and 26% respectively.

Table 2.3 Parameters obtained varying the output coupling transmission.

Output Coupler (%)	Pump Power (W)	Output Power (W)	Pump λ (nm)	Laser λ (nm)	Slope Efficiency (%)
2.5	26.5	2.54	980.5	1047.0	16
5.0	26.5	4.03	980.5	1038.5	24
7.0	26.5	2.87	980.5	1038.0	19
8.0	26.5	3.23	980.5	1036.5	24
10.5	26.5	3.18	980.5	1030.0	23
13.0	26.5	3.00	980.5	1030.0	23
15.0	26.5	2.85	980.5	1031.0	25
17.5	26.5	2.83	980.5	1030.5	24
20.0	26.5	2.92	980.5	1030.0	26
23.0	26.5	2.65	980.5	1029.5	26

A Rigrod analysis [39] was carried out to find the maximum power available from the oscillator and thus the absorption losses for unsaturated gain. If T_2 is the output coupler transmission and $r_1 = R_1^{1/2}$ and $r_2 = R_2^{1/2}$ are the reflection coefficients of each mirror with reflectivity R_1 and R_2 respectively, then the output intensity of the laser can be calculated from [38]:

$$I_{out} = \frac{T_2 I_{sat}}{(1+r_2/r_1)(1-r_1 r_2)}\left[InG_0 - In\left(\frac{1}{r_1 r_2}\right)\right] \tag{2.2}$$

where G_0 is the single pass unsaturated gain. This means that if the gain is low, when the losses in the cavity are smaller ($R_1 \rightarrow 100\%$), the output coupling transmission needs to be also small to obtain the maximum power available. Using this equation, the data obtained experimentally was fitted to find the power-extraction efficiency of the cavity. These measurements yielded parasitic losses of 1.8%, an optimum output coupling of 5%, maximum extractable power of 4 W, and a single pass unsaturated gain of 1.45 (Figure 2.18).

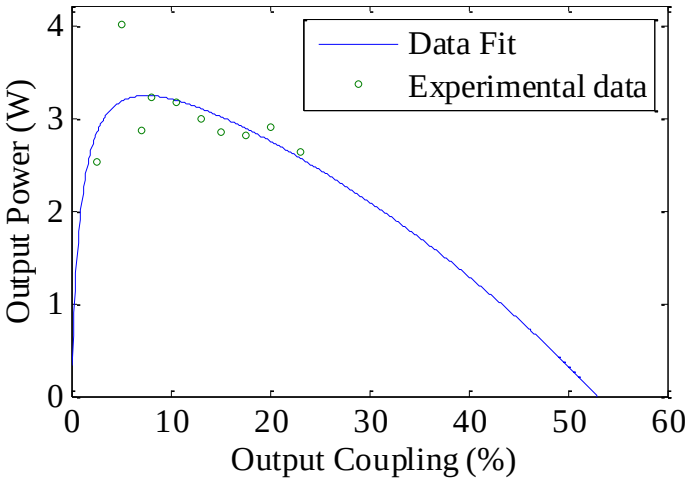

Figure 2.18 Rigrod analysis using the output couplers listed in Table 2.3 with an output power resolution of ±3% .

Although LCAV provided the parameters required for a stable resonator, a large thermal lens in the Yb:KYW crystal meant that some of the parameters of the cavity needed to be adjusted for optimal performance. We found the best performance of the laser was achieved for a distance of 1400 mm from SM1 to HR and 630 mm from SM2 to the output coupler. For the folding angle the best operation was found at 11.22°. After optimizing the cavity another Rigrod analysis was made using only four output couplers (2.5%, 5%, 8% and 15%) (Figure 2.19), getting this time parasitic losses of 1.17%, a best output coupling of 5%, maximum extractable power of 6.18 W, single pass unsaturated gain 1.21 and a 30% slope efficiency (Figure 2.20).

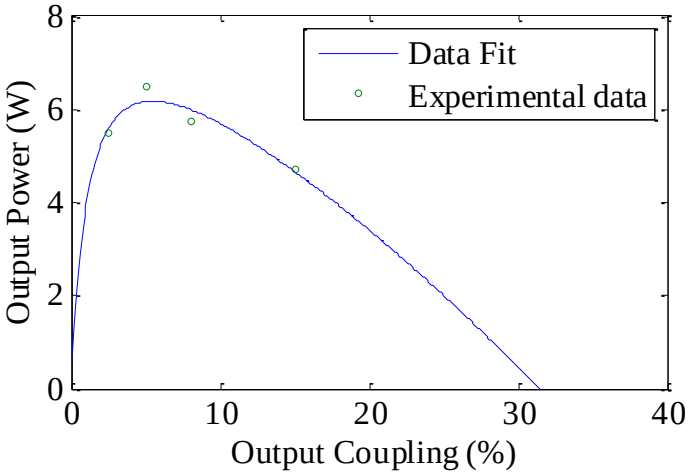

Figure 2.19 Rigrod analysis for the optimized cavity.

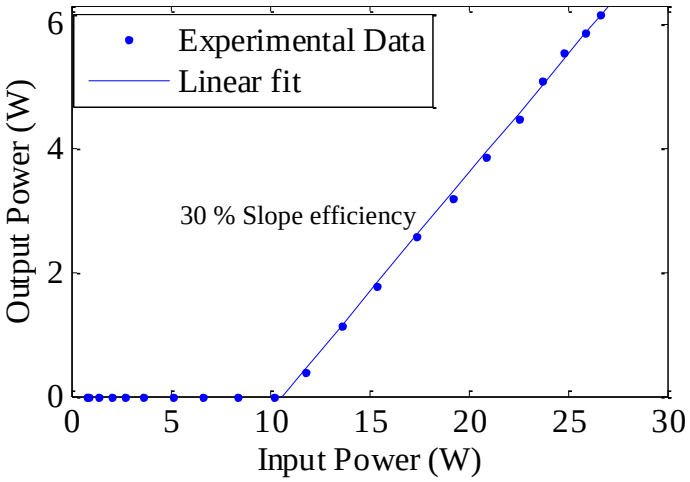

Figure 2.20 Variation of output power with the input power giving a slope efficiency of 30% with the oscillator optimized.

Tunability between 1020-1057 nm was obtained for three different output couplers (Figure 2.21), using an SF14 prism in the long arm of the cavity giving a maximum output power of 4.36 W. With these data we deduced from the gain-bandwidth obtained that it is possible to get pulses of the order of hundreds of femtoseconds.

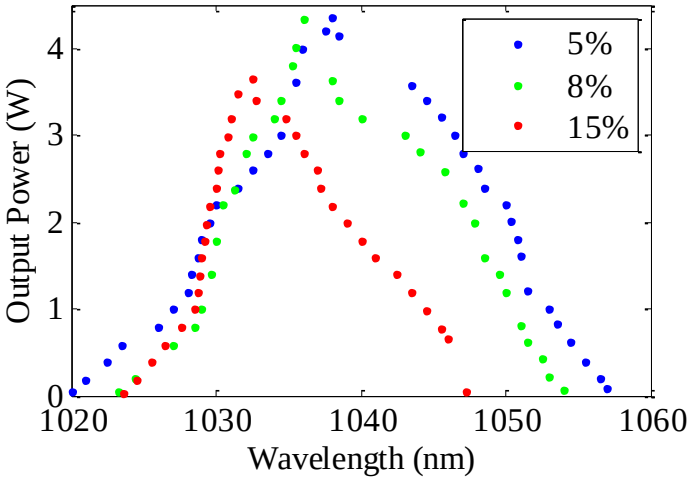

Figure 2.21 Spectral tenability of Yb:KYW CW laser, for 5%, 8% and 15% output coupling.

Due to the non-saturated reabsorption losses, when the transmittance increases the wavelength will move to shorter values [11]. This effect is shown on Figure 2.22, using the data from Table 2.3.

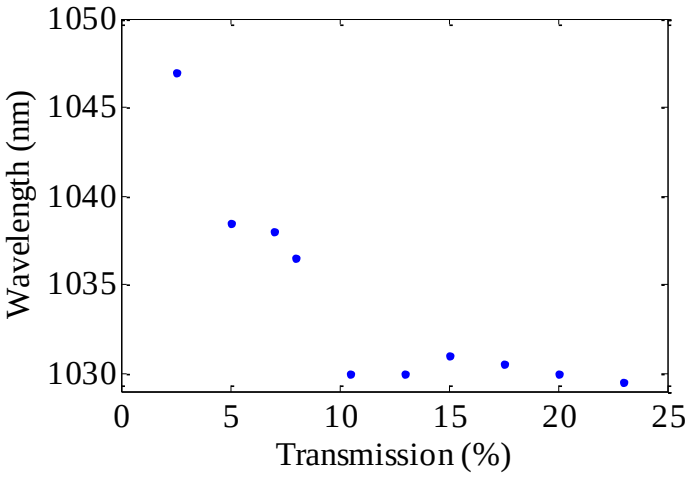

Figure 2.22 Variation of the wavelength with different output couplers.

2.5.4 Modelocked Operation of the Yb:KYW Laser

As mentioned in Chapter 1, passive modelocking was used in this project. A selection of SESAMs was evaluated for modelocking by replacing the HR mirror at the end of the short arm of the cavity with each of them in turn (Figure 2.23).

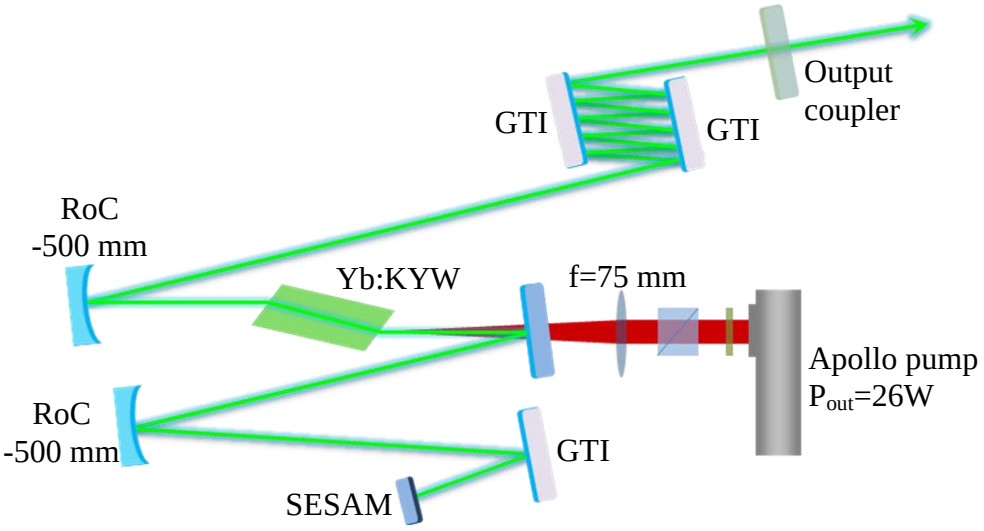

Figure 2.23 Actual cavity configuration, where the long arm corresponds to the distance from the Yb:KYW crystal to the output coupler, and the short arm from the crystal to the SESAM.

The SESAMs used were from BATOP (models: SAM-1040-1-x-500fs, SAM-1040-1.5-x-1ps and SAM-1040-2-1ps-x) [40]. The main characteristics of each SESAM are listed on Table 2.4. These SESAMs had a 4 × 4 mm effective area, and thickness of 400 µm.

Table 2.4 SESAM Characteristics [40].

Absorbance (%)	Modulation depth (%)	Non-saturable loss (%)	Saturation fluence (μJ/cm^2)	Reflectance @ 1030(%)	GDD @ 1030 (fs^2)
1	0.5	0.5	90	98.4	-13
1.5	0.8	0.7	70	97.4	0
2	1.2	0.8	60	99	-700

The SESAMs had a high-reflection band (>97%) between 980 and 1090 nm. For this cavity it was only fast saturable absorbers that were used. Some of the characteristics of each SESAM are shown in Figure 2.24. The 2% absorbance device had a resonant structure, which means that the dispersion changes rapidly over a narrow wavelength range. Because the expected pulses from this laser were in the range of a few hundred femtoseconds to sub-picoseconds regime, this device was found not to be very suitable for this cavity. The other two devices had an anti-resonant structure which makes the variation of the dispersion less rapid. According to the intracavity power obtained (30 W) and the length of the crystal, some thermal lensing effects were expected from the cavity, and therefore the spot size on the SESAM had to be manipulated to avoid the damage on the SESAM. In this case the 1.5% absorbance device was preferable because it had a lower saturation fluence than the 1% absorbance device and therefore helped avoid Q-switching of the system.

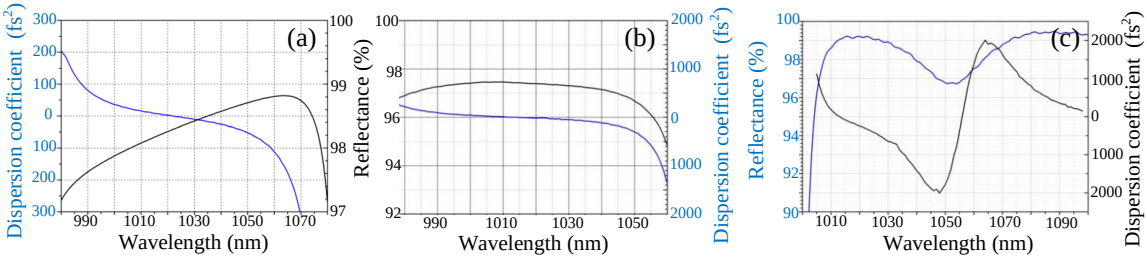

Figure 2.24 Low intensity spectral reflectance and GDD for: a) A_0 = 1 % SESAM, b) A_0 = 1.5% SESAM, and c) A_0 = 2% SESAM [40].

Because the Yb:KYW crystal introduced a large amount of positive dispersion [23], then a large amount of negative dispersion had to be used to compensate the GDD in the system. Initially an SF14 prism pair was used in the long arm of the cavity to compensate for intracavity dispersion and stabilise the mode locking but this led to a reduced output power of 1.5 W. An autocorrelation trace of the pulses is shown in Figure 2.25 assuming a sech^2 pulse shape, with a pulse repetition frequency (P.R.F.) = 53.5 MHz at 1047 nm. Pulses of ~700 fs were obtained with a duration bandwidth product of $\Delta\nu\Delta\tau = 0.51$, implying a small amount of chirp was present.

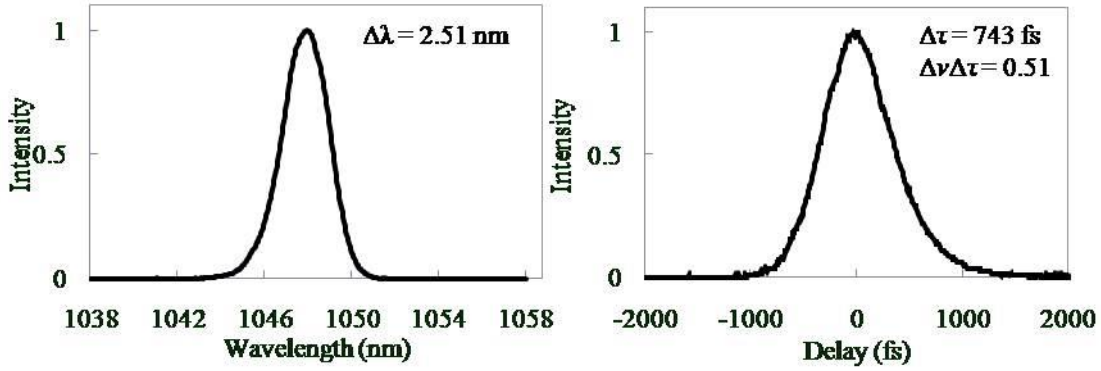

Figure 2.25 Pulse duration and bandwidth using prisms.

To allow easy integration of this laser into the amplifier, the laser was re-built on a breadboard, folding the cavity to fit on a smaller footprint. To improve the powers in the cavity and to compensate for the total dispersion inside the cavity, the prism pair was replaced by a pair of GTI mirrors coated with a high reflectivity of 99.9% at 970-1120 nm, which had a GDD of −1300±150 fs^2. One more GTI mirror was inserted as a folding mirror in the short arm, contributing a further GDD of −800±100 fs^2 to provide enough negative dispersion to the cavity (Figure 2.23). This was done to make the pulses more stable. A study of the effect of using different numbers of bounces between the GTI mirrors was made to find the best stability of the pulses without altering the long arm distance of 1400 mm. The analysis was made using a 10% output coupler and an absorbance A_0 = 1% SESAM. Figure 2.26 shows the change in the pulse spectrum for increasing numbers of bounces, producing output powers of 4.75 W without the GTIs, 4.9 W for 1 bounce, 5.1 W for 2 bounces, 4.8 W for 3 bounces, 4.8 W for 4 bounces, 4.1 W for 5 bounces and 3.6 W for 6 bounces.

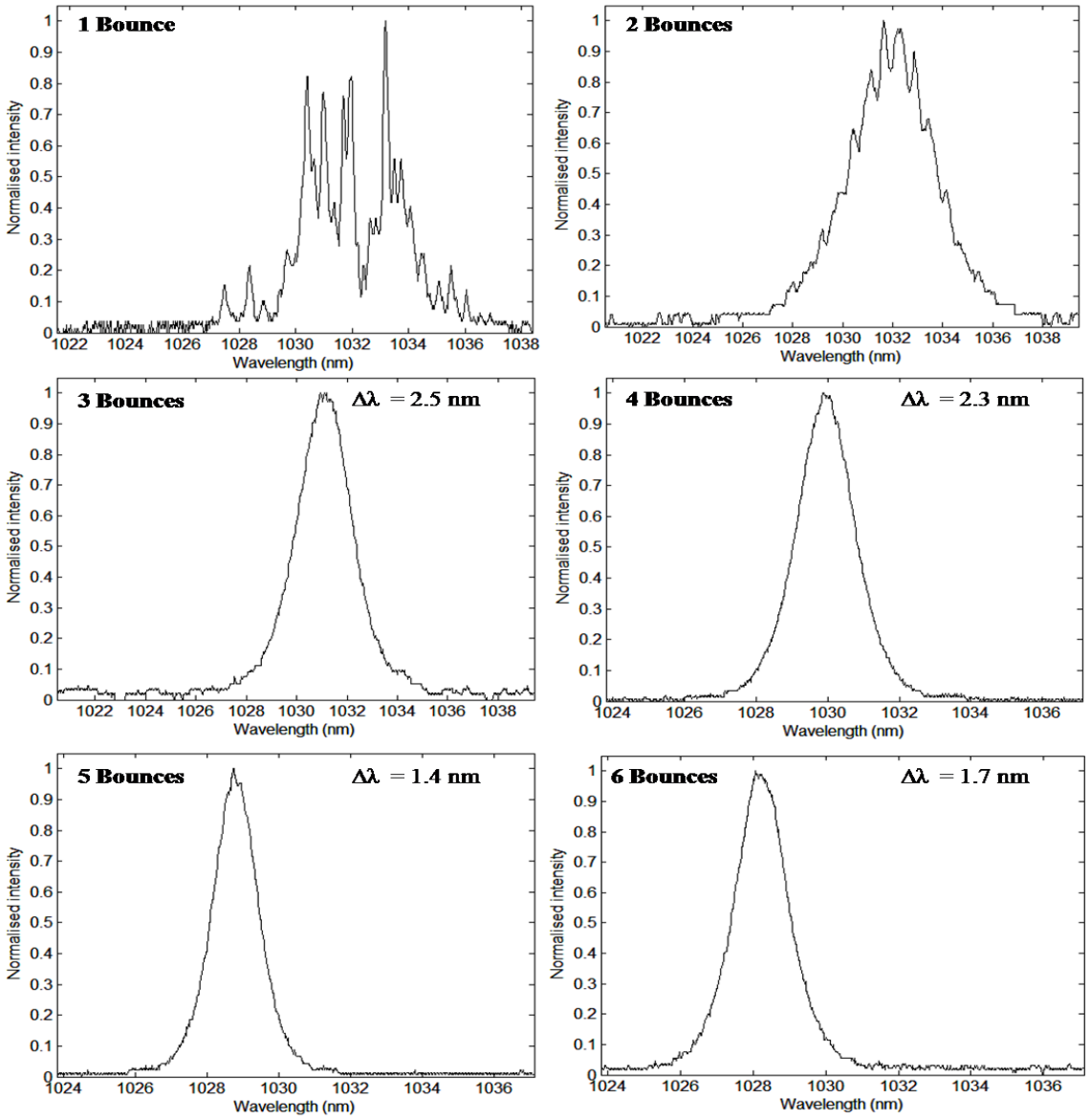

Figure 2.26 Pulse spectra for an increasing number of bounces on the GTI pair.

After the optimization process, which implied the best performance with three bounces on the GTIs, the pulses were measured to be ~500 fs at almost 1030 nm, with a power of 1.4 W and a bandwidth product of $\Delta\nu\Delta\tau = 0.39$ which implied that the pulses were close to the transform limit. The power had to be reduced to avoid multipulsing effects in the cavity. The repetition frequency was 52 MHz and the bandwidth was 2.5 nm. These pulses were produced with a 2% absorption SESAM and a 5% output coupler.

After a further optimization step the best stability was obtained with 5 bounces on the GTIs, which is the number of bounces used in the final configuration (Figure 2.23). For 5 bounces the total negative dispersion introduced to the cavity was -27600 fs^2 round trip.

Further optimisation of the cavity was performed by altering the length of the short arm of the cavity, which, in turn, altered the intracavity spot size on the SESAM. This was to avoid damage on the device due to high peak intensities and the analysis was made calculating the distance from the SM2 to the SESAM which had the best stability, according to the calculations made by using again LCAV design package. The results in Figure 2.27 show the spectrum of the laser for different lengths of the short arm.

Using the 10% output coupler and a A_0=1% SESAM, the beam radius on the SESAM and the laser output power were, respectively, 214 μm and 4.4 W for 800 mm; 257 μm and 3.8 W for 900 mm; 279 μm and 4.1 W for 950 mm; and 302 μm and 4.05 W for 1000 mm.

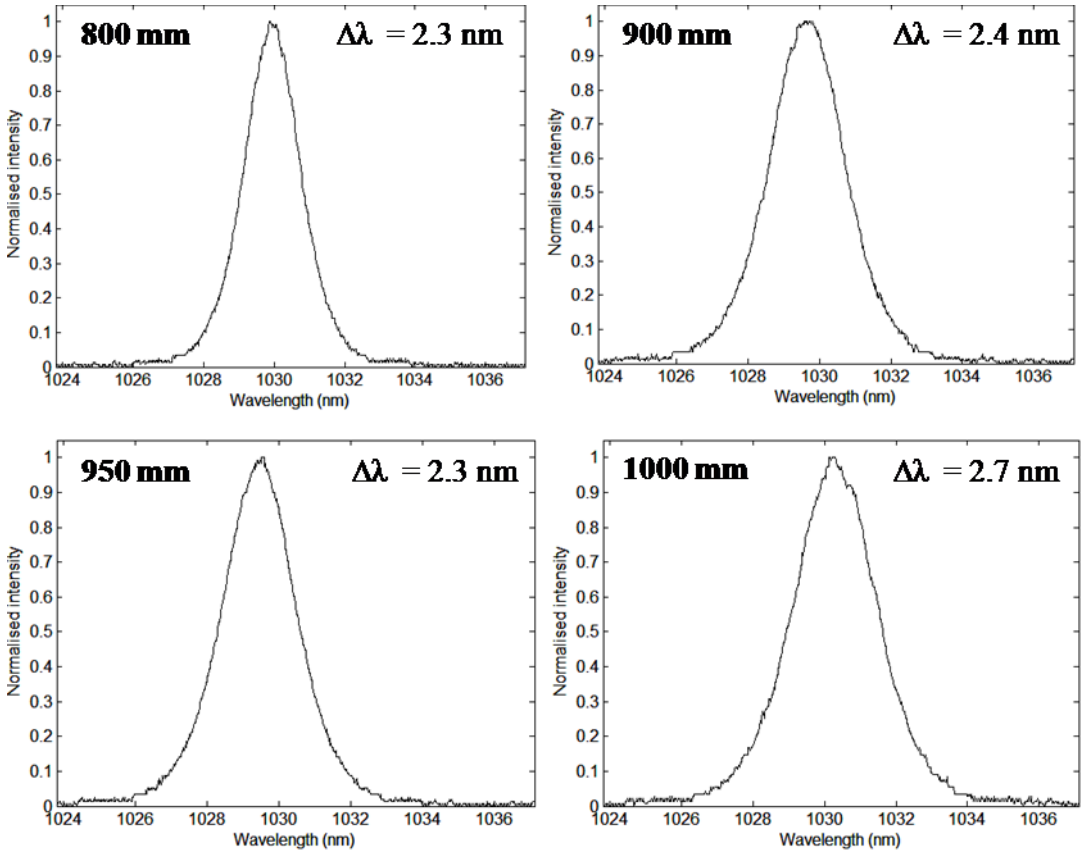

Figure 2.27 Laser spectra obtained for different lengths on the short arm.

A final configuration was investigated with a A_0=1.5% absorbance SESAM with a modulation depth of 0.8% and a saturation fluence of 70 μJ/cm^2; this SESAM was designed for work at 1040 nm with a high reflection coating between 990 nm and 1050 nm. Figure 2.28 shows the spectrum obtained for 950 mm and 1000 mm, with output powers of 3.95 W and 3.93 W in each case. Here the stability in the laser improved, although multipulsing was still observed for higher powers.

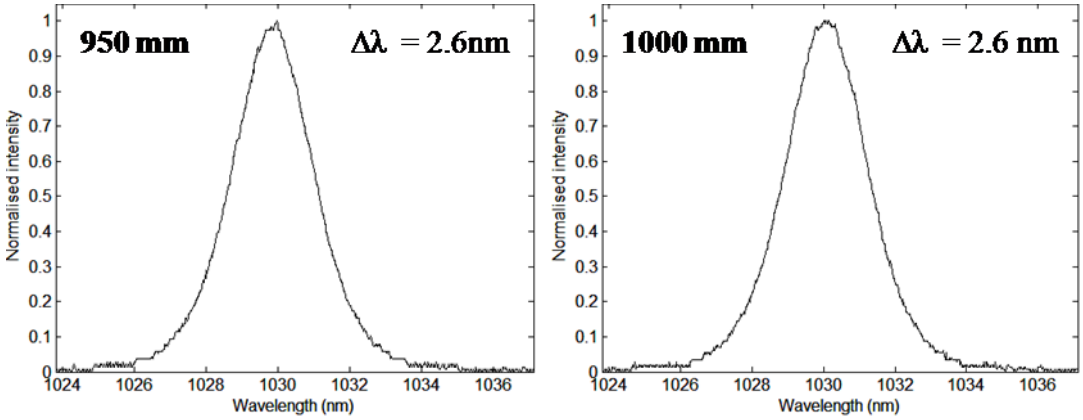

Figure 2.28 Spectral bandwith using an A_0 = 1.5 % SESAM.

The configuration with the 1000 mm distance between the spherical mirror and the SESAM in the short arm gave the best stability of the oscillator achieved at this point.

2.5.5 Temperature-dependent stability analysis

Due to the sensitivity of the multiple-bounce GTI mirror alignment to small changes in ambient temperature, another characterisation of the output of the oscillator was necessary to get the exact parameters for the best performance. Multiple bounces on the GTIs make the system lose its alignment very easily due to only small movements of them. Therefore when the temperature varies in the room some of the properties of the materials used in the cavity, like the mounts of the mirrors and the breadboard itself vary. Then, as the temperature rises, the materials expand making the alignment change, and thus the cavity has losses in the power and the modelocking is lost as well (Figure 2.29(a)). To avoid this, the breadboard was raised from the bench allowing it to float, and it also was thermally insulated underneath. In the case of the GTI mirrors, an invar bar was used to mount them together because it has a very low coefficient of thermal expansion. Lastly, the cavity was shielded into a box with aluminium tape inside and heated and maintained at 25°C using resistors driven with a 40 W controller. After all these improvements the oscillator could maintain its stability even with changes in the room temperature, as shown in Figure 2.29 (b).

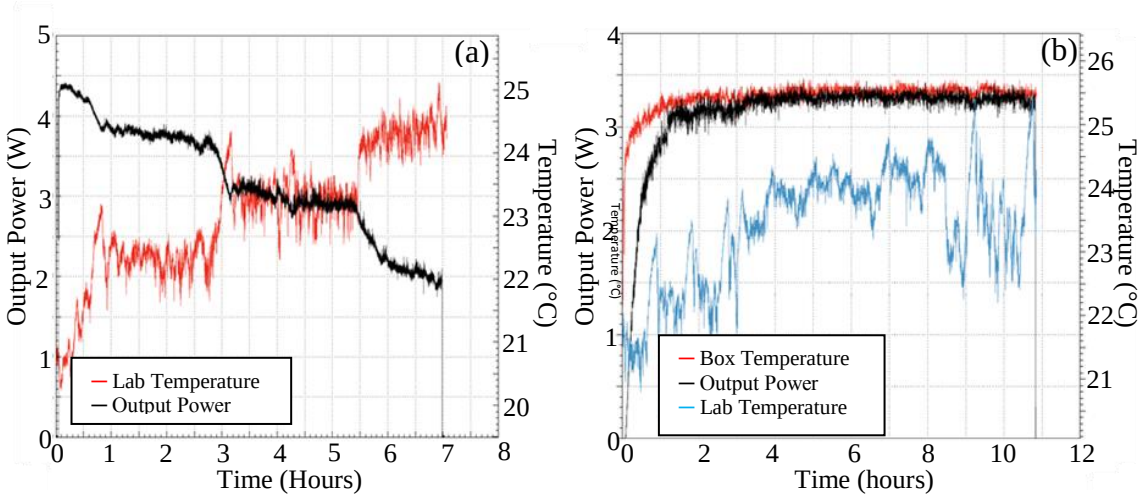

Figure 2.29 Power variation with temperature: (a) Open cavity; and (b) Cavity with box.

With this cavity configuration, and five bounces on the GTIs, it was possible to increase the power of the system to 5 W in CW operation and 4.5 W in modelocked operation at 1036 nm, using an output coupler of 10% and a A_0=1.5% SESAM. The pulse repetition frequency was 53 MHz. To be coupled into an amplifier, as required in the next part of the project, the wavelength needed for the master oscillator was 1032 nm. Figure 2.21 shows how by changing the output coupler from 10 % to 15% it was possible to force the wavelength to shift from 1036 nm to 1032 nm by increasing the non-saturated re-absorption losses in the crystal [11].

Finally, with these corrections incorporated within the oscillator, the final configuration gave 4.5 W average output power for pulses of 484 fs, a bandwidth of 2.6 nm and a pulse energy of 0.085 μJ (Figure 2.30).

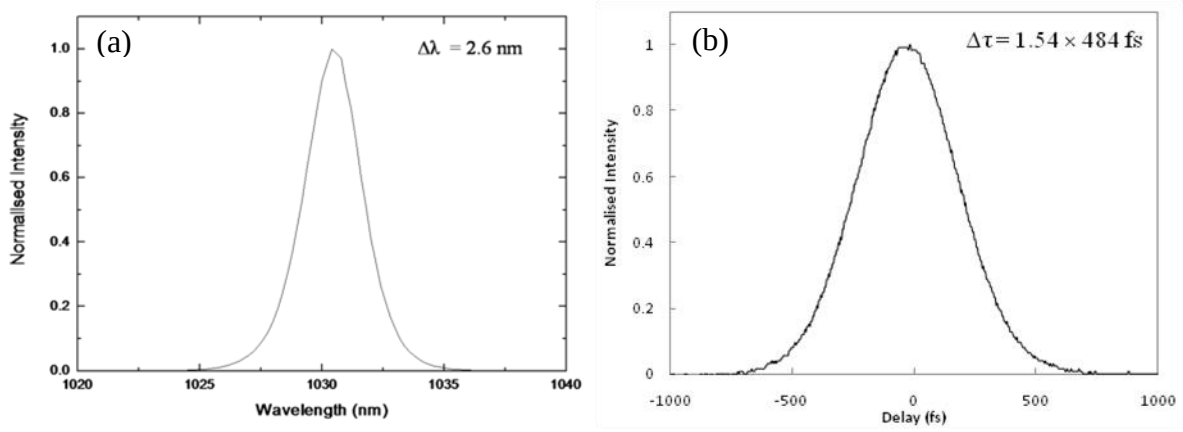

Figure 2.30 Final system (a) Spectrum (2.6 nm bandwith), and (b) Intensity autocorrelation (1.54×484 fs pulse duration).

The beam from this cavity had an M^2 = 1.20 in the horizontal axis, and M^2 = 1.19 in the vertical axis, calculated from the data and analysis presented in Figure 2.31.

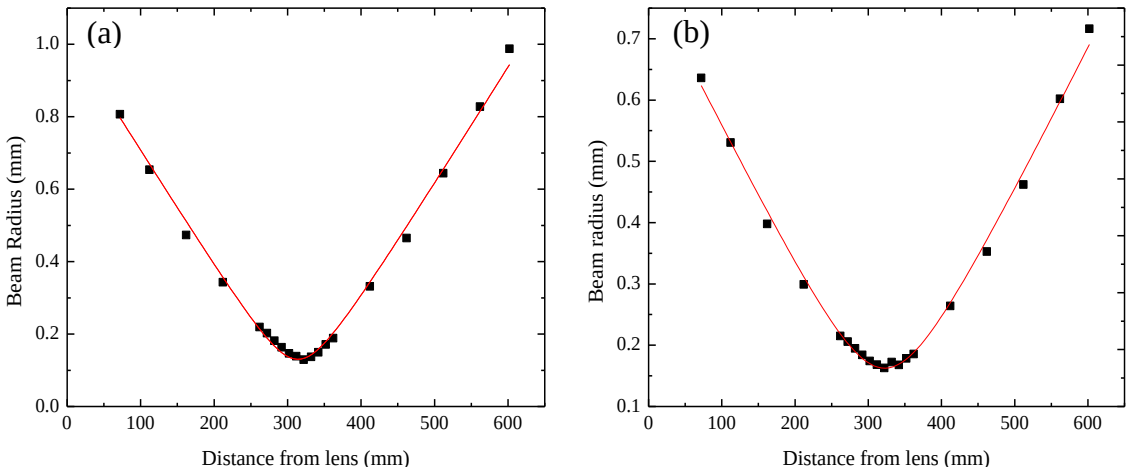

Figure 2.31M^2 measurement data for the final cavity (a) in the horizontal direction and (b) in the vertical direction.

2.6 Conclusions

A Yb:KYW laser oscillator was demonstrated in a cavity built using a Yb:KYW crystal with 1.5 at.% doping concentration. Two spherical mirrors were used for the folded z-cavity with -500 mm RoC. Three GTI mirrors compensated for the positive dispersion of the crystal, one in the short arm with -800 fs^2 negative GDD, and two with -1300 fs^2 negative GDD with five bounces on each. The long arm had a total distance from the crystal to the output coupler of 1670 mm with an angle of 8° on the spherical mirror, and the short arm had a distance of 1342 mm from the crystal to the SESAM, with an angle of 4° on the spherical mirror. The spot radius on the crystal was 97 μm at 1032 nm. The final spot diameter calculated on the SESAM was 516 μm, and on the output coupler was 1.35 mm. The SESAM used in this cavity had an absorbance of 1.5%.

Characterization of the cavity showed average modelocked output powers of up to 4 W and pulse durations of 500 fs with a good beam quality along both axes of M^2 = 1.2. The laser operated in the spectral range from 1020 nm to 1057 nm, with a center wavelength at 1032 nm, and had a repetition rate of 53 MHz. A duration-bandwidth product of 0.39 was obtained and, although this was obtained in a multipulsing mode, these results are good compared with those reported previously by others [14, 17, 18, 24, 36].

The achieved parameters of the laser are better than the ones originally aimed for in this project to seed the MOPA system, nevertheless more improvements can be done to get the best performance from the oscillator. In the next chapter the insertion of this oscillator into the master oscillator power amplifier will be detailed.

Because of all the improvements that were necessary to obtain stable modelocking operation for this oscillator, a next generation of the oscillator has been implemented using a different cavity geometry to improve some performance parameters and simplify the design. The low efficiency effects discussed in Section 2.5.1 due to using a long crystal made it necessary to change to a different crystal geometry to improve the performance of this oscillator. This will be discussed in Chapter 5.

2.7 References

[1] L. Macalik, J. Hanuza, and A. A. Kaminskii, "Polarized Raman spectra of the oriented $NaY(WO_4)_2$ and $KY(WO_4)_2$ single crystals," **555**, 289–297 (2000).

[2] M. Pujol, M. Bursukova, F. Güell, X. Mateos, R. Solé, J. Gavaldà, M. Aguiló, J. Massons, F. Díaz, P. Klopp, U. Griebner, and V. Petrov, "Growth, optical characterization, and laser operation of a stoichiometric crystal $KYb(WO_4)_2$," Physical Review B **65**, 165121–1–16521–11 (2002).

[3] G. Mérat, M. Boudeulle, N. Muhlstein, A. Brenier, and G. Boulon, "Nucleation , morphology and spectroscopic properties of Yb^{3+}-doped $KY(WO_4)_2$ crystals grown by the top nucleated floating crystal method," Journal of Crystal Growth **197**, 883–888 (1999).

[4] N. V. Kuleshov, A. A. Lagatsky, A. V. Podlipensky, V. P. Mikhailov, and G. Huber, "Pulsed laser operation of Y b-dope d $KY(WO_4)_2$ and $KGd(WO_4)_2$.," Optics letters **22**, 1317–9 (1997).

[5] A. A. Demidovich, A. N. Kuzmin, N. K. Nikeenko, A. N. Titov, M. Mond, and S. Kueck, "Optical characterization of Yb,Tm:KYW crystal concerning laser application," Journal of Alloys and Compounds **341**, 124–129 (2002).

[6] Y. Kalisky, O. Kalisky, U. Rachum, G. Boulon, and A. Brenier, "Comparative Performance of Passively Q-Switched Diode-Pumped Yb^{3+}-Doped Tungstate and Garnet Lasers Using Cr^{4+} : YAG Saturable Absorber," IEEE Journal of Quantum Electronics **13**, 502–510 (2007).

[7] C. T. A. Brown, M. A. Cataluna, A. A. Lagatsky, E. U. Rafailov, M. B. Agate, C. G. Leburn, and W. Sibbett, "Compact laser-diode-based femtosecond sources," New Journal of Physics **6**, 175–175 (2004).

[8] A. A. Lagatsky, E. U. Rafailov, C. G. Leburn, C. T. A. Brown, N. Xiang, O. G. Okhotnikov, and W. Sibbett, "Highly efficient femtosecond Yb:KYW laser pumped by single narrow-stripe laser diode," Electronics Letters **39**, 1108–1110 (2003).

[9] L. D. Deloach, S. A. Payne, L. L. Chase, L. K. Smith, W. L. Kway, and W. F. Krupke, "Evaluation of Absorption and Emission Properties of Yb^{3+} Doped Crystals for Laser Applications," IEEE Journal of Quantum Electronics **29**, 1179–1191 (1993).

[10] N. V. Kuleshov, A. A. Lagatsky, V. G. Shcherbitsky, V. P. Mikhailov, E. Heumann, T. Jensen, A. Diening, and G. Huber, "CW laser performance of Yb and Er,Yb doped tungstates," Applied Physics B: Lasers and Optics **64**, 409–413 (1997).

[11] A. A. Lagatsky, N. V Kuleshov, and V. P. Mikhailov, "Diode-pumped CW lasing of Yb : KYW and Yb : KGW," Optics Communications **165**, 71–75 (1999).

[12] A. Beyertt, D. Nickel, and A. Giesen, "Femtosecond thin-disk Yb:KYW regenerative amplifier," Applied Physics B **80**, 655–660 (2005).

[13] G. R. Holtom, "Mode-locked Yb:KGW laser longitudinally pumped by polarization-coupled diode bars.," Optics letters **31**, 2719–21 (2006).

[14] A. Lagatsky, C. Brown, and W. Sibbett, "Highly efficient and low threshold diode-pumped Kerr-lens mode-locked Yb:KYW laser.," Optics express **12**, 3928–33 (2004).

[15] A. A. Lagatsky, E. U. Rafailov, W. Sibbett, D. A. Livshits, A. E. Zhukov, and V. M. Ustinov, "Quantum-dot-based saturable absorber with p-n junction for mode-locking of solid-state lasers," IEEE Photonics Technology Letters **17**, 294–296 (2005).

[16] E. U. Rafailov, S. J. White, a. a. Lagatsky, a. Miller, W. Sibbett, D. a. Livshits, a. E. Zhukov, and V. M. Ustinov, "Fast Quantum-Dot Saturable Absorber for Passive Mode-Locking of Solid-State Lasers," IEEE Photonics Technology Letters **16**, 2439–2441 (2004).

[17] H. Liu, J. Nees, and G. Mourou, "Diode-pumped Kerr-lens mode-locked Yb:$KY(WO_4)_2$ laser.," Optics letters **26**, 1723–1725 (2001).

[18] M. Hildebrandt, U. Bünting, U. Kosch, D. Haussmann, T. Levy, M. Krause, O. Müller, U. Bartuch, and W. Viöl, "Diode-pumped Yb:KYW thin-disk laser operation with wavelength tuning to small quantum defects," Optics Communications **259**, 796–798 (2006).

[19] A. L. Calendron, K. S. Wentsch, and M. J. Lederer, "High power cw and mode-locked oscillators based on Yb:KYW multi-crystal resonators.," Optics express **16**, 18838–18843 (2008).

[20] F. M. Bain, A. A. Lagatsky, S. V. Kurilchick, V. E. Kisel, S. A. Guretsky, A. M. Luginets, N. A. Kalanda, I. . M. Kolesova, N. V. Kuleshov, W. Sibbett, and C. T. A. Brown, "Continuous-wave and Q-switched operation of a compact, diode-pumped Yb^{3+}:$KY(WO_4)_2$ planar waveguide laser," Optics express **17**, 1666–1670 (2009).

[21] P. Wasylczyk, P. Wnuk, and C. Radzewicz, "Passively modelocked, diode-pumped Yb : KYW femtosecond oscillator with 1 GHz repetition rate Abstract :," Optics express **17**, 5630–5635 (2009).

[22] A. A. Lagatsky, E. U. Rafailov, A. R. Sarmani, C. T. A. Brown, W. Sibbett, L. Ming, and P. G. R. Smith, "Efficient femtosecond green-light source with a diode-pumped mode-locked Yb^{3+}:$KY(WO_4)_2$ laser.," Optics letters **30**, 1144–1146 (2005).

[23] S. A. Meyer, J. A. Squier, and S. A. Diddams, "Diode-pumped Yb:KYW femtosecond laser frequency comb with stabilized carrier-envelope offset frequency," The European Physical Journal D **48**, 19–26 (2008).

[24] B. Jacobsson, J. E. Hellström, V. Pasiskevicius, and F. Laurell, "Widely tunable Yb:KYW laser with a volume Bragg grating," Optics Express **15**, 1003–1010 (2007).

[25] M. Siegel, J. Aus-der-Au, and A. Guandalini, "High Repetition Rate Cavity-Dumped Yb:KYW Femtosecond Oscillator," Conference on Lasers and Electro-Optics 2010 CTuV4 (2010).

[26] A. A. Demidovich, A. N. Kuzmin, G. I. Ryabtsev, M. B. Danailov, W. Strek, and A. N. Titov, "Influence of Yb concentration on Yb:KYW laser properties," Journal of Alloys and Compounds **300-301**, 238–241 (2000).

[27] X. Liu, D. Du, and G. Mourou, "Laser ablation and micromachining with ultrashort laser pulses," IEEE Journal of Quantum Electronics **33**, 1706–1716 (1997).

[28] A. A. Lagatsky, F. Bain, C. T. A. Brown, W. Sibbett, D. A. Livshits, G. Erbert, and E. U. Rafailov, "Diode-pumped femtosecond Yb:KYW laser incorporating a quantum-dot saturable absorber," 2007 Conference on Lasers and ElectroOptics CLEO 472–473 (2007).

[29] A. A. Lagatsky, F. M. Bain, C. T. A. Brown, W. Sibbett, D. A. Livshits, G. Erbert, and E. U. Rafailov, "Low-loss quantum-dot-based saturable absorber for efficient femtosecond pulse generation," Applied Physics Letters **91**, 231111–1–23111–3 (2007).

[30] A. Aznar, R. Solé, M. Aguiló, F. Diaz, U. Griebner, R. Grunwald, and V. Petrov, "Growth, optical characterization, and laser operation of epitaxial Yb:$KY(WO_4)_2$/$KY(WO_4)_2$ composites with monoclinic structure," Applied Physics Letters **85**, 4313–4315 (2004).

[31] P. Klopp, V. Petrov, U. Griebner, and G. Erbert, "Passively mode-locked Yb:KYW laser pumped by a tapered diode laser.," Optics express **10**, 108–113 (2002).
[32] G. Paunescu, J. Hein, and R. Sauerbrey, "100-fs diode-pumped Yb:KGW mode-locked laser," Applied Physics B **79**, 555–558 (2004).
[33] P. Klopp, U. Griebner, V. Petrov, X. Mateos, M. a. Bursukova, M. C. Pujol, R. Sole, J. Gavalda, M. Aguilo, F. Güell, J. Massons, T. Kirilov, and F. Diaz, "Laser operation of the new stoichiometric crystal $KYb(WO_4)_2$," Applied Physics B: Lasers and Optics **74**, 185–189 (2002).
[34] K. Ogawa, Y. Akahane, M. Aoyama, K. Tsuji, S. Tokita, J. Kawanaka, H. Nishioka, and K. Yamakawa, "Multi-milijoule, diode-pumped, cryogenically-cooled $Yb : KY (WO_4)_2$ chirped-pulse regenerative amplifier," Optics express **15**, 8598–8602 (2007).
[35] M. Jacquemet, F. Druon, F. Balembois, and P. Georges, "Single-frequency operation of diode-pumped Yb:KYW at 1003.4 nm and 501.7 nm by intracavity second harmonic generation," Applied Physics B **85**, 69–72 (2006).
[36] J. E. Hellström, B. Jacobsson, V. Pasiskevicius, and F. Laurell, "Quasi-two-level Yb:KYW laser with a volume Bragg grating," Optics Express **15**, 13930–13935 (2007).
[37] A. S. Grabtchikov, A. N. Kuzmin, V. A. Lisinetskii, V. A. Orlovich, A. A. Demidovich, M. B. Danailov, H. J. Eichler, A. Bednarkiewicz, W. Strek, and A. N. Titov, "Laser operation and Raman self-frequency conversion in Yb:KYW microchip laser," Applied Physics B: Lasers and Optics **75**, 795–797 (2002).
[38] A. E. Siegman, *Lasers* (University Science Books, 1986).
[39] W. W. Rigrod, "Homogeneously Broadened C W Lasers with Uniform Distributed Loss," IEEE Journal of Quantum Electronics **29**, 377–381 (1978).
[40] BATOP. http://www.batop.de/ (accessed on November 2012)

Chapter 3

Femtosecond pulses at 50 W average power from an Yb:YAG planar waveguide amplifier seeded by an Yb:KYW oscillator

3.1 Introduction

Over the next two chapters an application will be discussed for the oscillator presented in Chapter 2. These chapters will present the construction of a master oscillator power amplifier (MOPA) using two different configurations. This part of the project was made in collaboration with Prof. Howard Baker's group at Heriot-Watt University. The construction of the amplifier was started by Dr. Ian Thomson [1], and then continued by the two of us. Each of these configurations is characterized and described. In this chapter the construction of a MOPA is presented using the configuration in Chapter 2 as a master oscillator. This first amplifier design uses cylindrical mirrors to allow several bounces of the seed beam within a planar waveguide amplifier. Results from a design involving a single pass to five passes through the amplifier are presented.

3.2 The Waveguide Amplifier

As mentioned in Chapter 2, applications of ultrashort pulses at high energies have been increasing in areas such as micromachining [2-4] (including: ablation, cutting, welding, drilling and scribing), as well as telecommunications and medical sciences. To obtain high precision in these processes, femtosecond to picosecond pulse technology is being increasingly adopted [3]. For efficient ultrafast processing, high average power lasers are required, so it is necessary to improve the energy of the laser pulses or increase the repetition frequency [4]. Although now there are laser oscillators that can reach sufficiently high power levels, the increasing power of high repetition rate seed lasers by using multi-pass amplifiers have certain advantages over competing approaches.

Amplifiers use an input beam from a seed source, usually a laser diode, fibre laser or a solid state laser [5-13], and increase its power by stimulated emission in a gain material. The seed beam can be continuous or pulsed by different methods (Q-switched or CW-modelocking). The most commonly used in amplifiers as gain medium are disks [5, 6], solid-state crystals [7, 8], fibres [9], slabs [10] or planar waveguides [11-13]. In order to

achieve more power, some amplifiers must pass the seed beam several times through the gain material. This can be done in different ways. One method is to couple the seed beam on a single pass to a set of stages of gain material one after the other, generating amplification within each stage. Regenerative amplifiers use a gain material inside a resonator that is seeded using polarizers inside the cavity. After the pulse enters the cavity its polarization is rotated, then the pulse is amplified on each pass through the gain material [5-8]. Multipass amplifiers utilize a set of mirrors to reflect the beam many times through the gain material and generate amplification [11, 12, 14]. If more amplification is required, the first method can be optimized to form a set of multipass stage amplifiers coupled together. In this thesis is used the multipass amplifier method.

3.2.1 Amplification Theory

In multipass amplifiers, the amplification process usually modifies certain characteristics of the seed input while preserving others. The seed oscillator is used to define characteristics like the pulse repetition rate, wavelength, beam size, pulse duration and input power. To design an efficient amplifier it is necessary to know which properties are important to obtain the amplification needed. The most important are the absolute gain, the saturation energy, parasitic loss effects caused by focusing and reflection, amplification bandwidth and material dispersion.

One of the main influences on an amplifier's gain is the gain material itself. An important factor is the amount of useful energy that can be extracted from the pump energy introduced. This will define the length and thickness needed for the gain material. For optical amplification to occur, a population inversion in the gain material must be created by a pump source. After the medium is inverted, stimulated emission is produced when a seed signal is introduced to the material.

MOPA systems can be made by coupling a solid state oscillator into a bulk material. In this case, to obtain a better efficiency of the amplification, it is preferable to have the peak emission cross section of these materials in the same range. Therefore the materials used have to have similar energy level transitions. As Yb:KYW is a material already chosen for the master oscillator then Yb:YAG becomes a good option for the

amplifier. On an energy level system the ions in the lower level will move from the lower energy level to the higher level when absorption of the pump happens, and emission will be produced when the ions drop to a lower level (Figure 3.1).

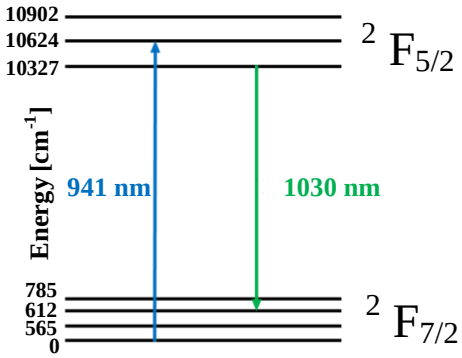

Figure 3.1 Energy level transitions of Yb:YAG.

In diode pumped amplifiers, a population inversion is achieved leading to higher gain coefficients. Usually the gain in an amplifier is determined by the intensity of the pump diodes and the intensity of the laser beam [15], which increase with the distance. When this intensity approaches the saturation intensity, the population inversion and thus the gain coefficient ($\alpha_0 = \Delta N \sigma$) becomes to saturate as well, then the increase of the intensity with the distance becomes more slowly as shown in Figure 3.2 [16].

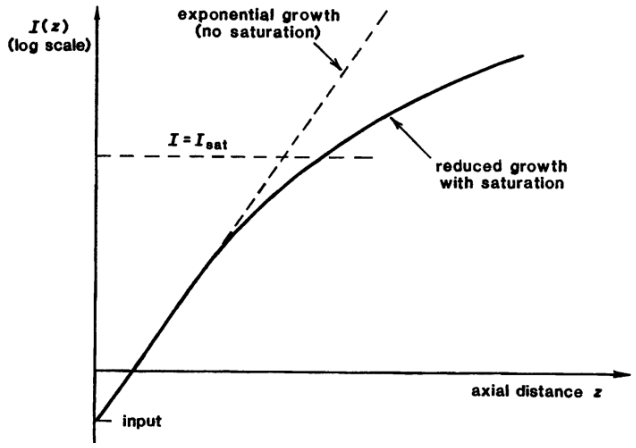

Figure 3.2 Intensity variation with propagation distance of the gain material [16].

If the saturation is homogeneous in the material and supposing that there are no linear losses, then the intensity will vary as:

$$\frac{1}{I(z)}\frac{dI(z)}{dz}=\frac{\alpha_0}{1+I(z)/I_s} \tag{3.1}$$

where I_{sat} corresponds to the saturation intensity of the medium. Then if the small signal gain is defined as $g_0 = e^{\alpha_0 L}$, with L the length of the amplifier.

Then the power gain in the medium can be defined as:

$$G=\frac{I_{out}}{I_{in}}=g_0\exp\left[-\frac{I_{out}-I_{in}}{I_{sat}}\right] \tag{3.2}$$

Then using equation 3.2 is possible to know the maximum extractable power that can be obtained from [16]:

$$I_{extr}=I_{out}-I_{in}=In\frac{g_0}{G}I_{sat} \tag{3.3}$$

Here the saturation intensity is the one that reduces the small signal gain to half of its value, and can be written as [16]:

$$I_{sat}=\frac{\hbar\omega}{\sigma\tau_{eff}} \tag{3.4}$$

where τ_{eff} is the recovery time. Then the intensity will saturate more easily for greater values of the transition cross section and the recovery time [16].

Therefore, for amplifiers, the maximum available power that can be obtained from the medium is given by:

$$P_{avail}=A\lim_{G\to 1}I_{extr}=A(In(g_0))I_{sat}=\frac{\Delta N\hbar\omega V}{\tau_{eff}} \tag{3.5}$$

where A and V are the total effective area and volume of through the amplifier respectively. Equation (3.5) tells us that the maximum power obtained from the

amplifier is determined mainly by the initial inversion energy in the medium and the recovery rate.

One way to increase the saturation intensity is for the population inversion energy to be increased or the recovery time lowered, which means that the pump intensity must be higher. While increasing the pump intensity will raise the single-pass gain in the material, it can lead to unwanted laser oscillation due to parasitic reflectivity of the facets of the material [15]. For this reason multipass amplification of the beam is generally needed [14]. In multipass amplification the input beam is sent many times through the gain media generating more gain on each pass.

3.2.2 Review of previous work

As mentioned before, many studies already exist on CW power amplification. Recently MOPA configurations have been applied increasingly for this purpose [5-14, 17-22]. As mentioned in the previous chapter, ytterbium-doped solid state lasers have become very common for master oscillators due to their ease of pumping commercially available diode lasers. This quality comes from the absorption cross section of such Yb-materials, which allow pumping in the near infra red (IR) region due to their broad absorption cross section from 915-976 nm. Power amplifiers in the near IR (1029 to 1065 nm), use Yb-doped master oscillators because they can be easily coupled with amplifiers using Yb-doped materials as gain media. As mentioned previously, different forms of Yb-doped material have been used for amplification. For fibre lasers, 20 W [9] and 26 W [19] amplified power have been reported, with repetition rates of 75 MHz and 100 kHz and pulse durations of 80 fs and 5 ns respectively. A semiconductor tapered Yb:YAG amplifier has given 50 W output power at 20 MHz [21]. Higher extractable powers have been obtained using slab based amplifiers reaching 1.1 kW amplification power at 20 MHz for pulses of ~600 fs [17, 18]. At the same time, planar waveguide amplifiers have been used successfully for high power amplification [20, 23]. Up to 16 kW have been demonstrated for these kind of amplifiers in CW operation and 4.5 kW in pulsed operation [23].

3.3 Planar Waveguide Characteristics

Planar waveguides are now widely used for solid state oscillators and amplifiers [1,12, 13, 23-27]. This is due to a variety of characteristics which represent a unique advantage for these systems. The fabrication of planar waveguides can be made through the modification of the index of refraction inside the material, or the bonding of plates with different indices of refraction (Figure 3.3). The last method is the most commonly used for high power applications. Usually the middle plate is a rare-earth doped material that has an index of refraction bigger than the plates at the edges or claddings ($n_2 > n_1, n_3$).

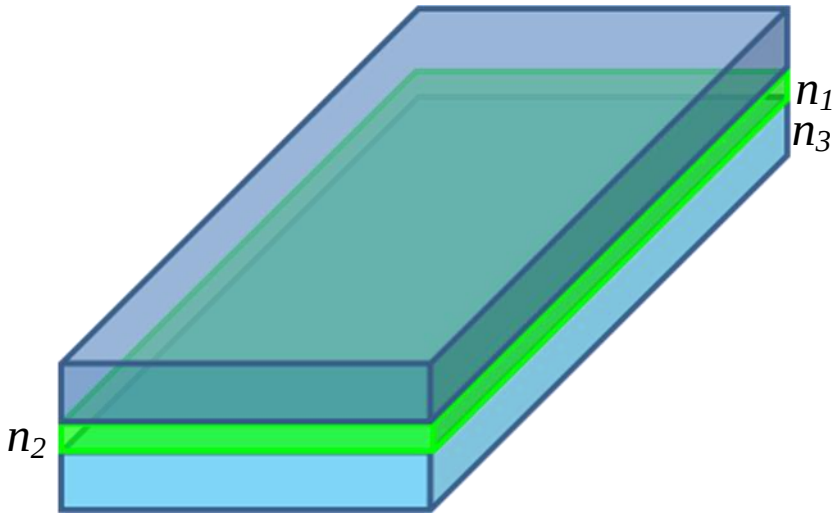

Figure 3.3 Planar waveguide structure, where $n_3 > n_2 > n_1$.

Bonding of materials with very different refractive index makes it possible to fabricate gain materials with high numerical apertures [26]. This makes this type of waveguide suitable for pumping with bar diodes, which are easily found at the required wavelengths for Yb^{3+} doped materials. An advantage of planar waveguides is that they can be pumped through three different directions (end pumping, face pumping and side pumping). This is very important, especially in amplifiers which require two beams to be coupled to the waveguide, the pump and the seed beams.

Because of the geometry of the waveguides, it is possible to pump them using diode bars or diode stacks which have the same (linear) shape. Using face pumping allows pumping with multiple diodes, nevertheless for good absorption, it requires multiple passes which adds more elements to the system and makes it more complicated. On the other hand, side pumping can be done through one or two opposite sides of the

waveguide. With this type of pumping, the direction perpendicular to the pump can be used to introduce the seed beam, and the faces of the waveguide can be used to control its temperature, giving the system greater flexibility [24, 26, 27].

When Yb^{3+} doped gain materials are subjected to high pump powers, the temperature increase inside the medium generates some undesired effects. Usually the rise in temperature causes the material to be under stress, which induces variations in the index of refraction inside the material. These changes can cause degradation in beam quality, losses in the system, depolarization and even fracture of the material [29-30]. For these reasons, due to its slab structure a planar waveguide offers a good beam quality. With that geometry, water cooling over the large faces of waveguides makes them capable of efficient heat removal, reducing to a large degree thermally induced problems at high powers [1, 11, 13, 26, 27].

3.3.1 Yb:YAG Optical Properties

Ytterbium-doped yttrium aluminium garnet or Yb:YAG ($Y_3Al_5O_{12}$), has been widely used for diode-pumped solid state lasers because its properties. YAG is an isotropic crystal with a cubic system of the space group I*a3d*, it is also centrosymetric with a symmetry m3m [30, 31]. Figure 3.4 shows the cubic cell for YAG which can be seen as an arrangement of octahedrons, tetrahedrons and dodecahedrons [30].

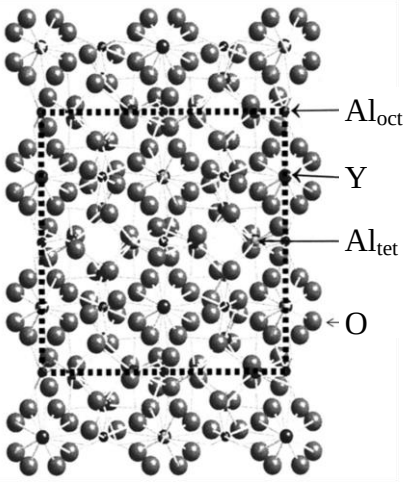

Figure 3.4 Crystal structure of YAG [30].

This crystal has a high optical transmission from 0.21 to 5.2 μm for a crystal sample of 1 mm thickness at 300 K. Its refractive index can be calculated for a particular wavelength by using [31]:

$$n^2 = 1 + \frac{2.293\lambda^2}{\lambda^2 - (0.1095)^2} + \frac{3.705\lambda^2}{\lambda^2 - (17.825)^2} \tag{3.6}$$

In the case of λ = 1032 nm, the refractive index can be found to be n = 1.818.

Because of its electronic structure (Figure 3.1), Yb^{3+} doped YAG has many advantages. It has a long upper-state lifetime (1.01 ms [32]) and a low quantum defect of 8.6% [33], which leads to a reduction in the thermal effects [34]. It also has low thermal expansion (7.7×10^{6} K) and high thermal conductivity (13.4 W/mK at 300 K) [31]. Other advantages including a high threshold for optical damage, with a fracture toughness up to 1.4 MPa $m^{1/2}$ at 300 K [31], and high stability against any chemical and mechanical variation, make these materials very appropriate for high power laser applications [30, 34]. The absence of concentration quenching allows for high doping concentrations, nevertheless a high doping concentration > 30 at.% causes unwanted effects such as wavelength shifts [34].

Yb:YAG, contrary to Yb:KYW, being a cubic isotropic crystal, only requires a single unpolarized beam to characterize completely its spectral properties. Figure 3.5 shows the absorption and emission cross section for this material. The peak absorption cross section for Yb:YAG is $\sigma_{abs} = 0.74\times10^{-20}\,\mathrm{cm}^2$ at 968 nm [35], and the peak emission cross section $\sigma_{em} = 2.03\times10^{-20}\,\mathrm{cm}^2$ at 1031 nm [32], which is the same peak emission wavelength as for Yb:KYW. This is important for this project because that allow us to couple an oscillator based on Yb:KYW into an amplifier constructed using Yb:YAG.

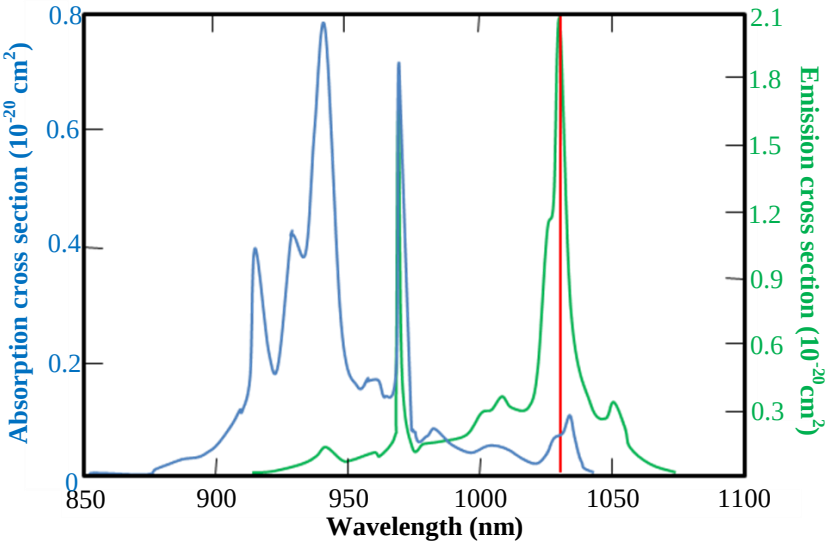

Figure 3.5 Absorption and emission cross sections of Yb:YAG [33].

3.4 Oscillator Properties and Settings

The master oscillator used for the MOPA was the one described in Chapter 2. This oscillator was built with Yb:KYW as a gain material. The output of this laser had an average output power of 4.5 W at 53 MHz repetition rate. The pulses from the output had a pulse duration of 484 fs at 1032 nm, with a beam parameter of $M^2 = 1.2$.

3.5 Amplifier design

The amplifier was built using a planar Yb:YAG waveguide as a gain material, pumped through one side by a diode stack. A short description of the amplifier configuration is given in this section. Detailed specification of this system used as a resonator can be found in Dr. Ian Thomson's thesis [1]. Amplification was made by multiple bounces of the seed laser through the core of the waveguide in a direction perpendicular to the pump beam.

3.5.1 Planar waveguide geometry

The planar waveguide used as the gain material for the amplifier was fabricated by Onyx Optics Inc. It had a 2 at.% doping concentration of Yb:YAG as a core material. Its dimensions were 12 mm wide by 13 mm long surface and 150 μm thicknesses (Figure 3.6). It had sapphire claddings of 1 mm thickness, making a total of 2.15 mm thickness for the waveguide. The index of refraction of Yb:YAG is $n = 1.82$ as specified in

Section 3.3.1, and for the Sapphire n = 1.77. Two opposite surfaces of the waveguide used for the pump were AR coated at 940 nm and had asymmetric unequal facets to stop parasitic oscillations in the amplifier. The other two were kept plane and AR coated for 1030 nm, perpendicular to the seed beam. One of the facets used for the pump had a 20-degree angle, to reduce the possibilities of having parasitic oscillations along the pump direction.

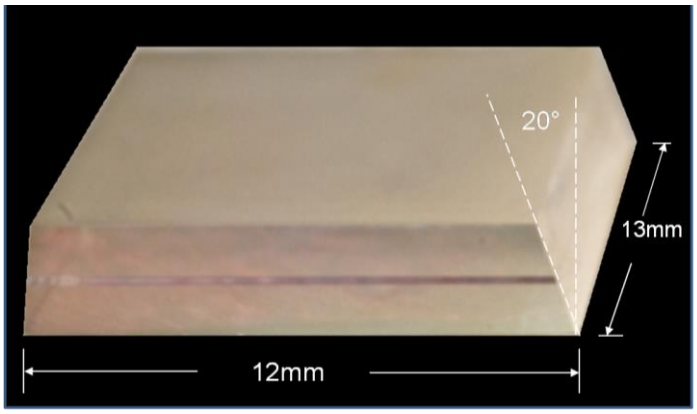

Figure 3.6 Yb:YAG Planar waveguide geometry.

The planar waveguide was mounted between two metal structures on the top and bottom faces to use them as a cooling system on the large surfaces of the waveguide (Figure 3.7). These structures were pressed on the top and bottom faces to secure the waveguide. Indium foil was used between the waveguide and the metallic structures for good thermal contact. Each of the structures had a water flow system which consisted of micro-channels that worked as a cooling device. As part of that system, water was flowed through copper fins of 200 μm by 1.5 mm inside the surface next to the waveguide. The water flow was made lateral and in opposite directions for the top and for the bottom faces.

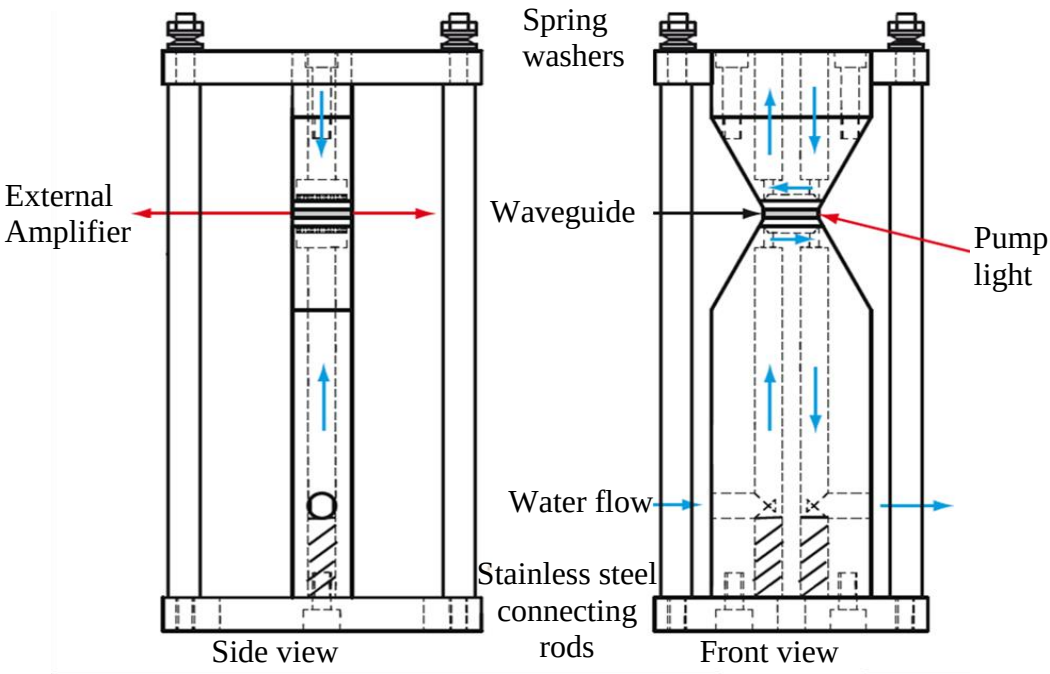

Figure 3.7 Complete heat sink structure of the waveguide mount [1].

The waveguide was set at 100 mm optical height. At one side of the waveguide mount was placed the diode stack that was the pump for the amplifier (Figure 3.8). This stack was made of six diode bars pumping at 940 nm. The width of the bars was ~13 mm which matched the dimensions of the waveguide. The output power of the stack was 480 W. To pump the waveguide the beams from the stack were focused using a 38 mm cylindrical lens. A custom phase plate was necessary between the diode stack and the waveguide to correct for collimation aberrations. A pair of golden coated side reflectors was used to homogenize the lateral beam profile. With this setting it was possible to focus the pump light to a thickness ~150 μm by 13 mm long. At a current drive of the stack of 100 A it was possible to obtain an intensity of 22.2 kW cm^{-2}. This diode stack was also water cooled by a chiller, and its temperature was maintained at 27±3°C which was the temperature necessary for the diodes to reach the absorption peak at 941 nm. The required pump wavelength of 941 nm was obtained only when the stack was pumped at full power (I = 100 A). This is the same effect observed in the Yb:KYW oscillator pump.

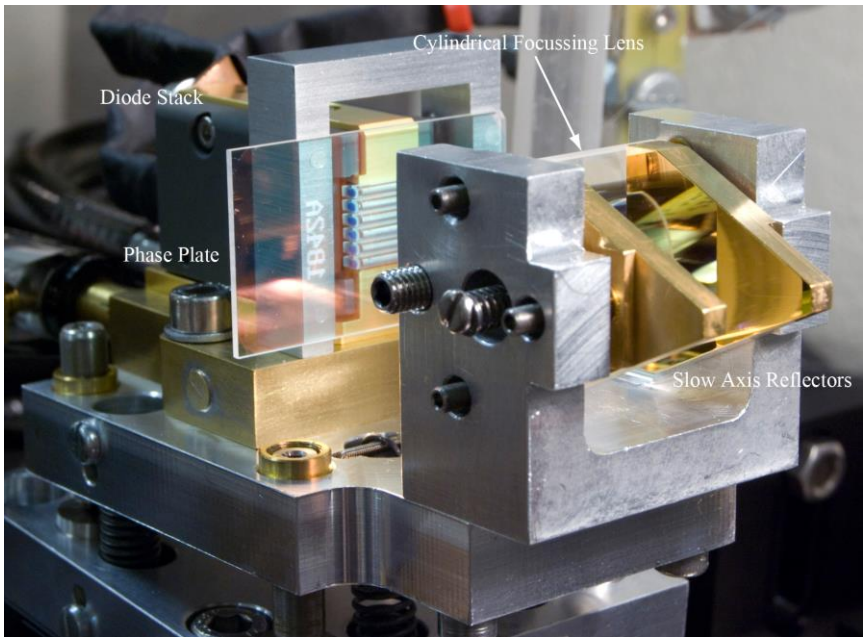

Figure 3.8 Diode stack mount [1].

After the cylindrical lens the maximum output power obtained was 442 W at 100 A, which is the maximum current at which the diode could be driven. Figure 3.9 shows the output power from the stack for different driver currents.

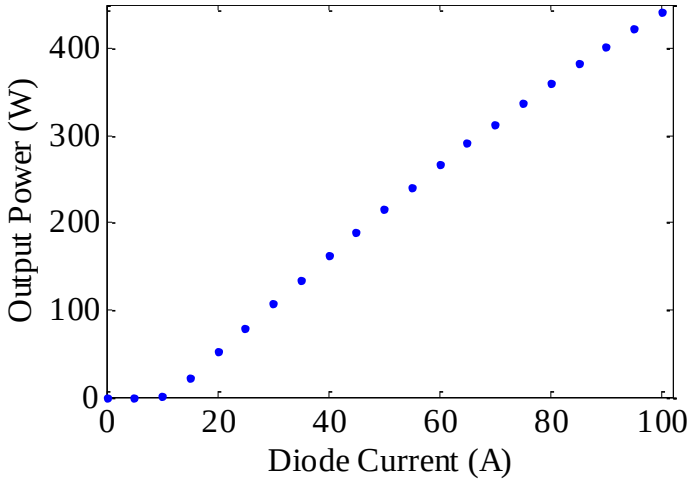

Figure 3.9 Output power of the diode stack.

Once the diode stack was properly mounted at the correct vertical and horizontal position to pump the waveguide, the pump beam was introduced through the side of the waveguide that had a surface angle at 20 degrees. The beam was directed to the planar waveguide parallel to the optical bench in the vertical direction (Figure 3.10). This allowed the light to be guided inside the waveguide parallel to the core.

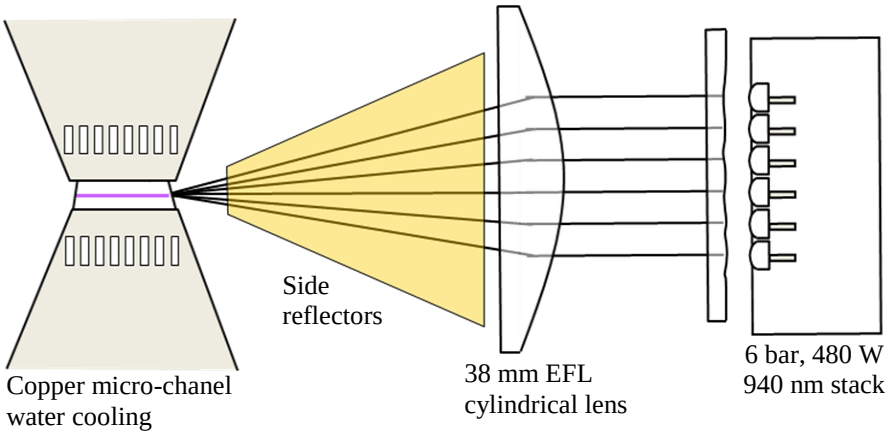

Figure 3.10 Optimal waveguide pumping scheme.

3.6 Measurement of gain coefficient across the waveguide

Once the amplifier pump set up was ready, the Yb:KYW oscillator was coupled to the amplifier. To do this, the beam size of the oscillator going into the amplifier in the unguided direction was reduced from 3 mm to ~2 mm through a telescope system consisting of two cylindrical lenses of 200 mm and 150 mm radius of curvature. This was done to mode-match the beam inside the waveguide after the telescope system. A free-space polarization-dependant isolator (Thorlabs model IO-5-1030-HP) was used to avoid feedback from the amplifier (Figure 3.11), which could cause the wavelength of the oscillator to change or even to shift from modelocked to CW operation. Because of the elements inside the isolator the coupled power from the oscillator was reduced to 3.5 W.

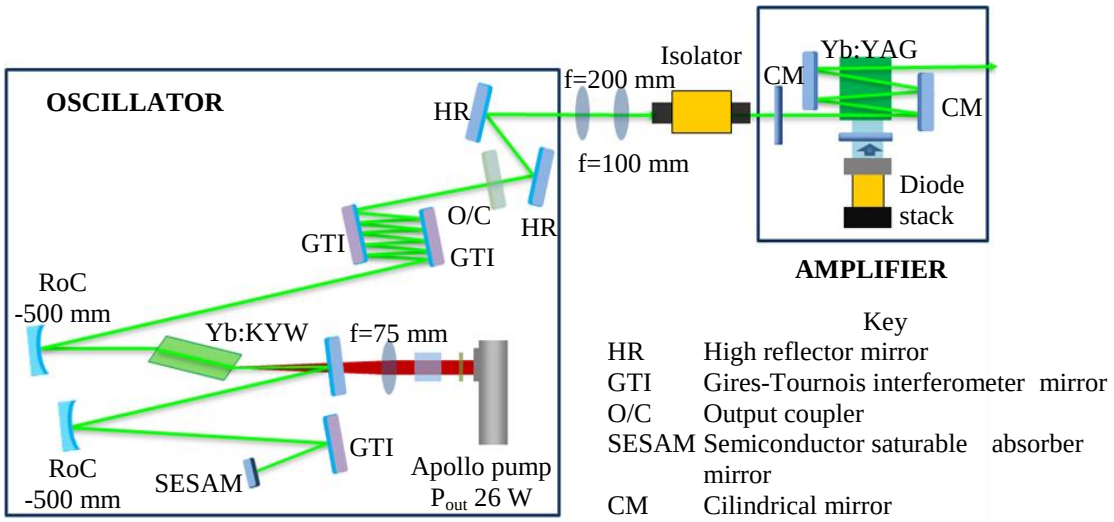

Figure 3.11 Coupling scheme between the oscillator and the amplifier.

After the isolator, the beam was focused into the waveguide using a 150 mm focal length cylindrical lens in the waveguide direction as shown in Figure 3.12. Then, the beam size at the entrance of the waveguide was 130 μm in the waveguide direction, and 1.8 mm in the unguided direction. To achieve multiple passes through the waveguide, two cylindrical mirrors were used, each coated for 95% reflectivity at 1030 nm. The reflectivity of the mirrors was chosen to avoid damage of the mirrors at high powers, this is due to the high probability of the system to start to work as a resonator at higher energies between the passes through the waveguide.

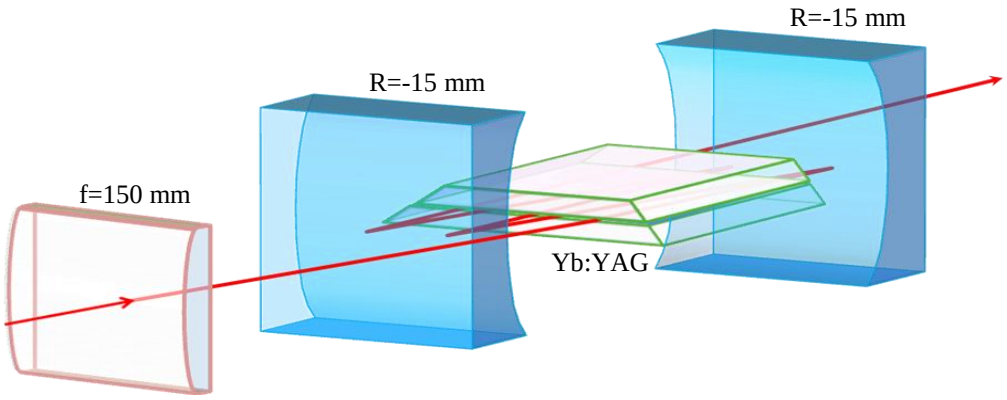

Figure 3.12 Folding system used in the amplifier.

As mentioned before, planar waveguide amplifiers have low losses. In this case the mirrors can be chosen accordingly with the characteristics of the waveguide, and the wavelength required [36]. In the unguided direction, the folding system is made with plane mirrors, maintaining a nearly constant beam size during the passes through the amplifier. For the guided direction, the folding mirrors required are chosen with the parameters in Figure 3.13 for the optimum radius of curvature. If a is half the waveguide core thickness, d is the distance from the waveguide to the centre of the mirror, and c is the radius of curvature of the folding mirror then c can be found with defining the parameters $\alpha = ka^2/c = 4Z_R/c$, $\beta = d/c$ [36] and $k = 2\pi/\lambda$, where $Z_R = \pi a^2/2\lambda$ is the Raleigh range.

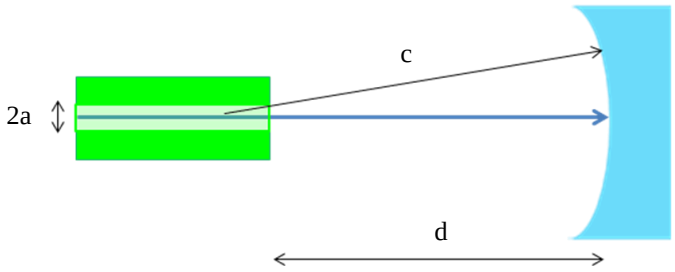

Figure 3.13 Side view of the folding system [36].

For systems with low loss there are three cases for an optimum configuration [36]: Case I is for a large radius of curvature, and the mirror close to the waveguide ($d << c$). Case II for large radius of curvature mirrors set at almost the distance of the centre of the curvature ($d \cong c$). And Case III for the mirror placed at half the radius of curvature ($d = c/2$), in which $\alpha = 2.415$ [36]. For this amplifier the best option was Case III which couples the fundamental mode into the waveguide again, suppressing higher-order modes and keeping a good beam quality at the output [1]. For the waveguide already described, $a = 75$ µm, then for a wavelength of 1030 nm the Rayleigh range is $Z_R = 8.6$ mm and thus, the required curvature is $c \cong 17$ mm and the distance from the mirror to the waveguide $d = 8.6$ mm. The mirror curvature which was available to be used was -15.5 mm.

3.7 Single Sided Amplification

The beam of the master oscillator was aligned into the amplifier using first the beam of a HeNe laser coming through the path of the incident beam. A pair of pinholes was placed before and after the waveguide for single pass alignment. After the first pass through the waveguide a CCD camera was placed to image the 1030 nm beam on a rotating aluminium disk, with a set of ND filters used on the lens of the camera to avoid saturation. The image of the beam is shown in Figure 3.14. In this way the beam was passed through the pinholes and then reflected on the disk to complete the alignment.

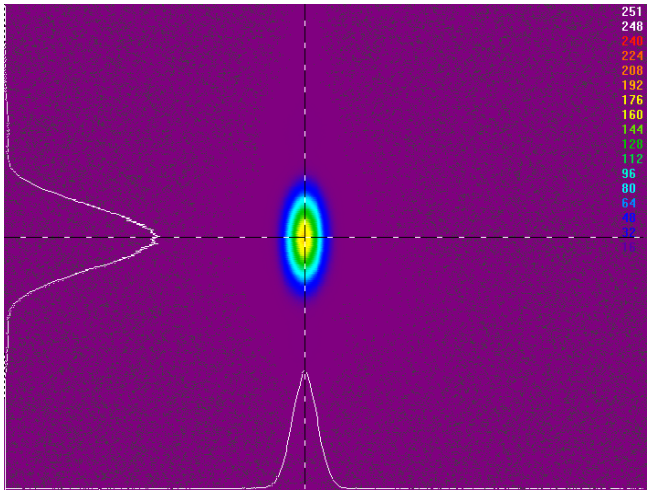

Figure 3.14 Beam profile of a single pass through the planar waveguide.

When the beam was properly aligned, the gain was calculated for different positions of the input seed beam through the front side of the waveguide at different currents from the output power measured, using the input beam from the oscillator as a probe beam. This calculation was done using the expression for the small signal gain (Equation 3.2) [16].

The measurement was done taking the output power of the probe beam when it was aligned to enter the waveguide from the side opposite to where the waveguide was pumped for the diode, and then moving towards it. Figure 3.15 shows the results of the gain of a 1 mm diameter beam, in the horizontal direction, at the maximum current of the diode (100 A). This shows that saturation occurs at the edge where the waveguide is being pumped. Maximum gain achieved is around 1 cm^{-1}. Then the position used for the input of the oscillator beam for the amplifier is at 0.5 mm from the edge that the pump stack is placed.

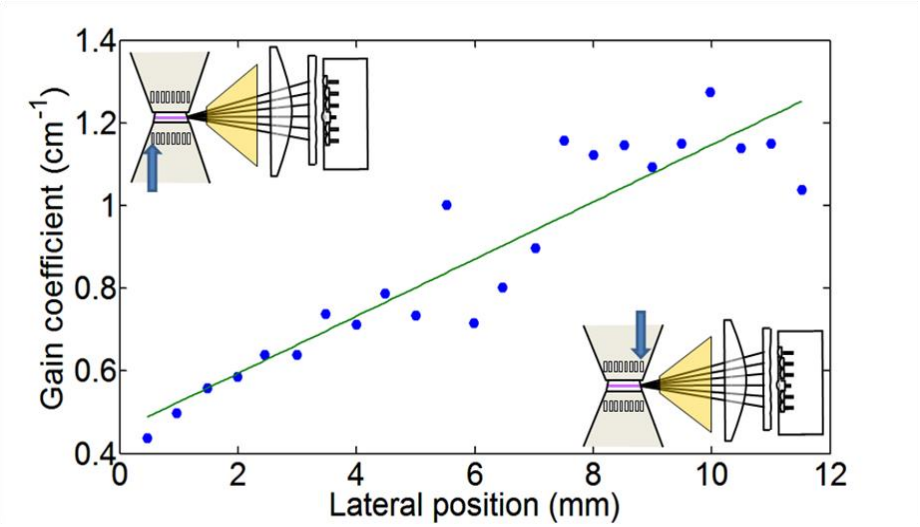

Figure 3.15 Gain coefficient at different input beam positions of the seed with respect to the surface of the waveguide, with the stack at the right side.

3.7.1 Configuration of a single pass Yb:YAG amplifier

A characterization of the amplifier was carried out for one to five passes through the gain material. For a single pass no mirrors were used; the seed beam simply passed through the waveguide once and was then directed to a detector. The power was measured for different pump currents from 0 A up to 100 A. The seed beam was injected at 0.5 mm from the edge of the waveguide, as mentioned in the previous section (Figure 3.16). Because the waveguide was only pumped on one side it was necessary to put a beam stop on the other side of the waveguide which was also water cooled due to the high power incident on it.

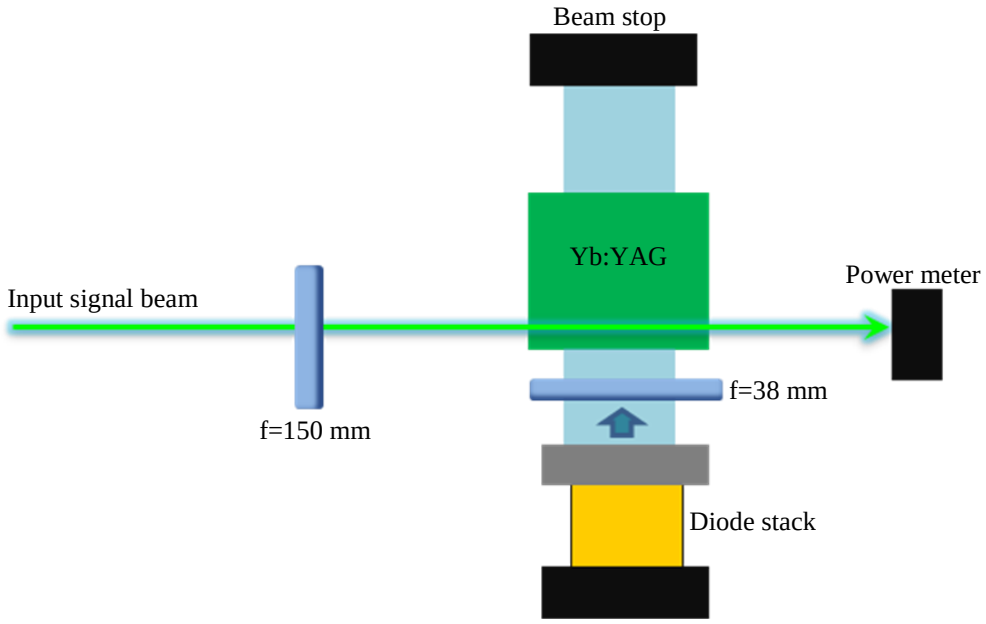

Figure 3.16 Single pass configuration of the amplifier.

Figure 3.17 shows the output powers obtained when the oscillator was operated in the CW and modelocking regimes. The maximum average output power was 12 W in the case of CW operation and 11 W when it was modelocked. To shift between modelocking and CW operation, the intracavity power of the oscillator was reduced to stop modelocking to happen, then the seed power in the CW operation was 3.3 W and 3.5 W when the oscillator was modelocked.

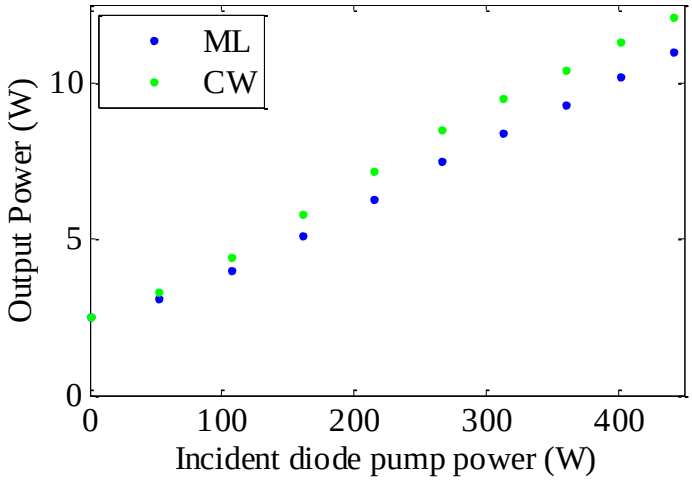

Figure 3.17 Output power as a function of the diode stack pump power for CW and modelocking operation of the oscillator.

An intensity autocorrelation was made to measure the pulse duration for each current from 0 to 100 A on 10 A steps. Figure 3.18 shows the variation of the pulse duration as

the current was increased. From this figure, pulse broadening can be observed as the pump power is increased. The pulse duration at the maximum current was 571 fs.

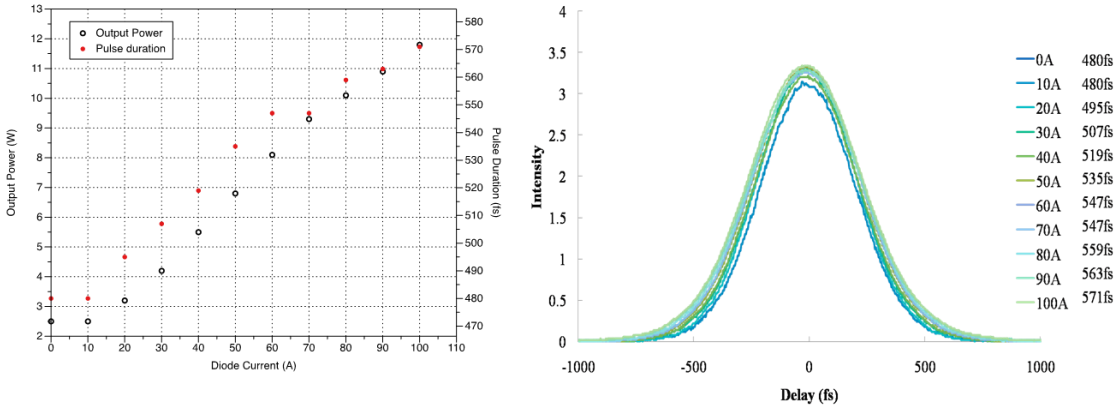

Figure 3.18 Single pass measurements of (a) output power and pulse duration, and (b) pulse shape showing broadening for various diode pump currents.

3.7.2 Configuration of a two pass Yb:YAG amplifier

For the second pass through the amplifier, the first cylindrical mirror with -15.5 mm radius of curvature was placed after the waveguide as shown in Figure 3.19. The distance between the mirror and the waveguide was 8 mm. The mirror was set on a xyz-translation stage to align the beam into the waveguide for a second pass. After the beam passed through the waveguide, it reached the cylindrical mirror, and then was reflected into the waveguide again and directed onto the power meter. To measure the power after the second pass a HR-coated mirror for infra-red was placed next to the entrance beam to reflect the beam to the power meter. This was done because the output beam was too close to the input beam and the space was too narrow to fit the power meter.

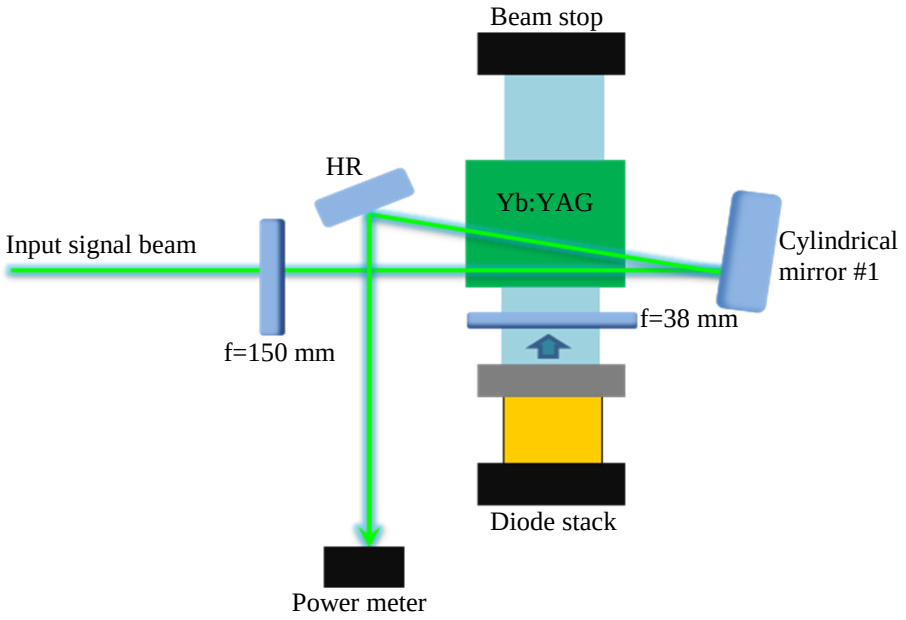

Figure 3.19 Double pass configuration of the amplifier.

Figure 3.20 shows the output power of the amplified beam after two passes through the waveguide.

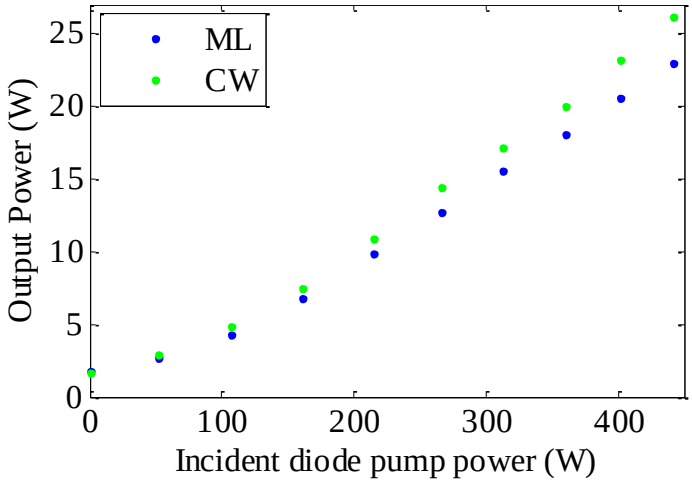

Figure 3.20 Output power after two passes though the amplifier.

The maximum output power obtained for two passes was 26 W when the oscillator was operated in a CW regime and 23 W when it was modelocked. For two passes broadening of the pulse duration was also observed. The pulse duration at the maximum current was 596 fs. Figure 3.21 shows the pulse broadening for two passes.

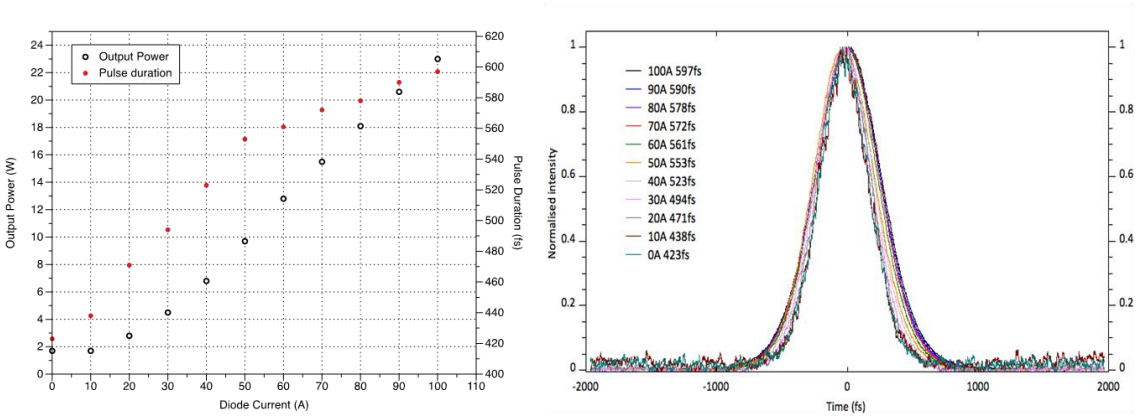

Figure 3.21 Double pass measurement for (a) output power and pulse duration, and (b) pulse broadening

3.7.3 Configuration of a three pass Yb:YAG amplifier

For the three-pass arrangement the second cylindrical mirror was placed next to the entrance beam, just close enough not to block the input beam. The distance from the waveguide to the mirror was also 8 mm. This mirror was also mounted on a xyz-translation stage to align the beam again into the waveguide for the third pass. The beam was folded for the third pass in such way to allow the output beam to pass close enough to the first mirror and not to clip on it as shown in Figure 3.22.

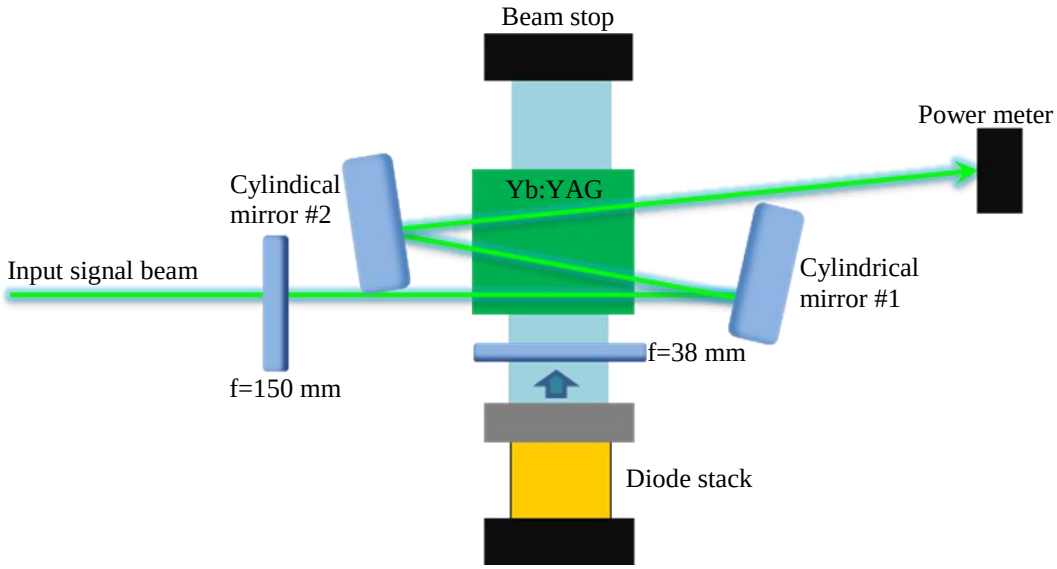

Figure 3.22 Configuration of three passes on the amplifier.

For this case the maximum output power was 34 W for CW operation of the oscillator and 35.1 W for modelocking. Figure 3.23 shows how the power for each current applied in both cases is similar.

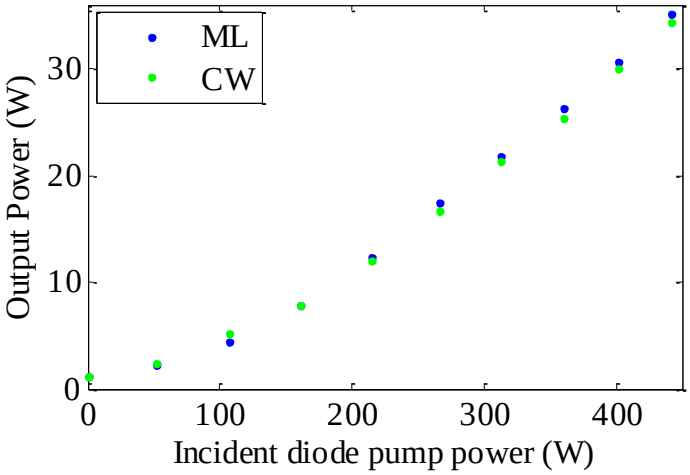

Figure 3.23 Output power for three pass amplification.

In this case the broadening of the pulses for the maximum current resulted in a pulse duration of 655 fs. Figure 3.24 shows the pulse duration for each current, as well as the intensity autocorrelation for three different currents.

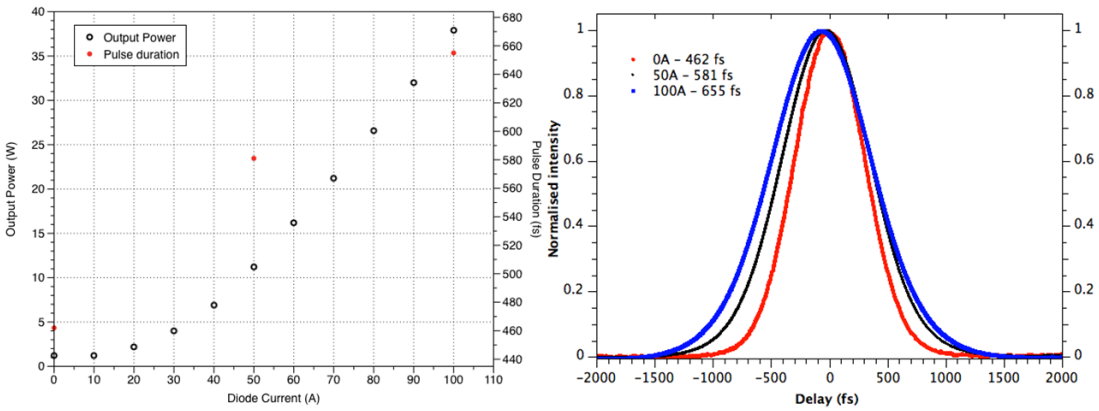

Figure 3.24 Triple pass measurements for (a) output power and pulse duration, and (b) pulse broadening

3.7.4 Configuration of a five pass Yb:YAG amplifier

Because of the length of the second cylindrical mirror, a four pass configuration could not be tested. For such cases it is necessary to use a thinner mirror which allows the beam to pass through its side without the mirror blocking the input beam to the amplifier. The final MOPA configuration used is shown in Figure 3.25. For five-pass amplification the cylindrical mirrors were tilted to get the output beam of the fifth pass next to the first mirror.

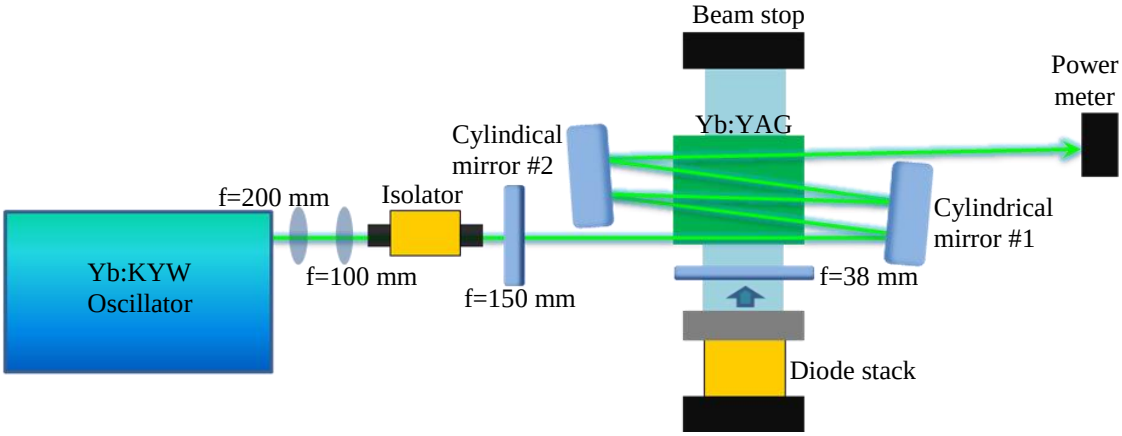

Figure 3.25 MOPA configuration.

For the final configuration average output powers of 40 W were reached for CW operation of the oscillator. In the case of modelocked operation, 50 W output power was obtained for the maximum current on the diodes, which corresponded to a pulse energy of ~1 μJ. This higher output is due to the repetition rate of the oscillator that generates a higher input power to the amplifier. Figure 3.26 shows the variation of the output power in both cases.

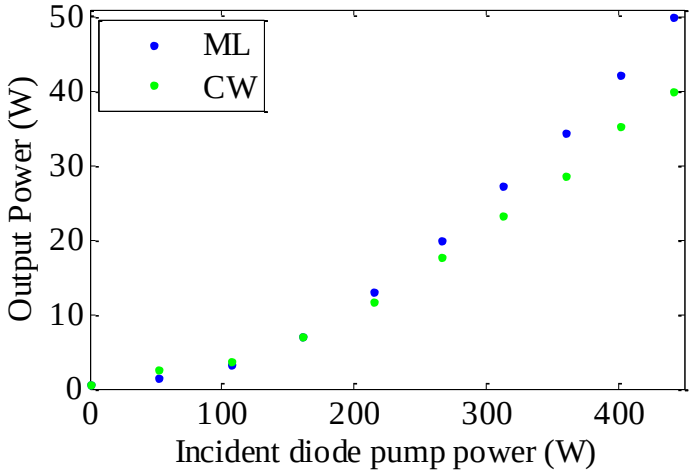

Figure 3.26 Output power for five pass amplification.

The continuous increase in output power shows that the device is not yet saturated. Figure 3.27 shows the variation of the spectrum and the pulse duration as the pump power was increased from 0 to 442 W. Pulses of 703 fs were obtained at the highest power with a spectral bandwidth of 2 nm at 1030 nm. As the beam is amplified, the spectrum of the output beam narrows and, this gain narrowing leads to pulse broadening. Figure 3.28 shows the pulse variation with the gain coefficient. This variation is linear as the gain coefficient increases.

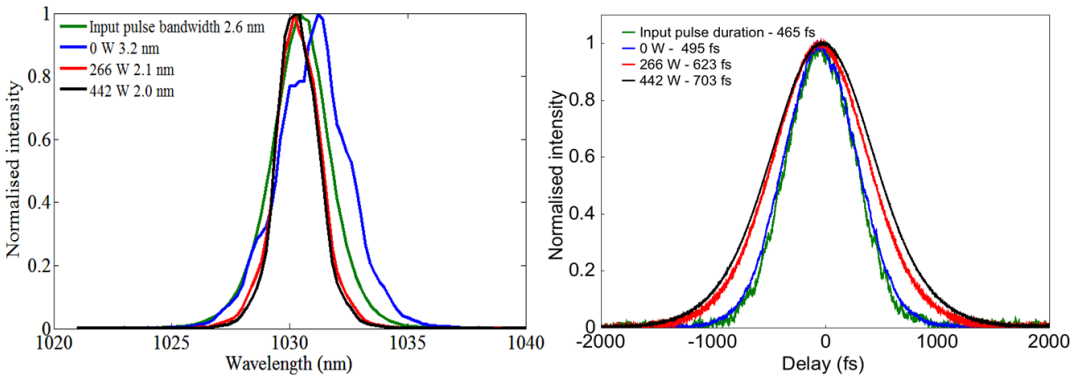

Figure 3.27 Five pass measurement for (a) output spectrum, and (b) pulse duration

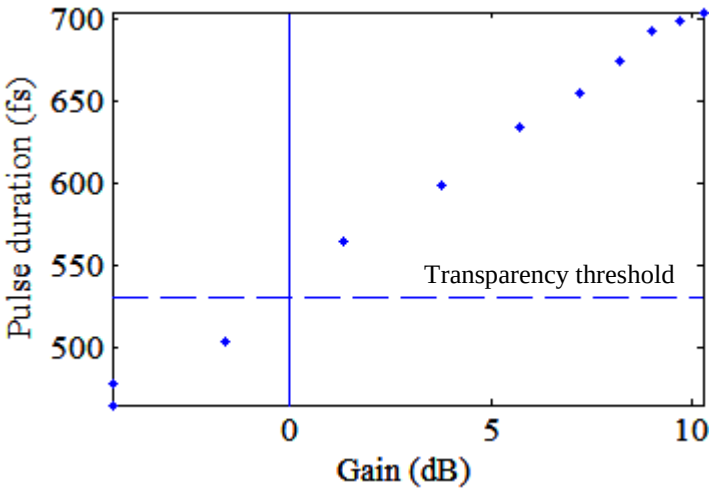

Figure 3.28 Variation of the pulse duration with the amplification gain for five passes.

Further increasing of the number of passes through the amplifier was not possible because of the geometry of the configuration which used cylindrical mirrors, and the length of the waveguide. With this geometry more passes of the amplifier required the mirrors to be almost parallel to each other, making the parasitic oscillations increase, changing the operation of the configuration from an amplifier to a resonating cavity.

Table 3.1 shows the results obtained for the configurations mentioned before. The output powers were obtained for CW operation of the oscillator and when it was modelocked. The best average output power of 50 W was obtained for five passes through the Yb:YAG planar waveguide, with a 2 nm bandwidth at 1030 nm. Pulse energy of 1 μJ was found for the maximum pump power. These results were obtained at the maximum pump power of 442 W from the diode stack.

Table 3.1 Data obtained for different passes through the amplifier.

	CW Output Power (W)	ML Output Power (W)	Δτ (fs)	Bandwidth (nm)	Pulse energy(μJ)
Oscillator	3.5	3.5	465	2.6	0.066
1 Pass	12	11	571	2.4	0.2
2 Passes	26	23	596	Not measured	0.43
3 Passes	34	35.1	660	2	0.66
5 Passes	**40**	**50**	**703**	**2**	**0.94**

Figure 3.29 shows how the spectrum narrowed as the number of passes of the planar waveguide was increased. This meant that the pulse duration broadened correspondingly as the spectrum narrowed.

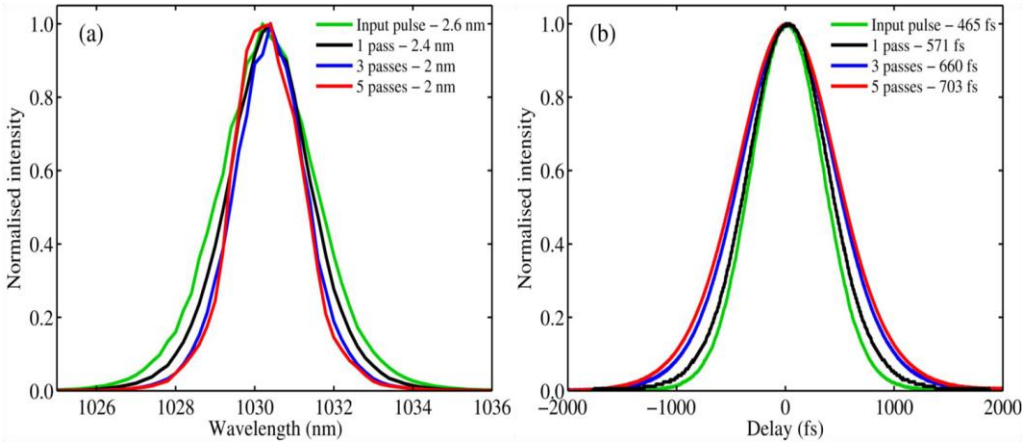

Figure 3.29 (a) Spectral narrowing and (b) pulse broadening for multiple pass amplification.

3.8 Analytical Amplification Model

As described in Section 3.2.1, during the amplification process, some of characteristics of the amplifier can modify the input pulse shape when it is amplified. That is why in this section the effects of all the changes involved in the amplification process are analysed. The pulse shape is modified with every pass through the amplifier, because of group delay dispersion, gain narrowing, gain saturation and self-phase modulation. By using the field of the input beam, it was possible to investigate the variation of each of these characteristics as the pulse propagated in the material. The gain saturation in the amplifier was analysed by using a model that includes this effects. The model was developed in the research group [37].

Using the data of Figure 3.15 for the gain of the pump on each amplifier pass, the characteristics of the pulse were modelled to fit the data of the experimental results from Table 3.1. Figure 3.30 shows the variation of the energy, bandwidth and pulse duration from 0 to 5 passes through the amplifier.

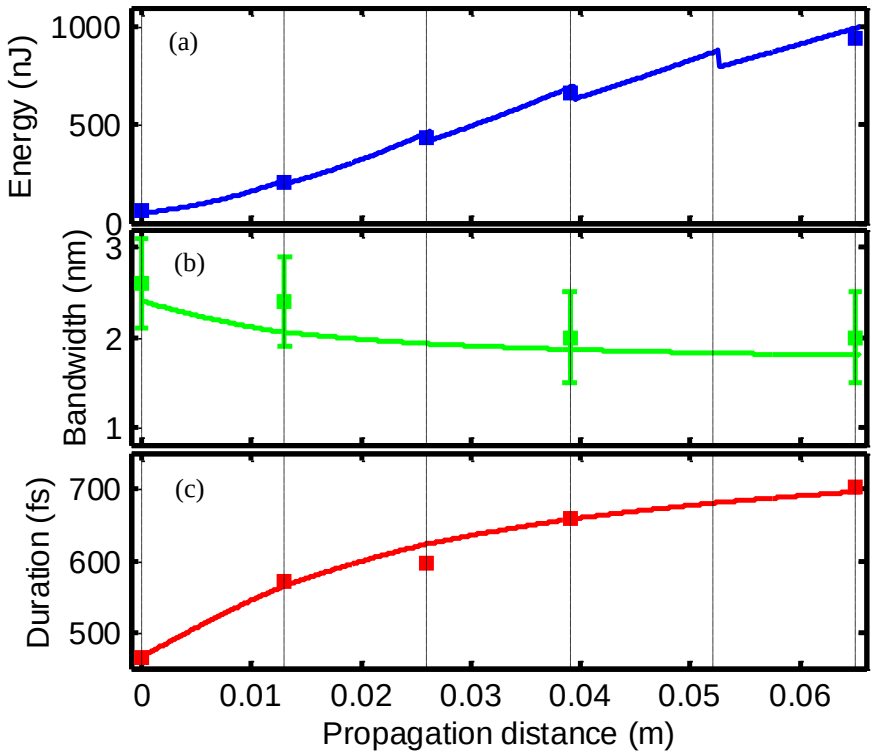

Figure 3.30 Numerical modelling results (solid lines) fitted to experimentally measured pulse parameters (symbols) by adjusting E_{sat}, G_o and λ_g. Showing the variation of (a) pulse energy, (b) bandwidth and (c) pulse duration.

The propagation between neighbouring dashed vertical lines represents one pass through the 13-mm-long Yb:YAG crystal. The error bars in Figure 3.30(b) represent the ± 0.5 nm resolution of the spectrometer used to record the pulse spectra. To calculate the energy it was considered the losses of the 95 % reflectivity mirrors used, which gives a 5% loss per bounce. A 5% coupling loss was also introduced in the calculations. In this calculation the saturation intensity, the small signal gain and the bandwidth were varied to get the best possible fit with the experimental data. The values obtained for this fit were 10 kW cm^{-1} for the saturation intensity, 1.6 cm^{-1} for the small signal gain and 3.7 nm bandwidth. These values agree with the ones previously reported of 9.5 kW cm^{-1} for the saturation intensity [33], 1.5-2 cm^{-1} for the small signal gain [12] and ≤5 nm bandwidth [38] for Yb:YAG.

To investigate the pulse shape effect after each pass of the amplifier, the group delay dispersion, gain narrowing, gain saturation and self phase modulation were modified in the model one by one to see which one generated the largest effect. Self phase modulation and group delay dispersion were found to cause only very small changes after the fifth pass on the amplifier. On the other hand gain narrowing and gain saturation were found to cause the biggest changes to the quality of the fit of the model. Using the model it was also possible to simulate the possible results for different changes to the configuration of the amplifier. For example in case of using 100% HR-mirrors instead of 95%, and using a double-sided pump scheme the model predicted 90 W of average output power, with pulses of 735 fs.

3.9 Conclusions

This chapter has presented the development of an Yb:YAG planar waveguide amplifier for ultrafast pulse amplification by combining it for the first time with a high-average-power Yb:KYW femtosecond oscillator in a MOPA configuration. The oscillator was the one described in Chapter 2. The amplifier consisted of a 12×13 mm Yb:YAG planar waveguide with a 2 at.% doping concentration, which had two planar faces and two faces angled at 20° and 7°. This amplifier was pumped by a 6-bar diode stack which generated 442 W at 940 nm. The pump was focused into the waveguide using a 30 mm lens and a phase plate to avoid aberrations. The input signal of the Yb:KYW oscillator was coupled into the amplifier using a 150 mm focal lens, and it was folded five times inside the configuration by two cylindrical mirrors with -15.5 mm radius of curvature and 95% reflectivity at 1030 nm. The amplifier produced 700 fs duration pulses at average powers of 50 W after five passes of the signal beam through the planar waveguide and at a repetition frequency of 53 MHz. An analytical model of the pulse amplification process showed that the changes in the pulse shape are mainly caused by the gain saturation and gain narrowing in the amplifier.

In the next chapter will be described the modifications made to the amplifier in order to scale to higher pulse energies and higher average output powers. Pumping the planar waveguide amplifier from two sides has been demonstrated in CW operation [12]. The numerical analysis predicted that it would be possible to extend the performance of the

existing configuration to average output powers of 90 W. By using toroidal mirrors it was expected to be able to increase the number of passes of the waveguide without risk of oscillation, which combined with double pumping should achieve around 265 W of output power with pulses of 780 fs.

3.10 References

[1] I. J. Thomson, Efficient , High-Power Operation of CW Yb : YAG and Q-switched Nd : YAG Planar Waveguide Lasers, PhD Thesis: School of Engineering and Physical Sciences, Heriot Watt University (2010).

[2] K.-H. Leitz, B. Redlingshöfer, Y. Reg, A. Otto, and M. Schmidt, "Metal Ablation with Short and Ultrashort Laser Pulses," Physics Procedia **12**, 230–238 (2011).

[3] A. Ancona, S. Döring, C. Jauregui, F. Röser, J. Limpert, S. Nolte, and A. Tünnermann, "Femtosecond and picosecond laser drilling of metals at high repetition rates and average powers.," Optics letters **34**, 3304–3306 (2009).

[4] R. Coppinger, "When fast isn't fast enough," Electro Optics issue 229 20–22 (2012).

[5] M. Larionov, F. Butze, D. Nickel, and A. Giesen, "High-repetition-rate regenerative thin-disk amplifier with 116 microJ pulse energy and 250 fs pulse duration.," Optics letters **32**, 494–496 (2007).

[6] C. Hönninger, R. Paschotta, M. Graf, G. Zhang, M. Moser, S. Biswal, J. Nees, and A. Braun, "Ultrafast ytterbium-doped bulk lasers and laser amplifiers," Applied Physics B: Lasers and Optics **17**, 3–17 (1999).

[7] S. Biswal, J. Itatani, J. Nees, and G. A. Mourou, "Efficient energy extraction below the saturation fluence in a low-gain low-loss regenerative chirped-pulse amplifier," IEEE Journal of Selected Topics in Quantum Electronics **4**, 421–425 (1998).

[8] G. H. Kim, J. Yang, S. A. Chizhov, E. G. Sall, A. V. Kulik, V. E. Yashin, D. S. Lee, and U. Kang, "High average-power ultrafast CPA Yb:KYW laser system with dual-slab amplifier.," Optics express **20**, 3434–3442 (2012).

[9] J. Limpert, F. Röser, T. Schreiber, I. Manek-Hönninger, F. Salin, and A. Tünnermann, "Ultrafast high power fiber laser systems," Comptes Rendus Physique **7**, 187–197 (2006).

[10] D. C. Brown, "Nonlinear thermal and stress effects and scaling behavior of YAG slab amplifiers," IEEE Journal of Quantum Electronics **34**, 2393–2402 (1998).

[11] H. Baker, J. Lee, and D. Hall, "Self-imaging and high-beam-quality operation in multi-mode planar waveguide optical amplifiers.," Optics express **10**, 297–302 (2002).

[12] I. J. Thomson, F. J. F. Monjardin, H. J. Baker, and D. R. Hall, "Efficient operation of a 400W diode side-pumped Yb:YAG planar waveguide laser," IEEE Journal of Selected Topics in Quantum Electronics **47**, 1336–1345 (2011).

[13] J. R. Lee, G. J. Friel, H. J. Baker, G. J, Hilton and D. R. Hall "A Nd:YAG planar waveguide laser operating at 121 W output with face-pumping by diode bars, and its use as a power amplifier". Advanced Solid- State Lasers, Trends in Optics and Photonics **50**, 36-40 (2001).

[14] W. H. Lowdermilk and J. E. Murray, "The multipass amplifier: Theory and numerical analysis," Journal of Applied Physics **51**, 2436–2444 (1980).

[15] W. Koechner, *Solid-State Laser Engineering* (Springer, 2006).

[16] A. E. Siegman, *Lasers* (University Science Books, 1986).

[17] P. Russbueldt, T. Mans, G. Rotarius, J. Weitenberg, H. D. Hoffmann, and R. Poprawe, "400W Yb:YAG Innoslab fs-Amplifier.," Optics express **17**, 12230–45 (2009).

[18] P. Russbueldt, T. Mans, J. Weitenberg, H. D. Hoffmann, and R. Poprawe, "Compact diode-pumped 1.1 kW Yb:YAG Innoslab femtosecond amplifier.," Optics letters **35**, 4169–4171 (2010).

[19] J. He, P. Yan, Q. Liu, L. Huang, H. Zhang, and M. Gong, "30 W output of short pulse duration nanosecond green laser generated by a hybrid fiber-bulk MOPA system," Laser Physics **21**, 708–711 (2011).
[20] Y. A. Zakharenkov, T. O. Clatterbuck, V. V. Shkunov, A. A. Betin, D. M. Filgas, E. P. Ostby, F. P. Strohkendl, D. a. Rockwell, and R. S. Baltimore, "2-kW Average Power CW Phase-Conjugate Solid-State Laser," IEEE Journal of Selected Topics in Quantum Electronics **13**, 473–479 (2007).
[21] S. Schwertfeger, A. Klehr, T. Hoffmann, A. Liero, H. Wenzel, and G. Erbert, "Picosecond pulses with 50 W peak power and reduced ASE background from an all-semiconductor MOPA system," Applied Physics B **103**, 603–607 (2011).
[22] K. Filgas, D. Rockwell, D., Spariosu, "Next-generation lasers for advanced active EO systems," Technology Today **1**, 9–13 (2008).
[23] M. Schulz, R. Riedel, A. Willner, S. Düsterer, M. J. Prandolini, J. Feldhaus, B. Faatz, J. Rossbach, M. Drescher, and F. Tavella, "Pulsed operation of a high average power Yb:YAG thin-disk multipass amplifier.," Optics express **20**, 5038–5043 (2012).
[24] J. Xu, "Diode Pumped Planar Waveguide / Thin Slab Solid-State Lasers," In Tech (2012).
[25] F. M. Bain, A. A. Lagatsky, S. V. Kurilchick, V. E. Kisel, S. A. Guretsky, A. M. Luginets, N. A. Kalanda, I. . M. Kolesova, N. V. Kuleshov, W. Sibbett, and C. T. A. Brown, "Continuous-wave and Q-switched operation of a compact, diode-pumped Yb^{3+}:$KY(WO_4)_2$ planar waveguide laser," Optics express **17**, 1666–1670 (2009).
[26] D. P. Shepherd, "High-numerical-aperture, contact-bonded, planar waveguides for diode-bar-pumped lasers," Optics Communications **160**, 47–50 (1999).
[27] T. S. Rutherford, W. M. Tulloch, E. K. Gustafson, and R. L. Byer, "Edge-Pumped Quasi-Three-Level Slab Lasers: Design and Power Scaling," IEEE Journal of Quantum Electronics **36**, 205–219 (2000).
[28] S. Chénais, F. Druon, S. Forget, F. Balembois, and P. Georges, "On thermal effects in solid-state lasers: The case of ytterbium-doped materials," Progress in Quantum Electronics **30**, 89–153 (2006).
[29] J. E. Hellström, S. Bjurshagen, V. Pasiskevicius, J. Liu, V. Petrov, and U. Griebner, "Efficient Yb:KGW lasers end-pumped by high-power diode bars," Applied Physics B **83**, 235–239 (2006).
[30] Y. Xu and W. Y. Ching, "Electronic structure of yttrium aluminum garnet (Y_3 Al_5 O_{12})," Physical Review B **59**, 530–535 (1999).
[31] E. M. J. Weber, A. V Dotsenko, L. B. Glebov, and V. A. Tsekhomsky, *Handbook of Optical Materials* (CRC Press, 2003).
[32] L. D. Deloach, S. A. Payne, L. L. Chase, L. K. Smith, W. L. Kway, and W. F. Krupke, "Evaluation of Absorption and Emission Properties of Yb^{3+} Doped Crystals for Laser Applications," IEEE Journal of Quantum Electronics **29**, 1179–1191 (1993).
[33] W. F. Krupke, "Ytterbium solid-state lasers. The first decade," IEEE Journal of Selected Topics in Quantum Electronics **6**, 1287–1296 (2000).
[34] H. Qiu, P. Yang, J. Dong, P. Deng, J. Xu, and W. Chen, "The influence of Yb concentration on laser crystal Yb : YAG," Materials Letters **55**, 1–7 (2002).
[35] X. He, G. Zhao, X. Xu, X. Zeng, and J. Xu, "Comparison of spectroscopic properties of Yb : YAP and Yb : YAG crystals," Chinese Optics Letters **5**, 295–297 (2007).

[36] J. J. Degnan and D. R. Hall, "Finite-Aperture Waveguide-Laser Resonators," IEEE Journal of Quantum Electronics **9**, 901–910 (1973).

[37] Leburn, C. G., Ramirez-Corral, C. Y., Thomson, I. J., Hall, D. R, Baker, H. J, Reid, D. T., "Femtosecond pulses at 50-W average power from an Yb:YAG planar waveguide amplifier seeded by an Yb:KYW oscillator," Optics Express **20**, 17367-17373, (2012)

[38] T. Südmeyer, C. Kränkel, C. R. E. Baer, O. H. Heckl, C. J. Saraceno, M. Golling, R. Peters, K. Petermann, G. Huber, and U. Keller, "High-power ultrafast thin disk laser oscillators and their potential for sub-100-femtosecond pulse generation," Applied Physics B **97**, 281–295 (2009).

Chapter 4

Double sided pumped MOPA system with 250 W average output power

4.1 Introduction

This chapter presents significant improvements made to the amplifier stage of the MOPA system described in Chapter 3. These modifications were implemented in order to obtain higher peak power per pulse from the amplifier by scaling its average power.

The function of an amplifier in a MOPA system is to increase the power from the seed master oscillator. In order to obtain the best efficiency from an amplifier it is best to operate it in the saturated region. When such amplifiers are used in a single-pass configuration the saturation region is almost impossible to reach. Working with MHz repetition rates from the master oscillator coupled into diode pumped amplifiers can be difficult because the gain per pass may be slightly too low in some cases [1]. This is the reason why in most cases multi-pass amplifiers are used because they allow us to increase the intensity of the seed beam sufficiently to saturate the amplifier and optimize the extraction efficiency. Despite this important advantage, multi-pass amplifiers also increase the probability of parasitic lasing, making alignment very critical.

In previously reported multi-pass amplifiers, the number of passes used has been between 6 to 11 passes depending on the choice of the gain material [2, 7]. Table 4.1 shows the characteristics of several multi-pass configurations, presenting results from a single pass to nine passes though the gain material. Nevertheless in all amplifiers more than 6 passes were required to reach the saturation region, and in some cases more than one amplifier has been necessary to reach the intensity needed to saturate the gain [3, 5]. In all of these cases the gain medium was pumped by diodes [2, 5] or YAG lasers [3, 4, 6, 7], depending on the pump wavelength needed for each material. Each amplifier was pumped from both sides of the gain material. For an Yb:YAG slab the maximum extractable power previously reported was 1.1 kW [2]. Energies on the order of μJ to mJ have been obtained with these configurations at pulse durations from 25 fs to 20 ns.

Table 4.1 MOPA configurations for different materials (*denotes peak power) .

Ref.	Power (W)	Gain material	Wavelength (nm)	Number of passes	Rep-rate (Hz)	Pulse duration(fs)
[2]	1100	Yb:YAG	1030.5	7+1	20×10^{6}	615
[3]	4×10^{12} *	Ti:sapphire	800	8, 5	100×10^{6}	45
[4]	-	Ti:sapphire	780	6	60×10^{6}	20×10^{6}
[5]	2.7	Yb:KYW	1030	10, 11	100	340
[6]	0.4	Ti:sapphire	803	8	70×10^{6}	67
[7]	1.4×10^{12} *	Ti:sapphire	-	8	-	25

The multi-pass configurations listed in Table 4.1 were based on unstable resonators. It has been shown that unstable resonators can support a near diffraction limited beam while still extracting efficiently the energy from a wide active region [8-10]. A confocal unstable resonator has even been shown to give a diffraction-limited collimated output beam [8]. The confocal resonator is very useful for gain materials with large areas because it can access almost all the energy available in the lateral direction [10]. There are two kind of confocal unstable resonators, the positive configuration and the negative one [8]. Figure 4.1 shows these two configurations.

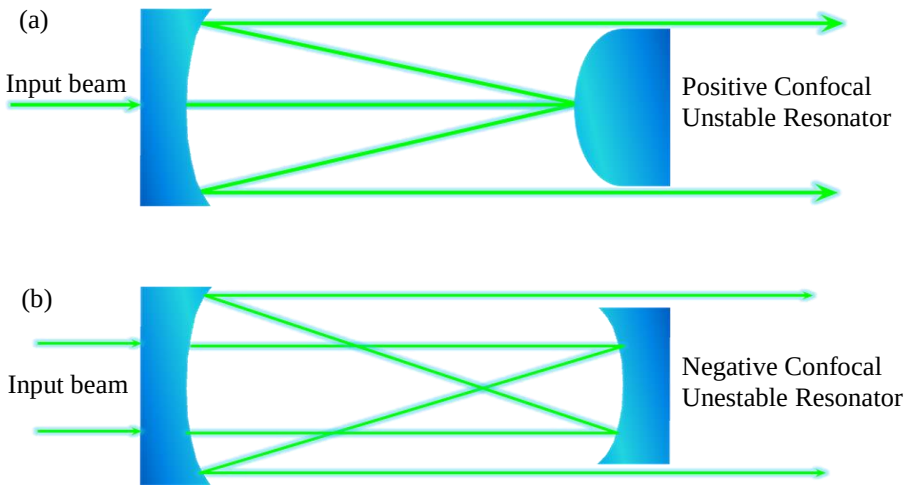

Figure 4.1 Confocal unstable resonator geometry for: (a) positive configuration and (b) negative configuration.

In these resonators L is the distance between the mirrors. If R_1 and R_2 are the curvatures of the mirrors then a new quantity can be defined as:

$$g_i = 1 - \frac{L}{R_i} \tag{4.1}$$

where i=1, 2 for the first and second mirrors. For a resonator to be confocal, it has to satisfy the condition $R_1 - R_2 = 2L$ for the positive case where one of the mirror curvatures is positive and the other negative, and therefore g_1 and g_2 are positive. The condition $R_1 + R_2 = 2L$ defines the negative case, when both mirrors have a positive radius of curvature but either g_1 or g_2 is negative. In a negative resonator, the wave front inverts in the optical axis on each pass, as shown in Figure 4.1(b). Then this means that there is at least one focal point inside the cavity. Therefore an associated disadvantage of these amplifiers can be the generation of high temperatures in the gain material, creating unwanted thermal effects or even damage. For the positive resonator a drawback can appear at the point of aligning this configuration, which is very critical for this case [8].

The use of planar waveguides is favourable for these kinds of resonators, because a waveguide provides effective control of the light injected to the system in one dimension [10]. A single sided version of a confocal unstable resonator has been used before with good beam quality in the output and lower beam divergence [10, 11, 12]. This kind of resonator has also been used to reduce losses or to mode match the resonator to improve the beam properties; in these cases a hybrid resonator combining a stable resonator in one direction with an unstable resonator in the other direction has been used successfully [11].

For an unstable resonator using a planar waveguide its large area becomes a disadvantage because it needs different configurations of unstable resonators for the lateral and transverse directions. When using only the simple unstable resonator, a good lateral beam profile is achieved, but the transverse beam quality becomes poor. In that case to improve the transverse beam profile with low losses a case III confocal unstable resonator is required [12, 13].

For the MOPA configuration previously described in Chapter 3, to get higher gain from the amplifier, it was therefore necessary to modify the configuration to a double sided pumped amplifier and increase the number of passes through the planar waveguide,

which as shown in the previous chapter was not possible by using simple cylindrical mirrors. Obtaining a bigger number of passes in the amplifier requires a ~17 mm radius of curvature mirror in the transverse direction to achieve the confocal condition, whilst the unstable resonator requires a 200 mm radius of curvature mirror in the lateral direction. In this case a pair of mirrors with specially designed toroidal characteristics had to be used.

4.2 Toroidal Mirrors

The toroidal mirrors were fabricated and characterized by the Lasers and Photonics Applications group (LPA) at Heriot-Watt University [14]. These mirrors are characterized by having a common (large) radius of curvature in one direction, whilst in the other direction, a number of stripes are generated each of which has a much smaller radius of curvature as shown in Figure 4.2. There are different polishing techniques to fabricate these mirrors, however some of them are very costly and take long time to complete. Krystian Wlodarczyk et.al [14] developed a new technique to fabricate these mirrors using CO_2 laser machining of fused silica to create the required surface. A previous technique already developed by the LPA group is based on a melt-ejection process [15]. This technique was used to fabricate the phase plate that was used to correct for aberrations from the diode stack [12]. In the new technique the lateral radius of curvature is given by the original cylindrical shape of the mirror, and the transverse radius of curvature is generated by CO_2 laser-induced vaporization of the glass.

The two cylindrical mirrors used were sourced from CVI Melles Griot. The curvatures of these mirrors were chosen to build a positive confocal unstable resonator configuration in the unguided direction. The first mirror was a plano-convex reflector (model SCX-20.0-152.6-UV), as shown in Figure 4.2.

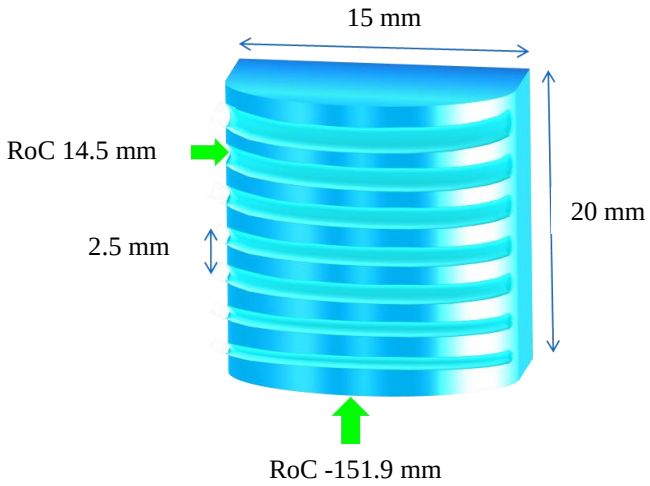

Figure 4.2 Plano-convex mirror with seven stripes of different curvatures, each separated by a distance of 2.5 mm, used for the new MOPA configuration

To make the stripes of the required radius of curvature the surface was submitted to a number of partially overlapped unidirectional CO_2 laser scans. To obtain a specific radius of curvature, the incident power on the surface, the number of scans and the spacing between the scans must be manipulated [14]. Table 4.2 describes the characteristics necessary to obtain each stripe in the plano-convex mirror. This table shows the power used for each stripe, which is treated as a separate mirror stripe (MS1-MS7), the transversal and lateral radius of curvature (RoCT and RoCL respectively) of the stripes, and the measured peak-to valley depth of the stripe (P-V depth).

Table 4.2 Fabrication values for the plano-convex toroidal mirror.

Mirror	Power (W)	RoCT (mm)	RmsRoCT (mm)	RoCL (mm)	P-Vdepth (um)
MS1	9.35	13.3	2.4	-151.9	0.202
MS2	9.30	14.5	1.4	-151.9	0.175
MS3	9.25	14.9	3.6	-151.9	0.225
MS4	9.20	16.9	2.9	-152.3	0.190
MS5	9.15	19.8	3.9	-152.9	0.180
MS6	9.20	21.2	4.2	-152.2	0.220
MS7	9.25	21.2	4.9	-152.2	0.220

The two mirrors used were fabricated with five scans on each stripe each, and a separation distance between the scans of 46 μm. For the first mirror, the wavelength of the CO_2 laser used was 10.59 μm [16].

The second mirror was a plano-concave reflector (model SCC-20.0-203.4-UV), to satisfy the positive confocal unstable resonator scheme. For this mirror the CO_2 wavelengths used were 10.59 µm, 10.57 µm and 10.61 µm [16]. This mirror also was fabricated with seven stripes, as shown in Figure 4.3.

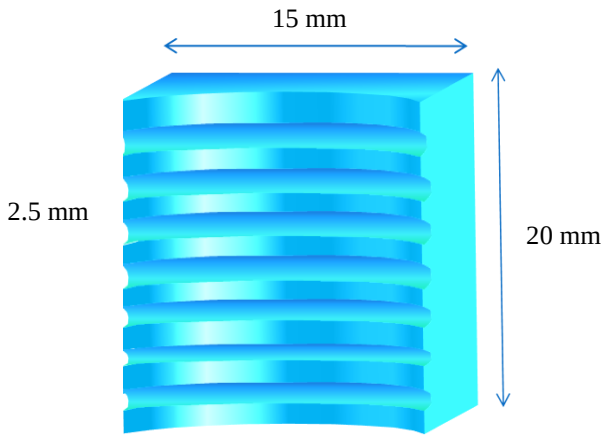

Figure 4.3 Plano-concave fabricated toroidal mirror.

For this mirror Table 4.3 shows the requirement for each stripe. Using the stripes in these mirrors, a configuration corresponding to a Case III resonator was possible in the guided direction whilst in the unguided direction a positive unstable resonator scheme was maintained.

Table 4.3 Fabrication values for the plano-concave toroidal mirror.

Mirror	Power (W)	RoCT (mm)	Rms RoCT (mm)	RoCL (mm)	P-V depth (µm)
MS1	9.35	35.9	11.2	202.7	0.140
MS2	9.30	-	-	-	-
MS3	9.40	22.9	5.0	202.5	0.130
MS4	9.35	28.1	5.6	202.7	0.135
MS5	9.30	17.6	2.7	202.5	0.120
MS6	9.25	19.1	6.4	202.4	0.130
MS7	9.20	21.5	6.0	202.7	0.090

After the mirrors were fabricated, they were sent to Layertec to deposit a 99% reflectivity high-damage threshold coating on each of them, centred at a wavelength of 1030 nm.

4.3 Pumping scheme

For this improved configuration the same waveguide was used which was a 2% at. doped Yb:YAG planar waveguide with 150 µm thickness in the core and 1 mm sapphire claddings, as shown in Figure 4.4. As mentioned previously, the waveguide was AR-coated for 1030 nm on two of the facets on the 12 mm side which had plane parallel surfaces, the other two sides had asymmetric unequal facets. On one side the edge was angled 7° from the vertical and was AR coated for 940 nm, and on the other side it was angled 20° from the vertical without coating due to the polishing of the facet to the desired angle. The angles were found by modelling the spontaneous emission using Zemax and Matlab [12] in order to suppress parasitic oscillations in the amplifier.

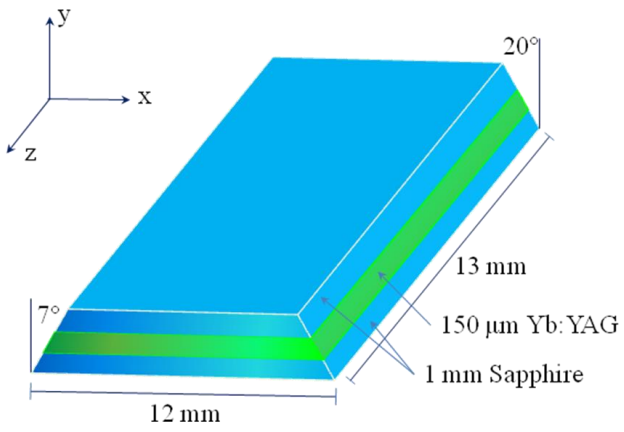

Figure 4.4 Yb:YAG planar waveguide dimensions.

The first modification that was implemented over the previous configuration was to add a second diode stack, in order to pump from both of the sides of the waveguide coated for 940 nm. To obtain the best results, the pump stack used in the previous configuration was also replaced. The two new pump sources were both six-diode bar vertical stacks from JENOPTIK, model JOLD-660-CAFN-6A which were collimated on the fast axis and had a 540 W average power at a maximum current of 105 A each. Each diode bar gave 110 W of pump power at 105 A of CW operation [17]. Figure 4.5

shows the output power of each of the stacks for different pump currents. As before, a water cooling system was used to maintain the temperature of the waveguide and the diodes at $23.7° \pm 0.3°$

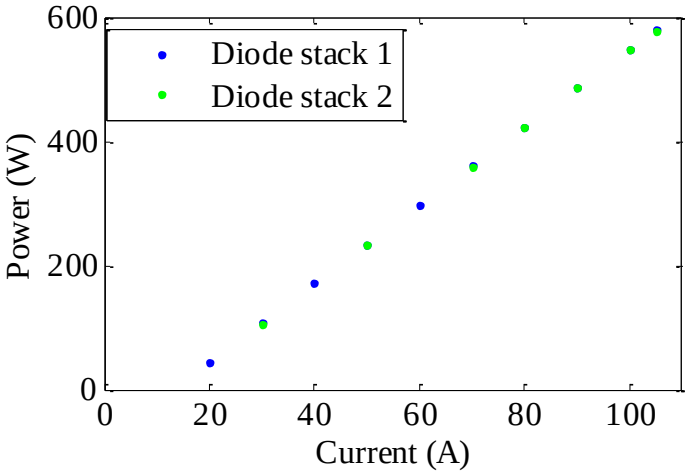

Figure 4.5 Average output power of each diode stack.

The first stack was aligned to the 7° facet side of the waveguide. According to Snell's law this stack was aligned to the waveguide at an incidence angle of $\theta = \theta_{air} - 7° = 5.85°$ [12] (with $\theta_{air} = \sin^{-1}[\sin(7)(1.82)]$ and $n_{Yb:YAG} = 1.82$), which allows the light to go parallel to the waveguide as it travels through it. The second diode stack was aligned in the direction parallel to the base of the waveguide, the same as the stack used in the previous chapter on the side of the 20° facet of the waveguide. This alignment allows the beam to pass through the waveguide without reaching the diode on the opposite side which could cause damage to each of the units. Figure 4.6 shows the beam incident on the waveguide from each of the stacks.

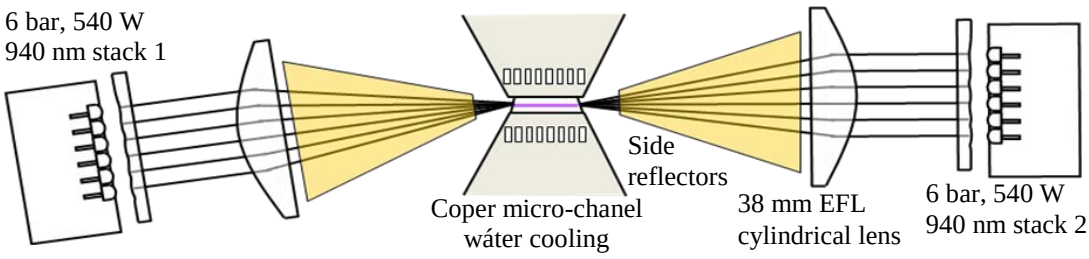

Figure 4.6 Diode stack pumping scheme.

Because the 20° angled facet was not coated, 7% of the light from the second stack was reflected [12] which is about 38 W of the total incident power. Therefore two beam

dumps were necessary to stop the beam at each side of the diode stacks. The alignment for the first stack was done using a power meter after the waveguide for the transmitted light and adjusting the alignment to maximize the amount of light absorbed. For the second stack, a fluorescence emission imaging technique was used to align it to the waveguide [12].

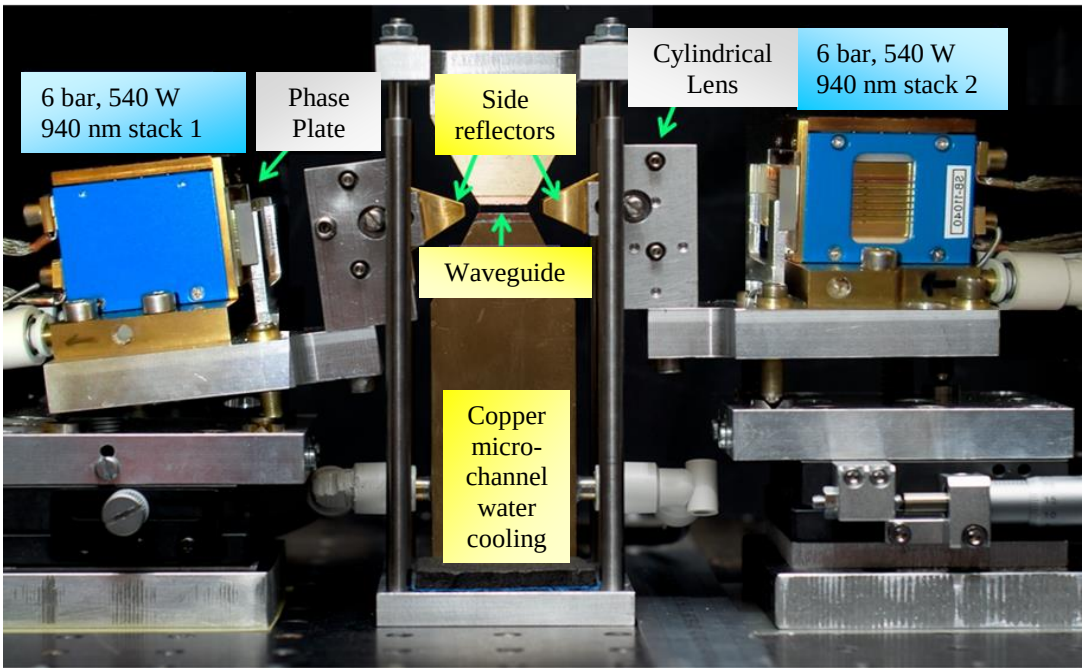

Figure 4.7 Amplifier pump configuration from the seed laser direction.

Figure 4.7 shows the final pump alignment for the amplifier. A phase plate was used after each stack to correct for aberrations. In this case, as in the previous configuration, the light from both stacks was focused into the waveguide using a 38 mm focal length lens. Side reflectors were also used to reflect back the light from the slow axis.

4.4 Single pass alignment

To increase to seven the number of passes in the amplifier from the five already achieved it was necessary to replace the cylindrical mirrors used in the first configuration (Chapter 3) with the toroidal mirrors detailed in Section 4.2. Using the software Zemax, a model of the seven passes of the toroidal mirrors was constructed to determine the beam characteristics of the seed required at the input of the waveguide as shown in Figure 4.8. From the calculations done with Zemax, a beam spot size ($1/e^2$

radius) of 0.54 mm was required to achieve seven passes. With the seed spot size in the waveguide ≅ 1 mm the output beam was estimated to be 1.51 mm, giving a magnification of 1.3 of the output beam compared to the seed beam.

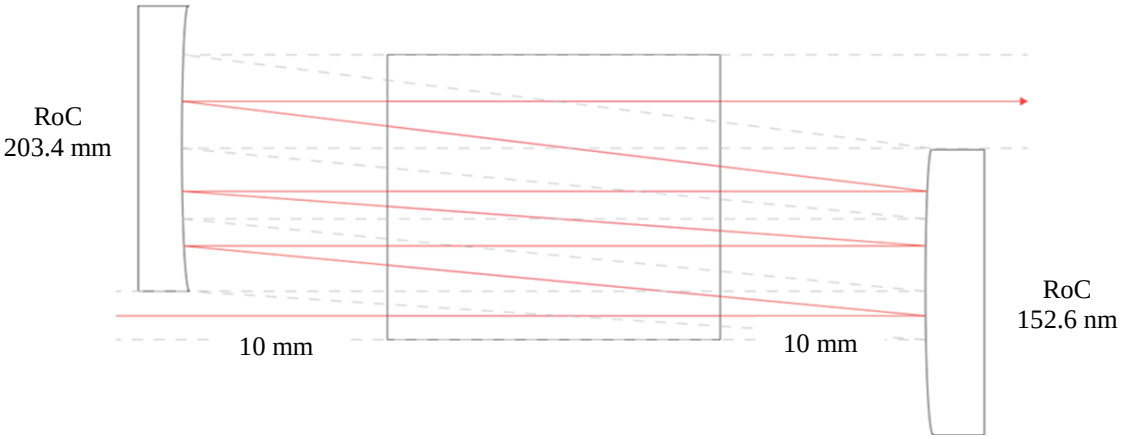

Figure 4.8 Seven pass configuration created using Zemax.

To have the correct beam size going into the waveguide, the telescope system was modified from the one used in the previous arrangement (see Chapter 3). Using again the SPIRICON system with a CCD camera the beam spot size was measured at the input of the planar waveguide. In this case two lenses with f = 150 mm and f = 75 mm were used, with a distance of 185 mm between them as shown in Figure 4.9. Because of the expected high powers from the amplifier as discussed in Section 3.8, a quarter-wave plate (λ/4) was also placed after the isolator for additional protection of the oscillator from feedback from the amplifier.

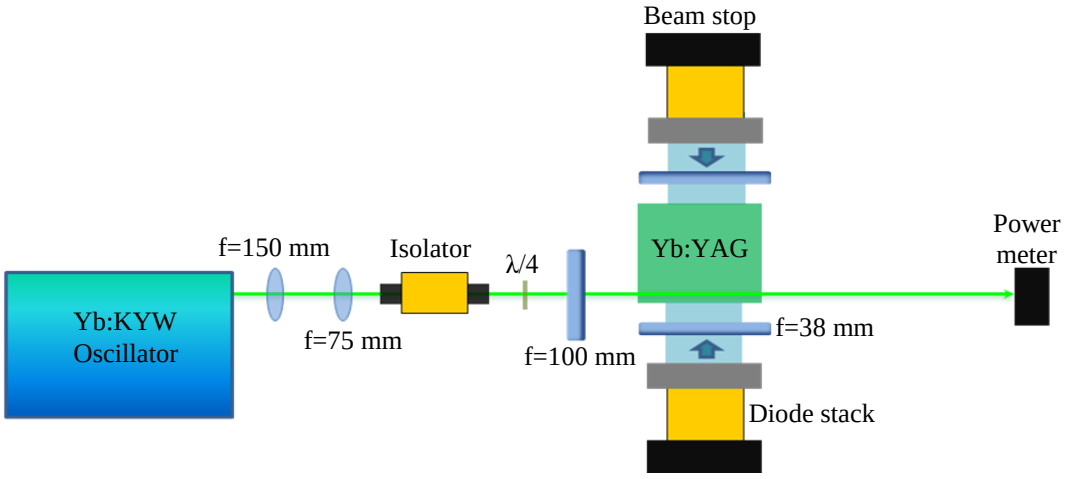

Figure 4.9 Single pass amplifier configuration.

When the telescope system was modified, and therefore the spot size was different, the focusing lens into the waveguide was changed from f = 150 mm to f = 100 mm. Using this lens the beam was aligned for a single pass through the planar waveguide. The alignment was done using a beam profiler (Thorlabs model BP109-IR) which was positioned at different distances after the waveguide to get the correct alignment. Images of the beam are shown in Figure 4.10, before and after the amplifier for a single pass configuration.

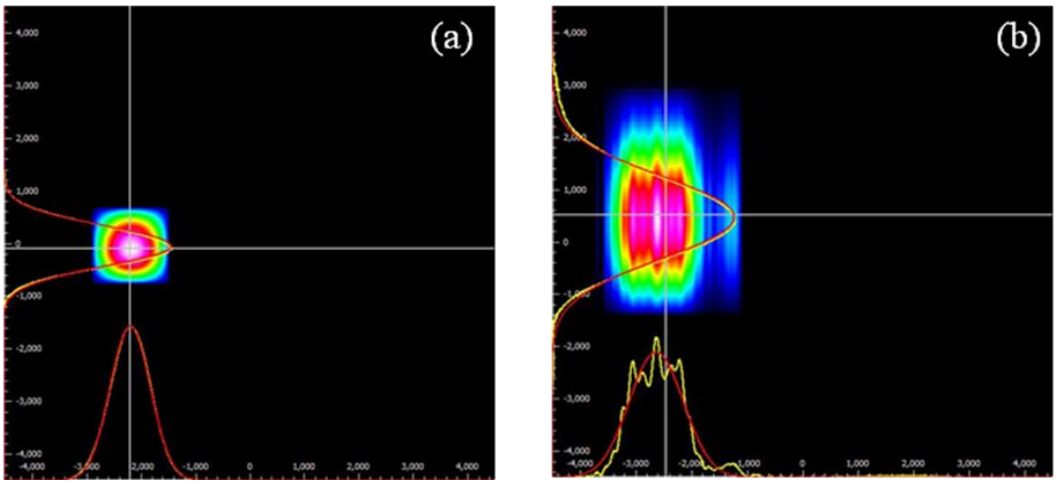

Figure 4.10 Beam shape obtained with the Thorlabs beam profiler a) before the planar waveguide, b) after the waveguide.

After aligning the beam, the average power obtained after the waveguide was 2 W with the pump diodes of the amplifier turned off. At 60 A drive for the pump diode stacks, or 253 W of pump power, 8.12 W were obtained for a single pass of the amplifier as shown in Figure 4.11.

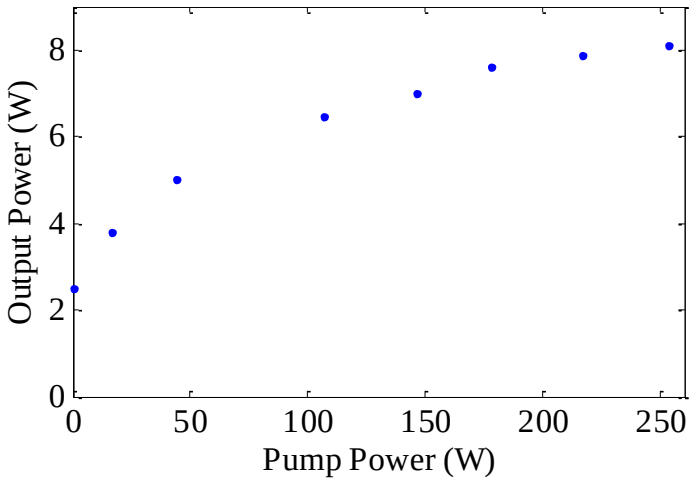

Figure 4.11 Output power versus pump power for a single pass through the amplifier

4.5 Seven Pass Amplification

In this configuration the mount used for the cylindrical mirrors of the previous configurations was modified slightly to allow the best alignment using the toroidal mirrors. The mount used was an xyz-translation stage as previously, but this time the mirror was mounted so that it could rotate in three dimensions too (see Figure 4.12). The mount was also covered with aluminium to reflect the fluorescence from the amplifier which could otherwise cause the mount to become hot, and therefore misalign the mirror from its correct position.

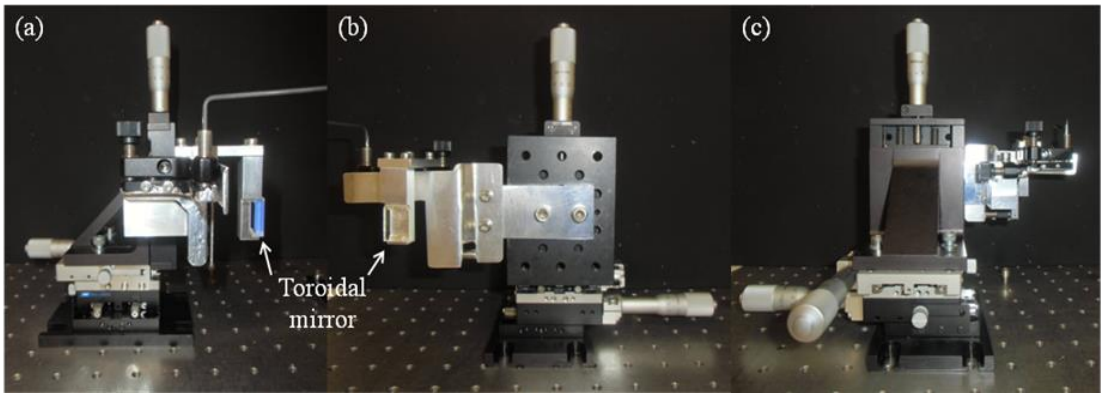

Figure 4.12 Toroidal mirror mount, (a) side view, (b) front view and (c) back view.

In the previous design (Chapter 3) a HeNe laser was used to align the mirrors in the amplifier system. This was no longer possible because the size of the stripes on the toroidal mirrors was smaller than the size of the beam, and the divergence properties of the HeNe and Yb:KYW beams after propagating through the waveguide were different. For the seven-pass configuration of the amplifier, the first toroidal mirror was placed to allow the seed beam to make two passes of the waveguide. Using the SPIRICON CCD camera system again the mirror was aligned by tilting it in the three dimensions and adjusting the height in an iterative process. After this the distance from the mirror to the waveguide was adjusted using the power meter to obtain a maximum efficiency. The final distance from the waveguide to the mirror was 7.2 mm.

After aligning the first mirror, the second mirror was placed to make more bounces through the planar waveguide. To align this mirror a second CCD camera was placed above the system to see the direction of the beam on each of the passes through the waveguide. Again a power measurement was used to obtain the maximum efficiency after iterative alignment. This mirror was placed at 7 mm from the waveguide, leaving a

gap of 1.33 mm from the edge of the mirror to the edge of the waveguide in the direction perpendicular to the seed beam, as shown in Figure 4.13(a). This was enough to allow the input beam to reach the waveguide. For the first mirror, the gap left for the output beam was around 1.87 mm (Figure 4.13 (b)). After testing each stripe for both mirrors the ones that were used were the fourth one on the first mirror (MS4 in Table 4.2), and the fifth one of the second mirror (MS5 in Table 4.3).

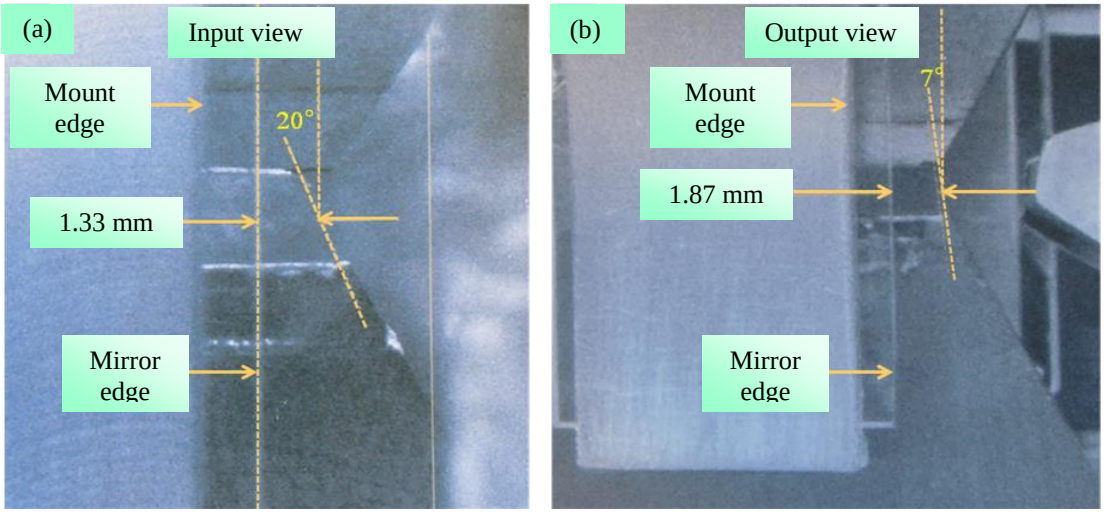

Figure 4.13 Toroidal mirror alignment a) from the input view and b) from the output of the beam.

For this configuration it was not possible to make measurements for each different number of passes from one to seven. In this case the folding system for two to five passes required moving the mirrors to a position not reachable due to the space between the mount of the 100 mm focal lens and the toroidal mirror 2. For this reason, the system was assembled only for one and seven passes. Figure 4.14 shows the seven-pass configuration for the amplifier.

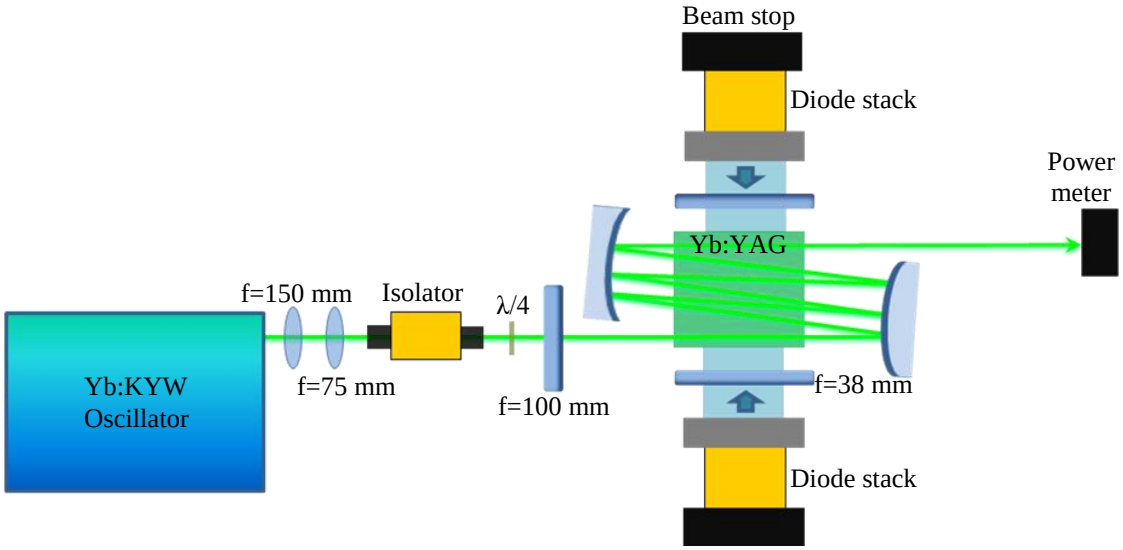

Figure 4.14 Seven-pass amplification configuration.

4.5.1 Beam Analysis

For seven passes a complete characterization of the beam was done for different amplifier pump-diode currents, which gave pump powers from 0 to 520 W. The output power and beam shape were analysed when the amplifier was seeded and when there was no seed. This means that, in the case with no seed, the system worked as a resonator. The output power for each case is shown in Figure 4.15.

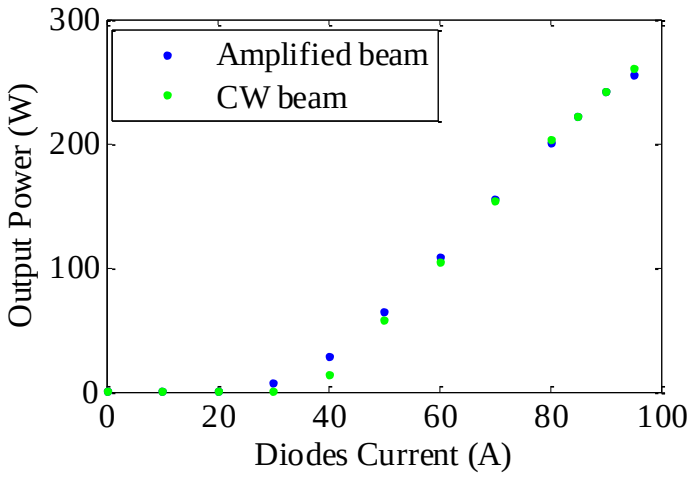

Figure 4.15 Amplified output average power and CW output power.

Using the CCD camera, the output beam was analysed for different pump-diode currents, from 10 A to 95 A, which corresponds to 0.17 W to 520 W of pump power.

Figure 4.16 shows the beam shape for each current. Because of the wavelength dependence of the material absorption cross section the best efficiency was reached at the highest pump current where the peak absorption wavelength of 940 nm was reached by the diodes [12]. Therefore at the highest current the beam shape would be better. For the first two current values, the system was still working as an absorber below the threshold value of transparency of the amplifier which generated a very noisy beam.

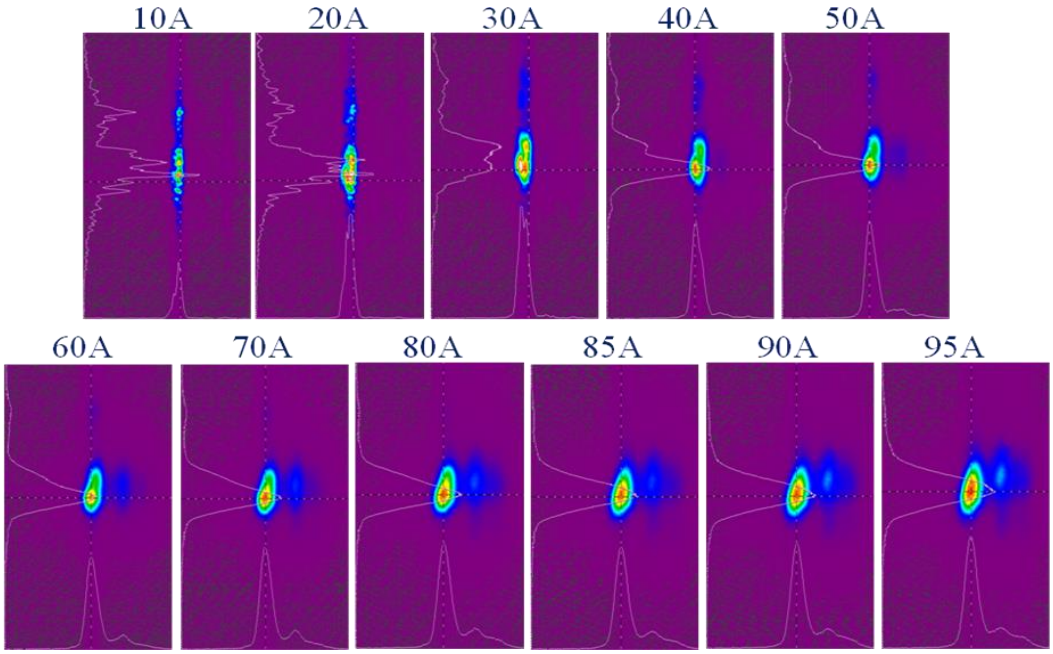

Figure 4.16 Beam shape for an increasing amplification current.

The beam was also recorded in the cases when the amplifier was seeded and when the system had only the pump power and worked as a laser oscillator. Figure 4.17 shows the beam for both cases for 40 A, 60 A and 80 A (i.e. 107 W, 253 W and 393 W of pump power respectively). These results showed that the CW beam from the resonator followed a slightly different output direction than the direction of the amplified beam and also had a noisier shape. To illustrate this better, the images of the recorded beams in the case of amplification were cut on the right to show the position of the CW beam with respect to the amplified beam. This is due to the configuration of the amplifier being designed for amplifying a seed beam and not as a resonator.

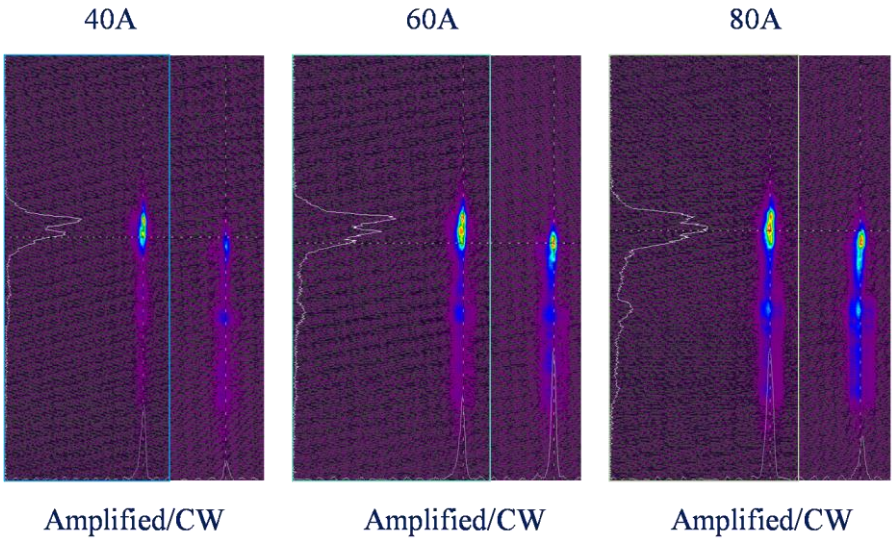

Figure 4.17 Beam shape for the amplified beam (left) and as a CW unstable resonator (right) for different currents. In this case the images of the two beams ore overlapped but the amplified one was cut to show the position of the CW beam.

After seven passes of the amplifier the output beam diverged considerably more in the vertical direction than in the horizontal direction as shown in Figure 4.18. The beam size at 136 mm from the waveguide was 3.6 mm in the horizontal direction and 5.6 mm in the vertical direction ($1/e^2$ beam diameter).

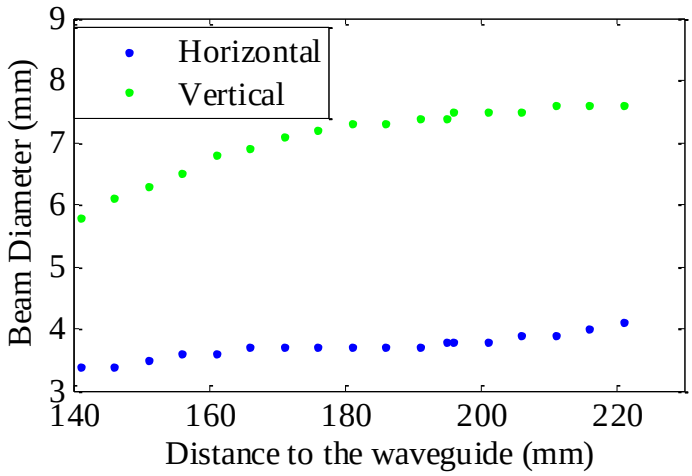

Figure 4.18 Beam diameter versus distance from the waveguide after the amplification process.

For the output beam an M^2 measurement was made using the Thorlabs beam profiler which gave an M^2 of 1.21 in the horizontal direction and 7.84 in the vertical direction. Figure 4.19 shows the results taken from the beam profiler.

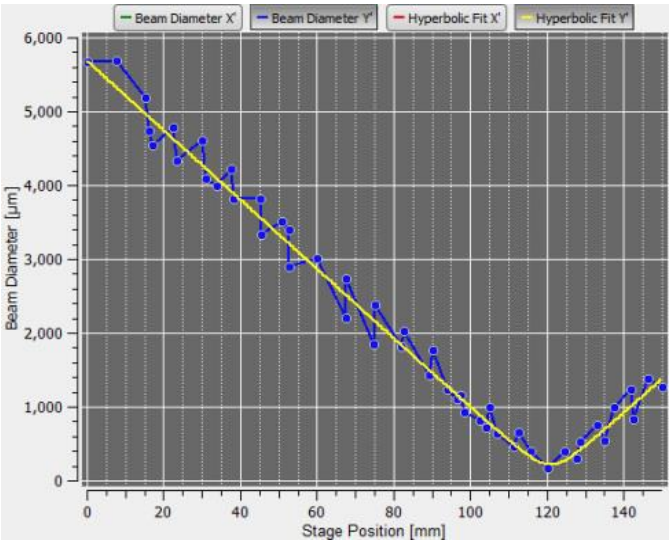

Figure 4.19 M^2 measurement in the horizontal direction for the seven pass amplified beam.

4.5.2 Spectral measurements

After characterizing the beam for seven passes through the amplifier, an assessment of the output beam characteristics was done for the final configuration shown in Figure 4.20. To take these measurements a beam splitter had to be used to decrease the output power and avoid damaging the measuring devices.

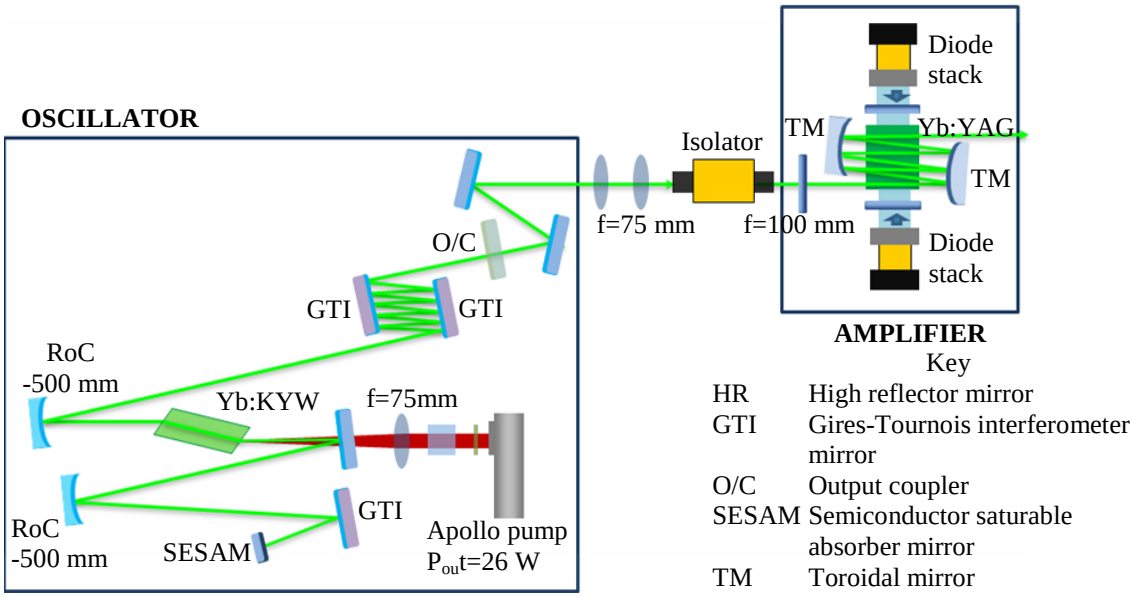

Figure 4.20 Final MOPA configuration.

The beam splitter used was an OPHIR model BEAM TAP I & II YAG designed to work at 1064 nm [18]. This model consisted of two reflecting surfaces AR coated at 1064 nm such that the planes of reflection are orthogonal, as shown in Figure 4.21. This

allows the output beam from the device to have the same mixture of *s* and *p* polarization components as the original input beam.

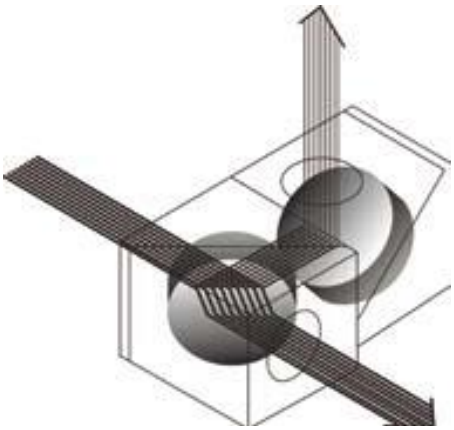

Figure 4.21 Polarization components of the beam splitter device used to take measurements [18].

The spectrum of the output beam was recorded for different pump-diode currents for seven passes of the amplifier. Figure 4.22 shows the spectrum obtained for pump-diode currents from 20 A to 95 A. To take these measurements an Anritsu optical spectrum analyser model MS9740A was used. From the spectrum obtained it was observed that the spectrum narrowed as the power was increased reaching a minimum 1.46 nm bandwidth for 95 A of current or 520 W pump power.

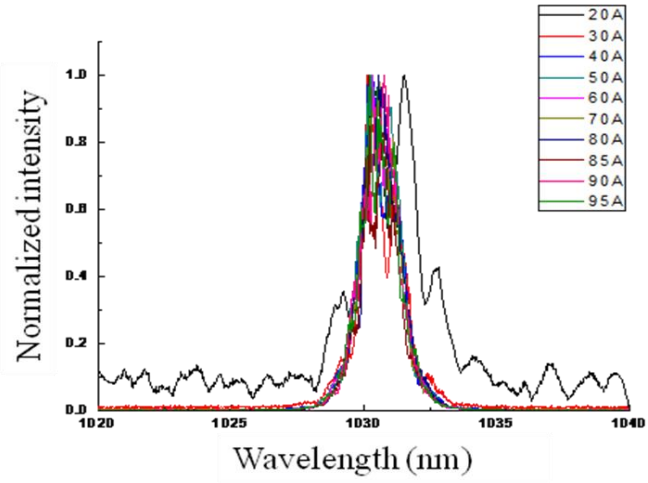

Figure 4.22 Amplifier output spectrum at different pump-diode currents.

4.5.3 Time-domain measurements

The duration of the pulses leaving the amplifier after seven passes were measured using the Femtochrome autocorrelator described in Chapter 1 (FR-103XL), which provided an

intensity autocorrelation of the pulses. Figure 4.23 shows the intensity autocorrelation obtained from 30 A to 95 A of pump current. This showed a pulse broadening up to 784 fs ($\times 1.54$) at the maximum pump power.

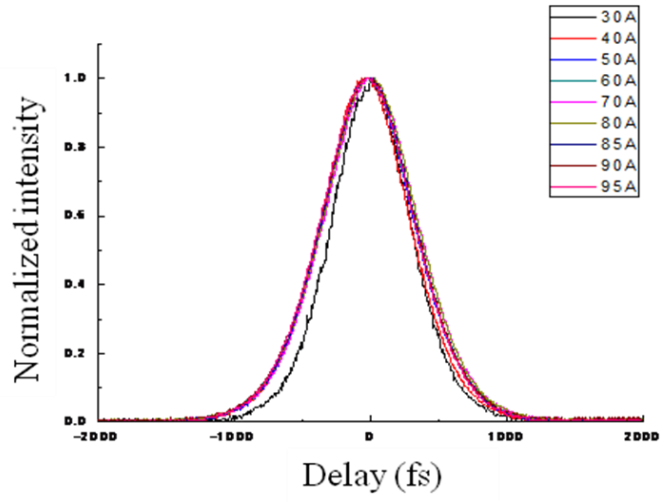

Figure 4.23 Pulse duration for different pump currents.

The maximum average output power obtained after seven passes of amplification was 255 W at 520 W of pump power, with a pulse energy of 4.81 µJ. Table 4.4 shows the results obtained for different pump current values in the MOPA.

Table 4.4 Output characteristics of the MOPA design.

Diode Current (A)	Output Power (W)	Δτ (fs)	Bandwidth (nm)	Pulse Energy (µJ)
Oscillator only	3.5	465	2.6	0.066
30	7.36	653	1.62	0.14
40	29.16	745	1.6	0.55
50	65	776	1.64	1.2
60	108.1	776	1.48	2.03
70	155.2	791	1.42	2.09
80	200.9	791	1.42	3.79
85	222.1	791	1.4	4.19
90	242.1	791	1.38	4.53
95	**255.1**	**784**	**1.46**	**4.81**

4.6 Conclusions

A significantly improved configuration of the MOPA design was presented in this chapter. Double sided pumping of the planar waveguide and the use of home-made toroidal mirrors provided a five-fold improvement in the output power obtained from

the amplifier. The use of toroidal mirrors also allowed more passes though the planar waveguide that helped to increase the final output power and pulse energy. The toroidal mirrors also allowed the use of two different resonator configurations for each direction of the amplifier to improve the beam quality. In the lateral direction the configuration used was a positive confocal unstable resonator whilst in the transverse direction the design was maintained as a Case III resonator used in Chapter 3.

With the modifications made, the final MOPA design generated an average output power of 255 W that was five times more than the power of 50 W obtained with the previous configuration. At this power pulses of 784 fs durations were obtained at 1032 nm with a bandwidth of 1.46 nm, and pulse energy of 4.81 μJ. These are the best results achieved until now with this configuration. In principle, still higher pulse energies and output powers could be achieved using nine passes through the planar waveguide, although a modification of the seed input beam size would be needed again in order to align the system.

4.7 References

[1] J. J. Ramsay, I. A.Degnan, "A Ray Analysis of Optical Resonators," Applied optics **9**, 385–398 (1970).

[2] P. Russbueldt, T. Mans, J. Weitenberg, H. D. Hoffmann, and R. Poprawe, "Compact diode-pumped 1.1 kW Yb:YAG Innoslab femtosecond amplifier.," Optics letters **35**, 4169–4171 (2010).

[3] P. F. Curley, C. Le Blanc, G. Ch, G. Darpentigny, P. Rousseau, F. Salin, J. P. Chambaret, and A. Antonetti, "Multi-pass amplification of sub-50 fs pulses up to the 4 TW level," Optics Communications **31**, 72–76 (1996).

[4] P. Georges, F. Estable, F. Salin, J. P. Poizat, P. Grangier, and A. Brun, "High-efficiency multipass Ti:sapphire amplifiers for a continuous-wave single-mode laser.," Optics letters **16**, 144–146 (1991).

[5] D. N. Papadopoulos, A. Pellegrina, L. P. Ramirez, P. Georges, and F. Druon, "Broadband high-energy diode-pumped Yb:KYW multipass amplifier.," Optics letters **36**, 3816–3818 (2011).

[6] A. Ruiz-De-La-Cruz and R. Rangel-Rojo, "Compact multi-pass amplifier for chirped-pulse amplification," Journal of Modern Optics **53**, 307–311 (2006).

[7] H. Teng, J. F. Xia, Z. Y. Wei, and J. Zhang, "Efficient Chirped-Pulse Multi-Pass Preamplifier," Jounal of the Korean Physical Society **39**, 831–833 (2001).

[8] W. F. Krupke and W. R. Sooy, "Properties of an unstable confocal resonator CO2 laser system," IEEE Journal of Quantum Electronics **5**, 575–586 (1969).

[9] A. E. Siegman, "Unstable optical resonators.," Applied optics **13**, 353–367 (1974).

[10] Y. A. Anan'ev, "Unstable resonators and their applications," Soviet Journal of Quantum Electronics **1**, 565–586 (1972).

[11] P. E. Jackson, H. J. Baker, and D. R. Hall, "CO2 large-area discharge laser using an unstable-waveguide hybrid resonator," Applied Physics Letters **54**, 1950 (1989).

[12] I. J. Thomson, Efficient , High-Power Operation of CW Yb : YAG and Q-switched Nd : YAG Planar Waveguide Lasers, PhD Thesis: School of Engineering and Physical Sciences, Heriot Watt University (2010).

[13] H. Baker, J. Lee, and D. Hall, "Self-imaging and high-beam-quality operation in multi-mode planar waveguide optical amplifiers.," Optics express **10**, 297–302 (2002).

[14] K. L. Wlodarczyk, I. J. Thomson, H. J. Baker, and D. R. Hall, "Generation of microstripe cylindrical and toroidal mirrors by localized laser evaporation of fused silica.," Applied Optics **51**, 6352–6360 (2012).

[15] G. A. J. Markillie, H. J. Baker, F. J. Villarreal, and D. R. Hall, "Effect of vaporization and melt ejection on laser machining of silica glass micro-optical components.," Applied Optics **41**, 5660–5667 (2002).

[16] F. J. M. Harren, J. Reuss, E. J. Woltering, and D. D. Bicanic, "Photoacoustic measurements of agriculturally interesting gases and detection of C_2H_4 below the PPB level," Applied Spectroscopy **44**, 1360–1368 (1990).

[17] http://www.jenoptik.com/en-diode-stack-product-overview (accessed on February 2013).
[18] http://www.ophiropt.com/ (accessed on February 2013).

Chapter 5

Simplified Yb:KYW ultrafast oscillator for an Yb-based MOPA

5.1 Introduction.

As mentioned in Chapter 2, Yb:KYW is a material which is easy to use, because of its broad absorption and emission cross sections, which mean that we can find pump sources for it which are commercially available [1]. These pump sources (see Table 2.1) range from Ti:sapphire lasers to diodes, with the most frequently used being fibre coupled laser diodes.

Due to the anisotropic characteristics of the Yb:KYW material it is necessary to align the pump light with the most appropriate polarization direction within the crystal, as mentioned in Chapter 2. Normally this is possible due to the linear polarization of most of the pump sources. Single mode fibres can provide the polarization orientation required to pump the gain material. Polarization-maintaining fibres can be used, in which strong birefringence prevents coupling between orthogonal states [2]. Another way to manage the polarization in fibres is by straining the fibre to control the polarization at the output [3]. This is done mainly in single mode fibres but it can be used also in multimode fibres [2]. Because of the broad absorption cross section of Yb:KYW, it is also possible to pump it with sources that are randomly polarized [4, 5] resulting in only a small reduction in the absorption efficiency of the pump scheme.

This Chapter presents a new configuration of an Yb:KYW oscillator, different from the one presented in Chapter 2. In this case the oscillator is pumped by a randomly polarized multimode fibre-coupled diode at 980 nm with an output power of 10 W, and a new crystal geometry and doping concentration is used. This cavity configuration allows the repetition frequency of the oscillator to be changed to various values using a relay imaging system. Results for a range of repetition frequencies are presented.

5.2 Yb:KYW Crystal Design

The crystal for this cavity was a Yb:KYW gain media with 5 at. % doping concentration of Yb^{3+}. It had a triangular geometry of $9.39 \times 5.22 \times 3\,\text{mm}$ (see Figure 5.1) to allow the variation of the gain by adjusting the crystal insertion. Variation of thickness of the crystal allowed the optimization of the efficiency of system in a manner which could not be carried out with the previous design described in Chapter 2. The plane side of the crystal was anti-reflection coated at 980 nm to be used as the input of the pump beam and high reflecting at 1030 nm to be used at the same time as one end of the cavity. The aim with this was to reduce the number of elements in the cavity compared with the cavity already described. Due to the properties of Yb:KYW described in Chapter 2, the crystal had a plane-Brewster cut such that the p-polarization at 981 nm and 1030 nm was incident along the N_m axis.

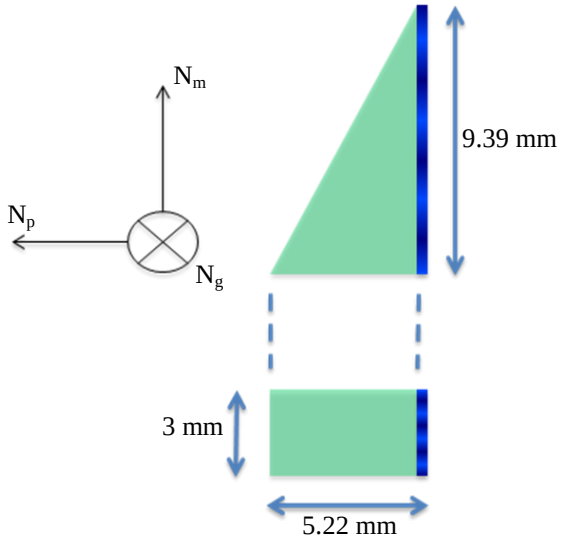

Figure 5.1 Crystal geometry of Yb:KYW

5.3 Fibre Coupled Diode Pump Laser Characterisation

The pump laser for this system was a fibre-coupled diode laser array (*JDSU L4-9897510-100C*) at 980 nm, which had a multimode fibre with a 105 µm core diameter and a 0.15 numerical aperture. The fibre was spliced to another multimode fibre with the same core size which had an angled ending for coupling into the crystal. The pump uses the multimode fibre to be able to manage a larger amount of power than can be handled by single-mode fibre-coupled diodes [2]. This pump was a randomly polarized source, so a polarization variation measurement was made to evaluate the stability and of the polarization state (Figure 5.2). This measurement was done by placing a polarizing beam splitter cube at the output of the fibre, and measuring the power after

the cube. The drop at the beginning of the graph on Figure 5.2 is due to movement on the fibre that will be discussed in Section 5.4.4.

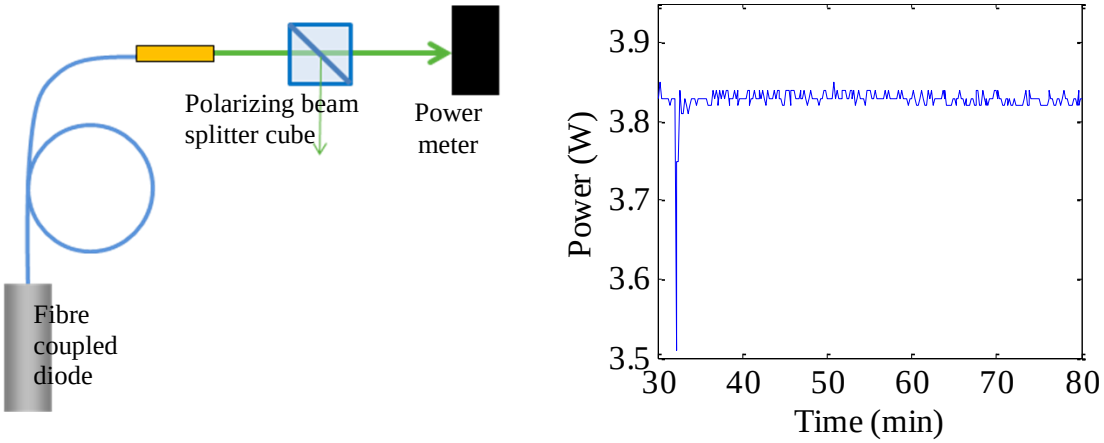

Figure 5.2 Power variation in time for a transmitted polarized beam showing polarization variation for the pump diode laser at 3.8 W input power.

5.3.1 Temperature Tuning

The fibre diode temperature, in contrast to the first oscillator built which was water-cooled (Chapter 2), was electrically controlled using a separate peltier element and a TEC driver. The diode was mounted on an aluminium plate, and the peltier located in the middle between the plate and the breadboard. The breadboard also served as a heat-sink for a proper heat removal from the peltier. An analysis of the variation of the diode wavelength with the temperature set by the TEC driver showed that only at certain temperatures was the diode wavelength the one needed for pumping the crystal. For lower drive currents and diode output powers the wavelength was as short as 968 nm (Figure 5.3). This diode was specified to produce 10 W of output power. Only above 7 A (5.9 W) did the wavelength shift to 980 nm, that needed for pumping the Yb:KYW laser. The change in wavelength as the power increased varied in 4 nm steps from 968 nm, slightly missing the exact wavelength of 981 nm needed for the optimum absorption in Yb:KYW.

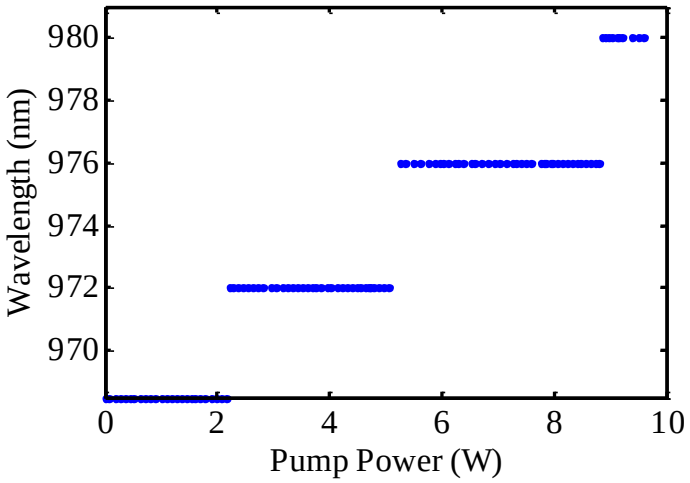

Figure 5.3 Wavelength variation with power at 33°C.

To get the correct value of the wavelength, and obtain the best efficiency of the device, it was necessary to vary the temperature of the diode for different drive currents (Figure 5.4). The best performance for an output wavelength of 980 nm was obtained when the diode was maintained at a temperature of 33°C. Finally the maximum power obtained at 11.5 A was 9.5 W at 980 nm instead of the 10 W ideal specification of the device.

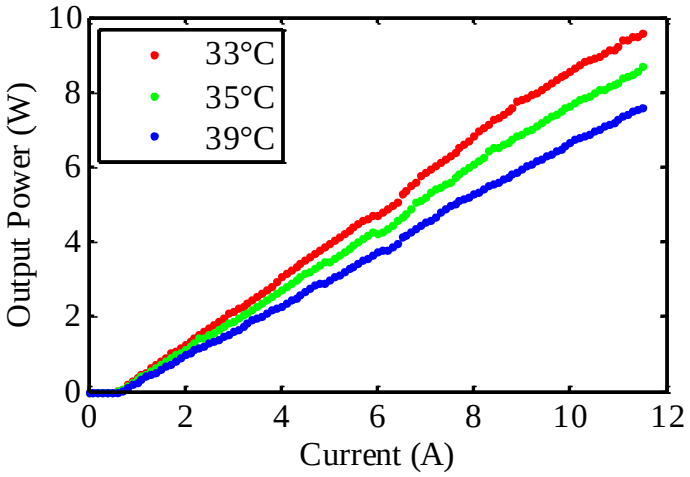

Figure 5.4 Output power at different temperatures.

5.4 The Yb:KYW Laser

5.4.1 Yb:KYW Crystal Mounting and Thermal Stabilization

The crystal was mounted on two copper plates above and below it, each with a peltier attached, in order to provide homogeneous control of the temperature though the crystal (see Figure 5.5). For this cavity the temperature scheme was changed from the previously water-cooled to an electronically controlled one. Both plates were attached to each other using plastic screws to reduce thermal coupling. A layer of indium foil was also used between the crystal and the copper plates to allow better temperature

exchange. Two TEC controllers were used to separately drive each of the peltiers, since the required cooling load was different due to the different thicknesses of the plates between each peltier and the crystal. It was also necessary to add two heat-sinks above and below the crystal, each one cooled by a fan, to avoid overheating and thus malfunctioning of the peltiers. The plates on which the crystal was sitting were isolated from the rest of the mount with a plastic layer on each leg, reducing the cooling load to only the small local area of the crystal.

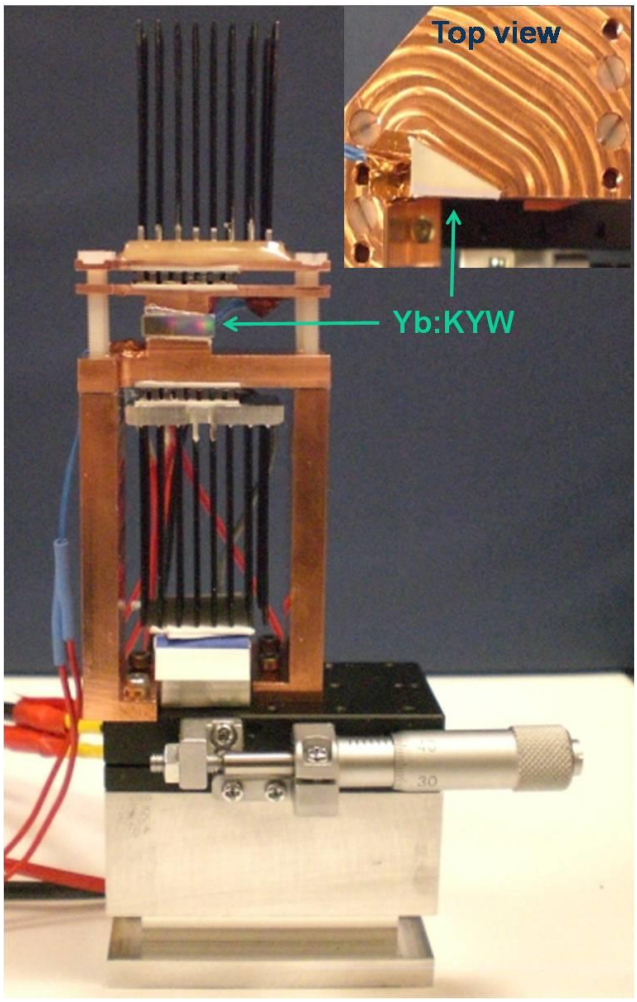

Figure 5.5 Crystal mount.

This mount was placed on a translation stage with movement along the direction parallel to the surface that acted as the end mirror.

5.4.2 CW operation of a 3 mirror cavity design

For this oscillator, a three mirror cavity was built with a plane-Brewster crystal as the gain material. Using this geometry allowed the study of the efficiency depending on the

variation of the thickness of the material. This also made it possible to use an unpolarised diode as a pump beam, as shown in Figure 5.6. In this cavity the crystal worked as an end mirror as well as a gain material.

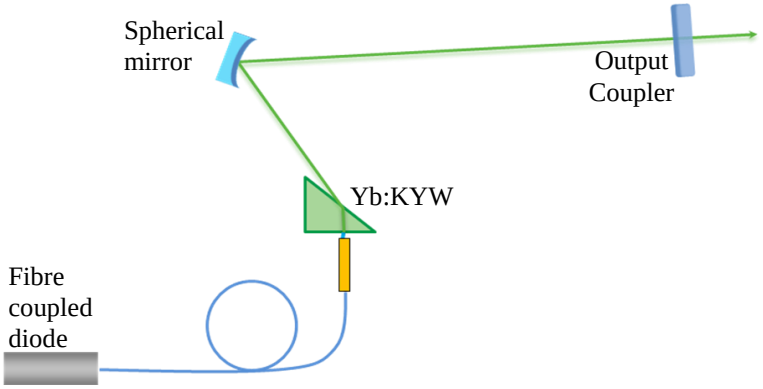

Figure 5.6 First cavity design.

Using the laser design package LCAV again to model the cavity, a first configuration was built comprising three mirrors and the gain material as shown in Figure 5.6. The pump beam was placed directly next to the plane surface of the crystal; this is possible because the core size of the fibre (105 μm) matches the lasing mode, which means that the beam size of the pump in the crystal will be the same size as the fibre core that is comparable to the lasing beam size of ~120 μm (see Figure 5.7). This pumping scheme also makes an improvement from the previous design because the system can be mode-matched to a smaller spot size in the crystal. After the beam enters the crystal it was expanded until it reached the spherical mirror which focused the beam again to the output coupler. The fibre had an angle cut at the output to avoid back reflections from the crystal. Different spherical mirrors were tested to get the best efficiency of the system and find the most convenient arrangement for every element used.

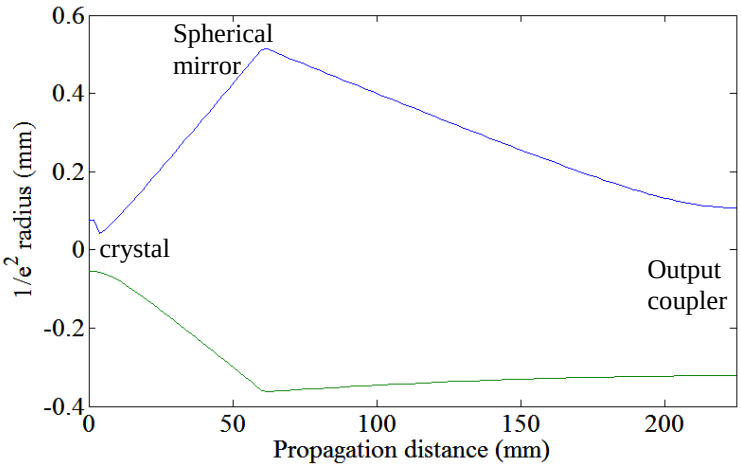

Figure 5.7 Beam propagation through the cavity showing the tangential beam radius in blue and the saggital beam radius in green.

The compactness of the pump diode and the fact that it was fibre coupled reduced significantly the space occupied by the device (Figure 5.8). The crystal, as mentioned before, was coated on the plane surface to reflect 1030 nm and transmit 980 nm, to act as an end mirror on the cavity. The spherical mirror was coated for >95% transmittance from 979-983 nm and ≥ 99.9% reflectance at 1035 nm. A set of output couplers with different transmissions was used at one end of the cavity. The temperature of the crystal was kept at 18°C.

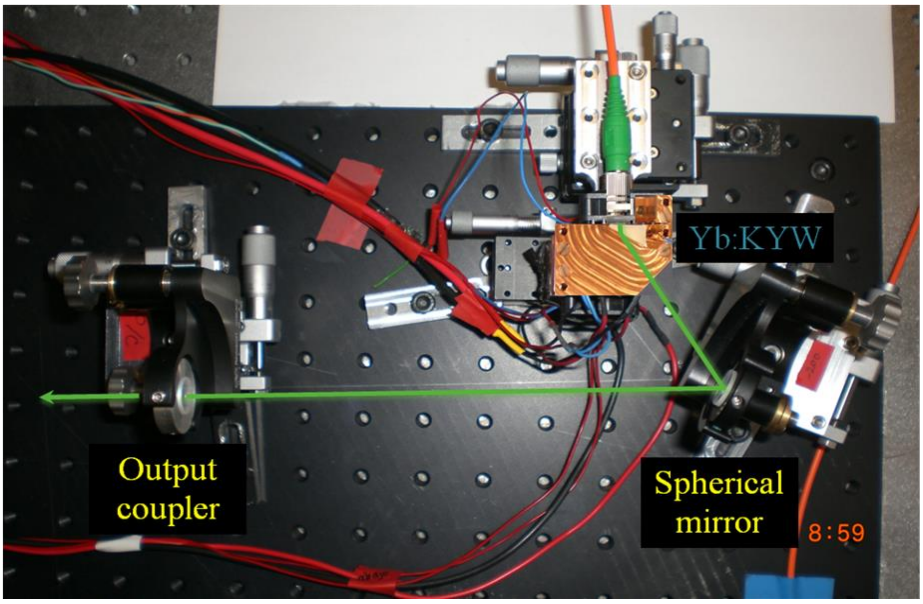

Figure 5.8 Three mirror cavity.

Performance as a function of crystal thickness

As mentioned before the plane-Brewster crystal was pumped through the plane HR-coated surface. Its mount allowed for the crystal to be moved in the direction

perpendicular to the beam, making it possible to vary the thickness of the crystal used in the laser. For this particular crystal it was not possible to obtain laser oscillation close to the edges of the crystal. The operation was possible throughout the middle section of the crystal, with the best efficiency at 1.87 mm thickness as shown in Figure 5.9. For this measurement the diode was set at a current of 9 A corresponding to 7 W of pump power.

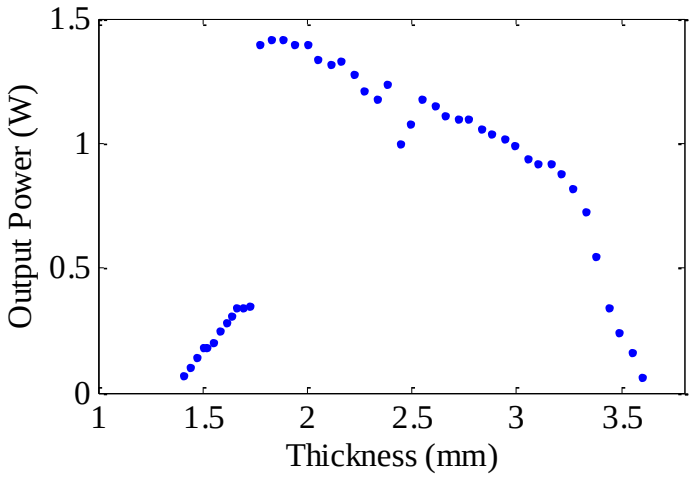

Figure 5.9 Output power for different thickness of the crystal used in the oscillator using a 10% output coupler and a -200 mm radius of curvature mirror.

The experiment was carried out starting from the thinnest part of the crystal to the thickest part, or from right to left according to Figure 5.5. The measurements were taken every 0.05 mm.

With this cavity a set of spherical mirrors was used to characterize the system. Three different curvatures were used: -100 mm, -150 mm and -200 mm.

-100 mm RoC mirror cavity

Using a -100 mm RoC as the spherical mirror in the configuration shown in Figure 5.6, the cavity was built based on the calculations of the design package. The configuration had a distance of 58.8 mm between the crystal and the spherical mirror and 165 mm between the spherical mirror and the output coupler. The total cavity had a length of 225.7 mm on a single pass of the beam. The angle of incidence on the spherical mirror was 28°. Figure 5.7 shows the beam diameter at different positions inside this cavity modelled with LCAV. For this case the beam diameter at the plane surface of the crystal is 129 μm, at the spherical mirror the beam diverges to a spot size of 876 μm, and at the

output coupler the beam diameter is 428 μm. Using this cavity a slope efficiency of 45% was obtained as shown in Figure 5.10.

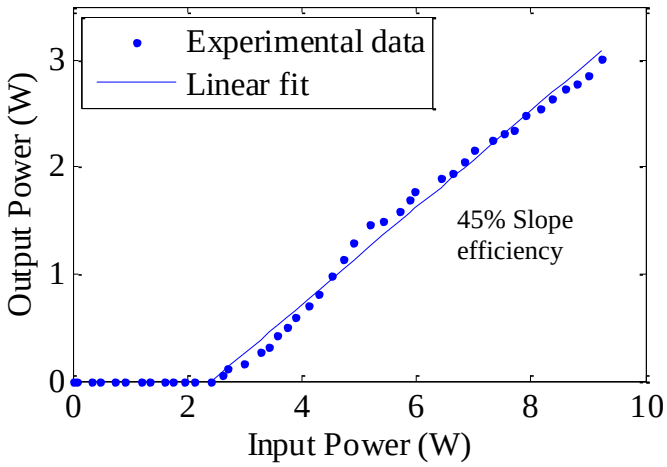

Figure 5.10 Average output power of the oscillator versus pump power.

A Rigrod analysis [6] was carried out at 8.5 W input power (Figure 5.11). Using a range of output couplers of 5%, 7.5%, 10%, 15% and 25% transmission, the best efficiency was found with a 10% output coupler, with parasitic losses of 3%, and an unsaturated gain of 1.42. The average output power was 3.01 W at the maximum input power of 9.5 W.

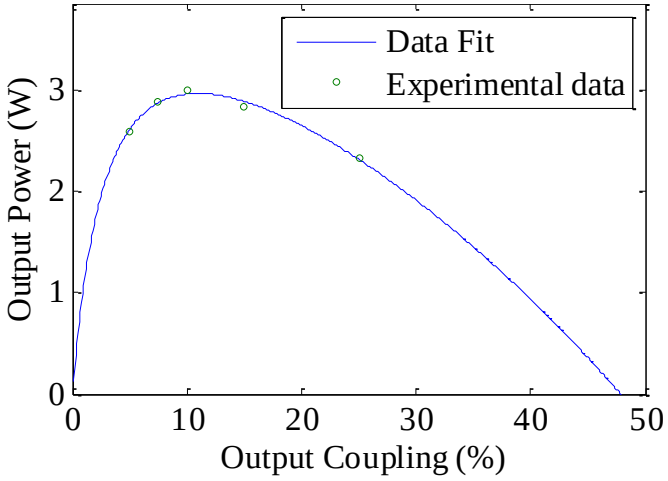

Figure 5.11 Rigrod analysis showing the best efficiency at 10% output coupler transmitance.

-150 mm RoC mirror cavity

When using the -150 mm RoC mirror, the distances between the mirrors had to be modified to get the correct spot size on the crystal compensating for astigmatism. In this case the distance between the crystal and the spherical mirror was 84.5 mm, and the distance from the spherical mirror and the output coupler was 343 mm. The angle of incidence on the spherical mirror was set to 24°. Using these distances the beam size

($1/e^2$ beam diameter) on the plane surface of the crystal was 123 µm, on the spherical mirror it expanded to 1.311 mm and on the output coupler was 615 µm (Figure 5.12(b)). Because the distances inside the cavity changed, when using this mirror the total cavity length was 429.4 mm. Using a 10% transmittance output coupler, the best output power achieved was 2.87 W (see Figure 5.14).

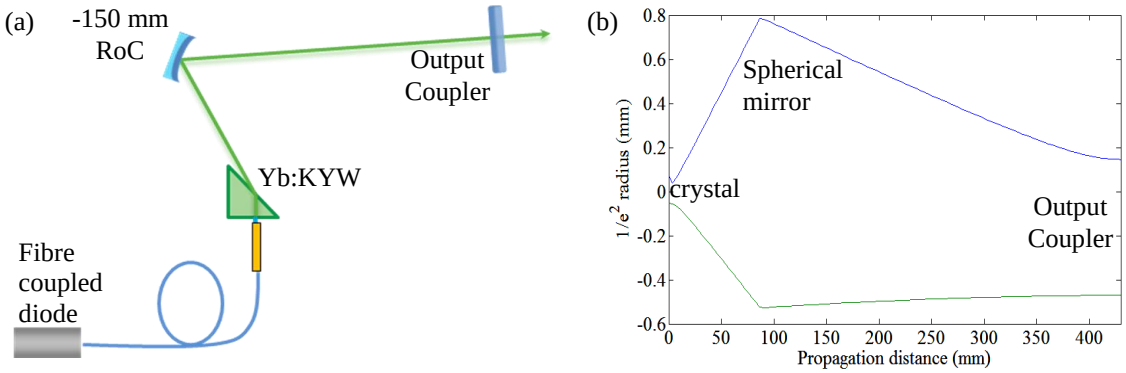

Figure 5.12 (a) Cavity configuration using a -150 mm RoC mirror and (b) beam width as it travels through the cavity.

-200 mm RoC mirror cavity

From the calculation using the laser design software for this cavity, the stability region using a -200 mm curvature mirror was found to be larger than the previous two cases. The distances in this case were 110 mm from the crystal to the spherical mirror and 620 mm from the spherical mirror to the output coupler. An angle of 20° was used for the incidence on the spherical mirror for best efficiency. In this case the beam sizes were 115.7 µm in the crystal, 1.838 mm on the spherical mirror and 750 µm on the output coupler (Figure 5.13). This configuration gave a closer mode-match between the pump and the lasing beams.

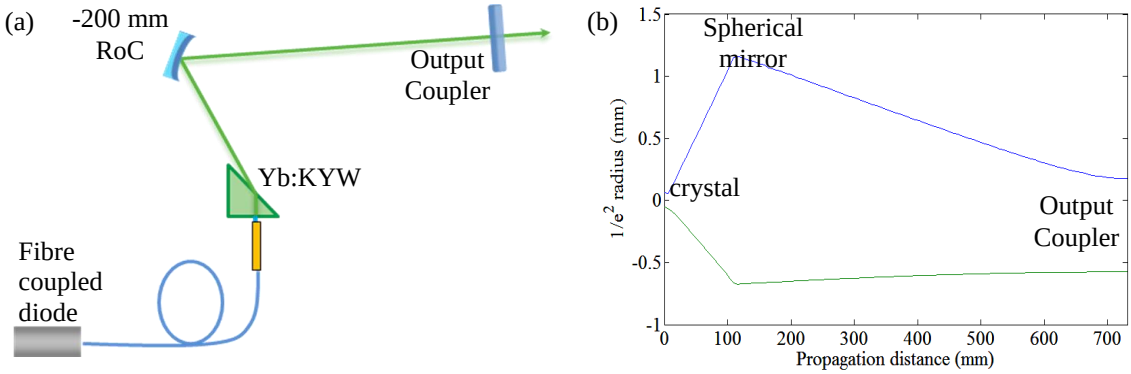

Figure 5.13 (a) Cavity configuration with a -200 mm RoC mirror and (b) beam width through the cavity.

The total cavity length in this case was 731.9 mm. The best output power was found again with a 10% output coupler, obtaining 2.79 W. Figure 5.14 shows the output performance for the different spherical mirrors used.

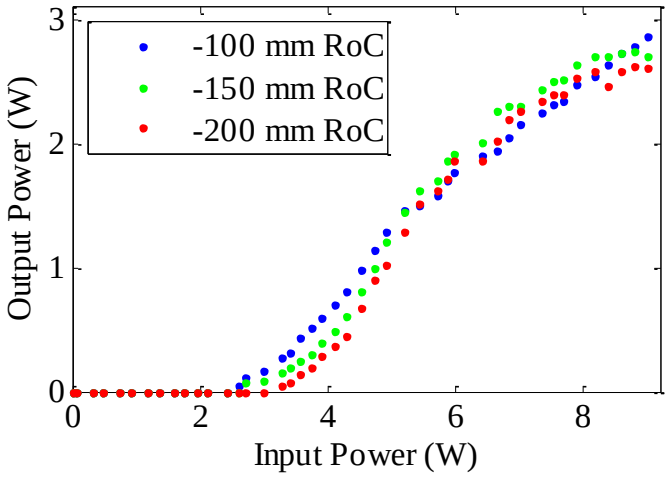

Figure 5.14 Output power using different spherical mirrors and a 10% output coupler.

The main characteristics of the three cavities are shown in Table 5.1, where D1 corresponds to the distance between the crystal and the spherical mirror, and D2 to the distance from the spherical mirror to the output coupler. In the table is shown the angle of incidence on the spherical mirror.

Table 5.1 Parameters obtained using different radius of curvature mirrors.

RoC Spherical Mirror (mm)	D1 (mm)	D2 (mm)	Incidence angle (°)	Output Power (W)	Slope Efficiency (%)	Cavity length (mm)
-100	58.8	165	28	3.01	45	225.7
-150	84.5	343	24	2.87	49	429.4
-200	110	620	20	2.79	48	731.9

5.4.3 CW operation of a 4 mirror cavity design

According to the calculations made by using the laser design software, the divergence of the intracavity beam that comes directly from the AR-coated crystal face grows as it travels through and after the crystal until it reaches the spherical mirror. After that, the beam is focused again. To get modelocked operation, a SESAM was again used in the cavity. To achieve a suitable spot size on the SESAM, it was necessary to place it between the crystal and the spherical mirror, which is the only place where the size is small enough to get the saturation fluence necessary to obtain modelocking. To set this up, a plane mirror (HR mirror coated for >95% transmittance from 979-983 nm and ≥99.9% reflectance at 1035 nm) was first placed on the position where the absorber would later be.

Because the distance from the crystal to the spherical mirror is very short for the three cavities mentioned in Section 5.4.2, the most suitable design for inserting a mirror in this place was the cavity containing the -200 mm radius spherical mirror. The system using this spherical mirror was folded after the crystal with a plane mirror as shown in Figure 5.15(a).

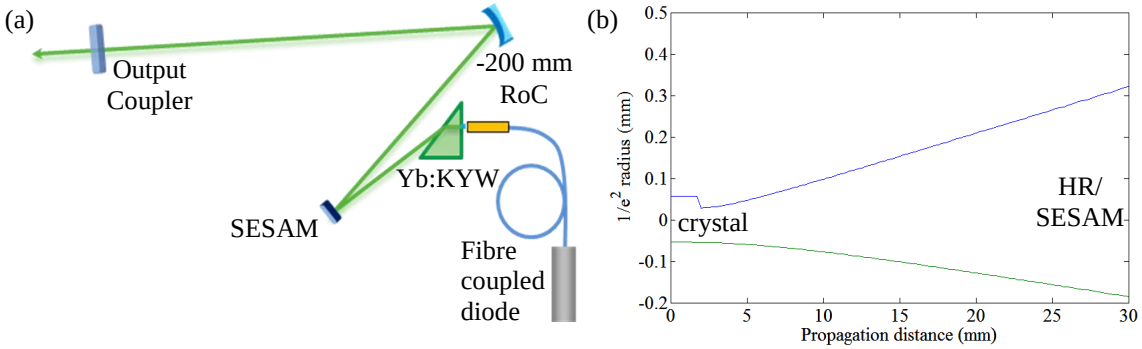

Figure 5.15 Four mirror cavity design.

For this new configuration the HR mirror was placed at 30 mm from the crystal. At this point the beam diameter on the HR was 507.7 µm as shown in Figure 5.15(b). To keep the cavity with the same parameters as the one discussed in the previous section the spherical mirror was placed at 80 mm from the HR. The angle formed by the incident and the reflected beam on the HR was set to 10 degrees. The incidence angle of the beam on the spherical mirror was kept at 20° as before. After the cavity was optimized, the HR was replaced for a SESAM to get modelocking. Using a 10% output coupler an output power of 2.80 W was obtained with a slope efficiency of 44% (Figure 5.16).

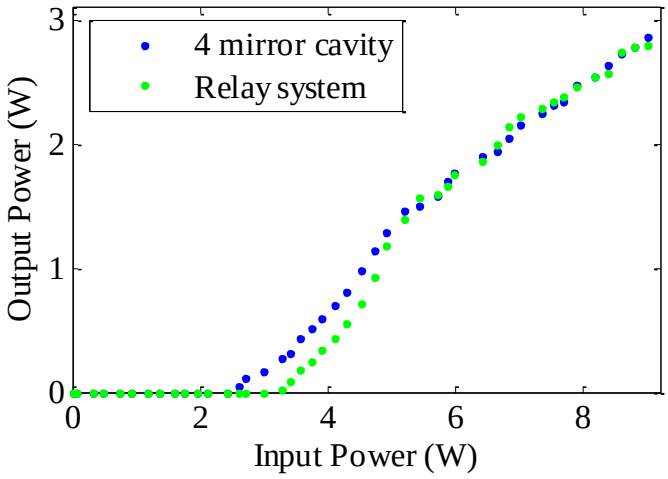

Figure 5.16 Output power for two cavity lengths, the short cavity with a 4 mirror arrangement and the cavity including a relay system.

5.5 Cavity length extension using relay imaging

This cavity was built as an improvement for the one described in Chapter 2, therefore their operating characteristics had to be made similar. In order to have a repetition frequency closer to the one provided by the previous oscillator, a relay system was added to the cavity (Figure 5.17). This relay system consisted of four extra mirrors; two of them were -1000 mm RoC, and had a negative dispersion of -600 fs^2, and the other two were GTI mirrors, one of them with a -1300 fs^2 negative dispersion, and the last element being the output coupler. The mirror that was on the output coupler position for the previous cavity was replaced by a plane GTI mirror with a GDD of -1300 fs^2. The cavity repetition frequency was 54.8 MHz.

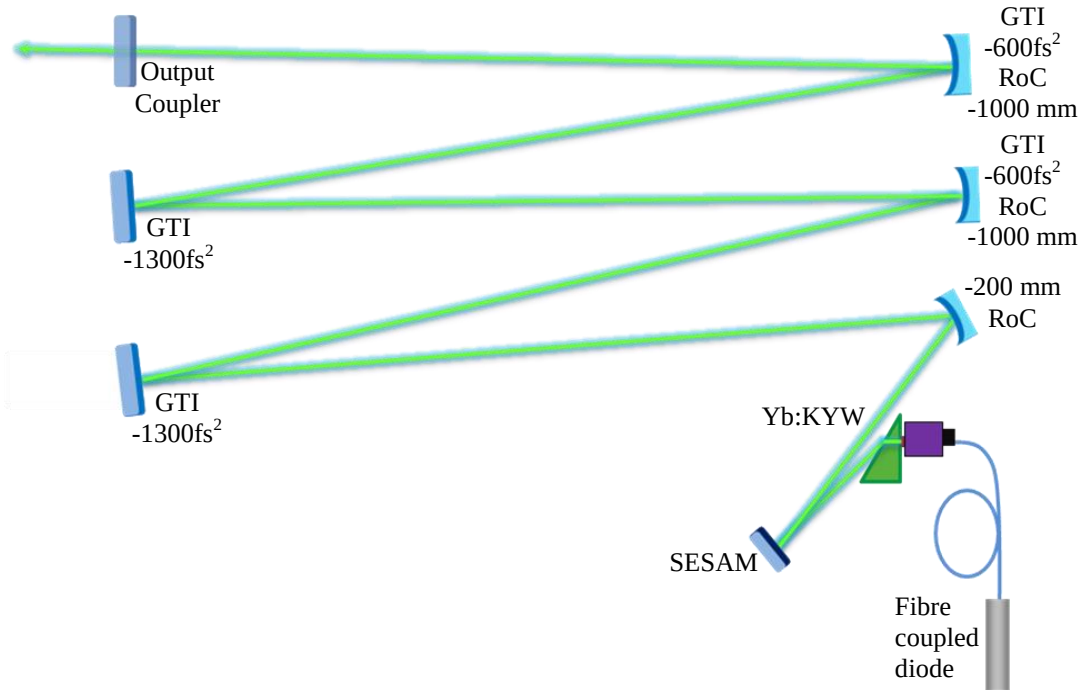

Figure 5.17 Layout of the 54 MHz Cavity.

The distances between each of the extra mirrors was 500 mm, and the folding angles were maintained at 10 degrees in each bounce, to avoid unwanted effects and to control the spot size at the end of the cavity. The beam sizes at the crystal and the SESAM were maintained at 112 μm and 507 μm respectively whilst the size on the output coupler was 743 μm as shown in Figure 5.18, similar to the short cavity configuration using only 3 and 4 mirrors. The total length of this cavity was 2732 mm single pass.

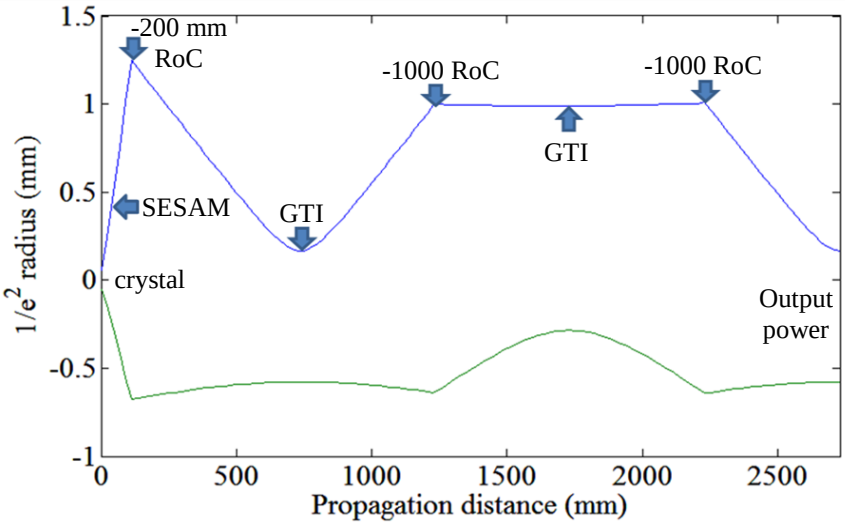

Figure 5.18 Beam propagation through the extended cavity showing the tangential beam radius in blue and the saggital beam radius in green.

Insertion of the extra mirrors comprising the relay system made the laser have higher losses, and thus the output power decreased. A new Rigrod analysis [6] was made for this cavity (Figure 5.19) obtaining the best output coupling for 7.5 % transmittance, with parasitic losses of 2%.

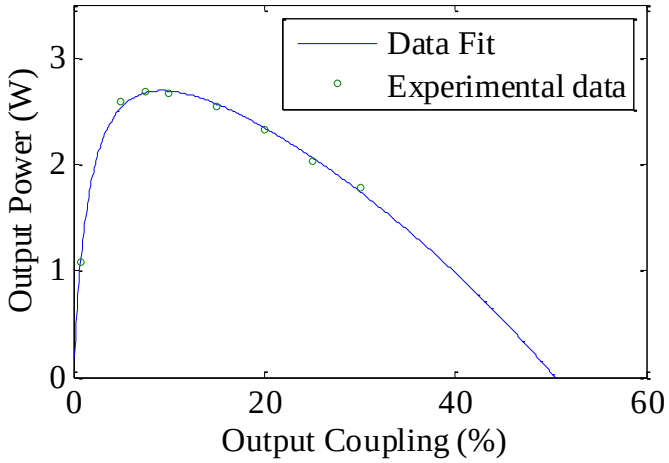

Figure 5.19 Rigrod analysis [6] for output couplers between 0.8 and 30% transmission.

As discussed previously in Chapter 2, the wavelength required for the oscillator was 1032 nm. From the data on Table 5.2 it was decided to use the 10% transmittance output coupler to obtain the wavelength needed [7], which gave almost the same output power as the 7.5% transmittance, for a pump power of 9 W at 980 nm.

Table 5.2 Parameters obtained varying the output coupling transmission.

Output Coupler (%)	Output Power (W)	Laser λ (nm)
0.8	1.08	1051.0
5.0	2.60	1038.5
7.5	2.69	1035.0
10.0	2.67	1032.0
15.0	2.55	1031.0
20.0	2.33	1030.0
25.0	2.03	1029.5
30.0	1.79	1026.0

Section 5.1 mentioned how polarization can vary when travelling through fibres [2, 3]. In this oscillator, because a fibre coupled diode was used, the polarization of the beam that comes out of the fibre can change if the fibre is put under any kind of external stress. When the fibre path was moved, the power of the oscillator varied depending on the fibre position. To increase the efficiency of the laser it was necessary to optimize the polarization state leaving the fibre. As mentioned before, the fibre polarization can be controlled by bending the fibre [3]. The fibre from the laser diode was formed into a loop and positioned so that the best efficiency of the oscillator was achieved; by doing this the power of the oscillator was increased to 2.94 W with a 62% average slope efficiency.

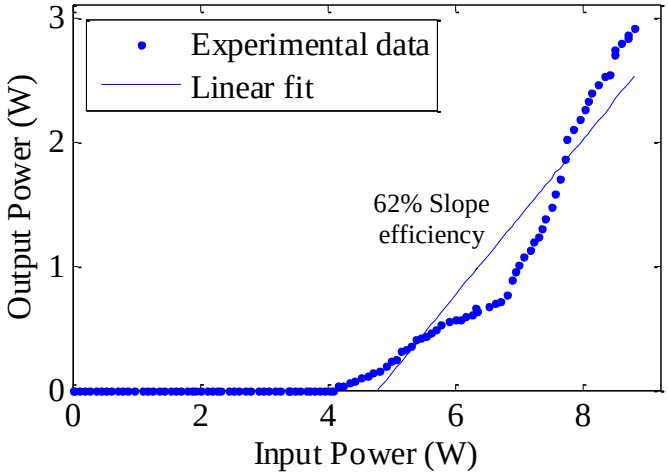

Figure 5.20 Output power of the extended cavity.

5.6 Modelocked Operation of the Yb:KYW Laser

Modelocked operation for this oscillator was achieved using again the set of SESAMs described in Chapter 2. In this case, again because of the high intracavity powers (29.4 W) and the pulse durations expected (~500 fs), after testing the other SESAMs mentioned in Chapter 2, the best option was the 1.5 % absorbance SESAM (BATOP model SAM-1040-1.5-x-1ps). The saturation fluence was 70 μJ/cm^2, and the

modulation depth was 0.8%. The SESAM replaced the HR mirror next to the crystal (Figure 5.21). At this position the spot size on the SESAM had a calculated diameter of 524 μm.

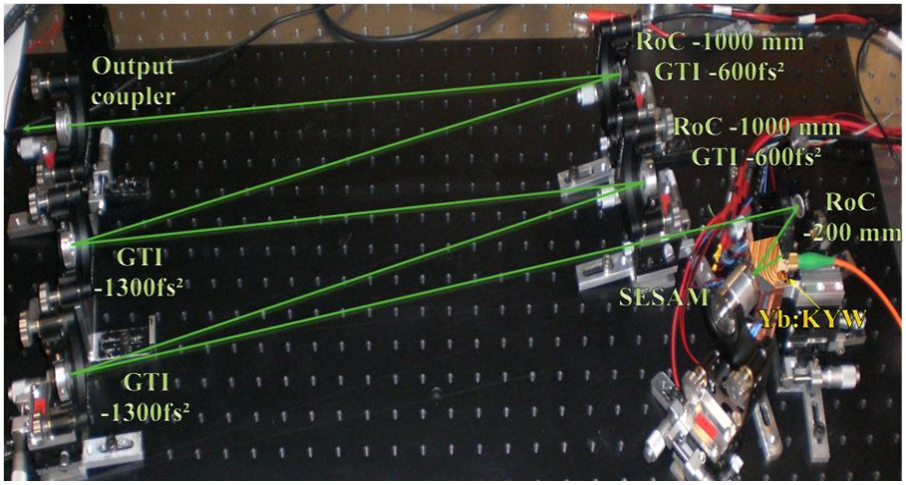

Figure 5.21 Complete cavity configuration (54 MHz).

The high positive dispersion generated by the Yb:KYW crystal in this oscillator, the same as in the case of the previous oscillator (Section 2.5.4), had to be compensated as before. Four of the mirrors used in this cavity were GTI mirrors with different amount of negative dispersion, as described before; nevertheless the negative dispersion was not enough to get stable modelocking, the same as in the previous case where the spectrum for low negative dispersion showed a poor modelocking (Figure 2.26). To find the correct amount of negative dispersion needed for this configuration, one of the GTI mirrors with -1300 fs^2 was replaced by a GTI mirror with -800 fs^2. Then again two mirrors with -1300 fs^2 dispersion were placed between the last two mirrors of the cavity to make bounces on them and get the best performance of the oscillator as shown in Figure 5.22.

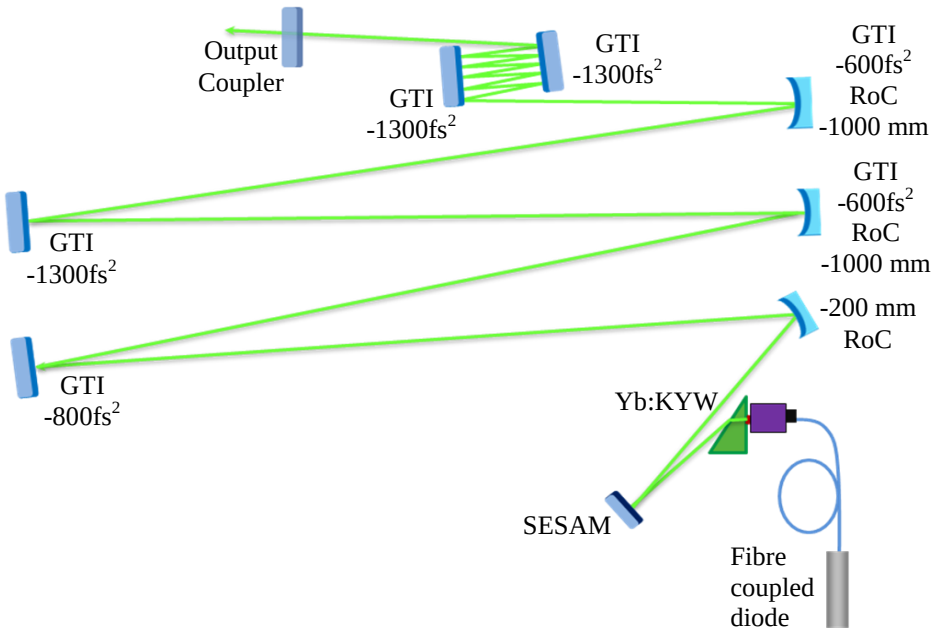

Figure 5.22 GDD compensation using bounces on GTI mirrors. As mentioned previously the fibre was placed next to the plane surface of the crystal.

One to seven bounces were analysed. Table 5.3 shows the data obtained on each bounce on both GTI mirrors. For the first two configurations stable modelocking could not be achieved.

Table 5.3 Output data for different bounces though the GTI mirrors.

No of bounces	Output Power (W)	GDD (fs^2)	$\Delta\tau$ (fs)	Bandwidth (nm)	$\Delta\nu\Delta\tau$
1	2.7	-11800	Not stable	--	--
2	2.55	-17000	Not stable	--	--
3	2.55	-22200	629.9	1.65	0.29
4	2.49	-27400	526.2	2.08	0.30
5	2.48	-32600	591.7	2.1	0.35
6	2.34	-37800	611.3	1.97	0.34
7	2.30	-43000	718	1.75	0.34

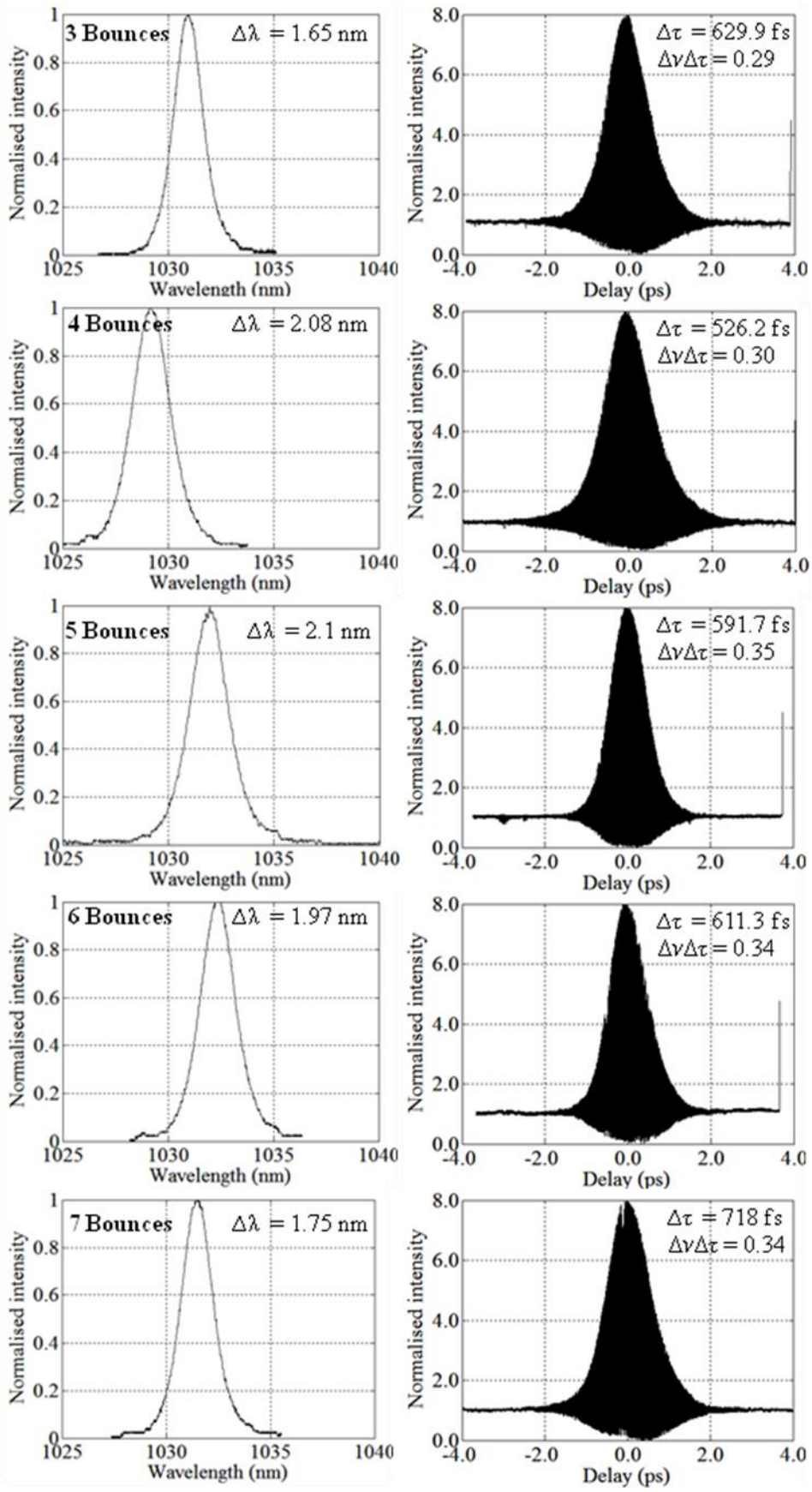

Figure 5.23 Spectrum and interferometric autocorrelation for different number of bounces on the GTI mirrors

Figure 5.23 shows the variation of the spectrum and the interferometric autocorrelation containing the pulse duration for all the bounces on the GTI mirrors in which stable modelocking was achieved. From these results, it was found that the optimum amount of GDD compensation producing the shortest bandwidth limited pulses was -27000 fs^2.

After analysing the system for dispersion compensation the GTI mirrors used for the analysis were taken out of the cavity, and the GTI mirror with -800 fs^2 was replaced with a -10000 fs^2 GTI mirror; with this and the previous dispersion introduced by the other mirrors the total final negative dispersion used was -25000 fs^2. This final oscillator system had an average output power of 2.42 W using an output coupler of 10% transmittance. The pulses obtained had a duration of 521.8 fs with a bandwidth product of 0.31 for $sech^2$-shaped pulses, similar to the pulse duration obtained with the oscillator described in Chapter 2. The bandwidth product in this case was closer to the value of 0.315 for $sech^2$-shaped pulses, than that the one of the previous oscillator where this was 0.39. Figure 5.24 shows the spectrum and autocorrelation for the final system.

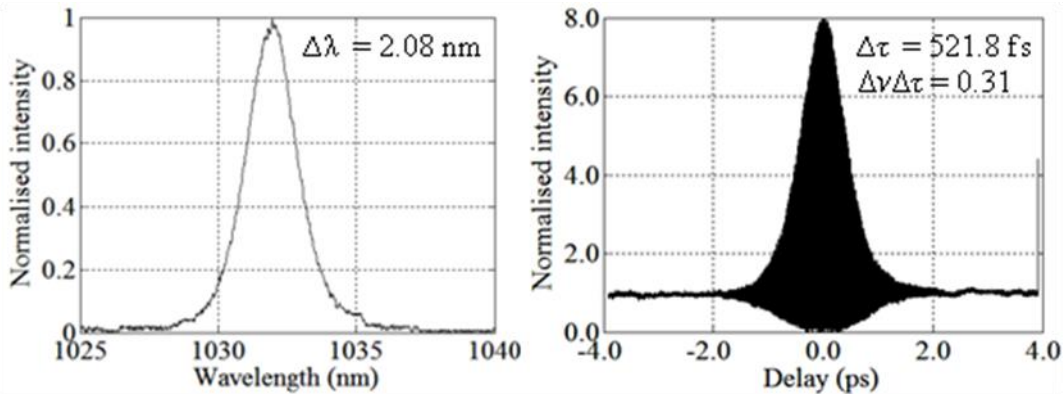

Figure 5.24 Spectrum and interferometric autocorrelation for the 54 MHz cavity.

Beam quality analysis was made for the output beam from the cavity. In this case instead of the knife-edge method a beam profiler (Thorlabs model BP109-IR) was used, which included beam analysis software that shows the beam diameter data before and after a 150 mm lens and an M^2 fit for both axes of the beam. Figure 5.25 shows the results revealing that M^2_x = 1.46 and M^2_y = 1.93. The beam diameter on the output coupler was 2.04 mm in the horizontal direction and 1.96 mm in the vertical direction.

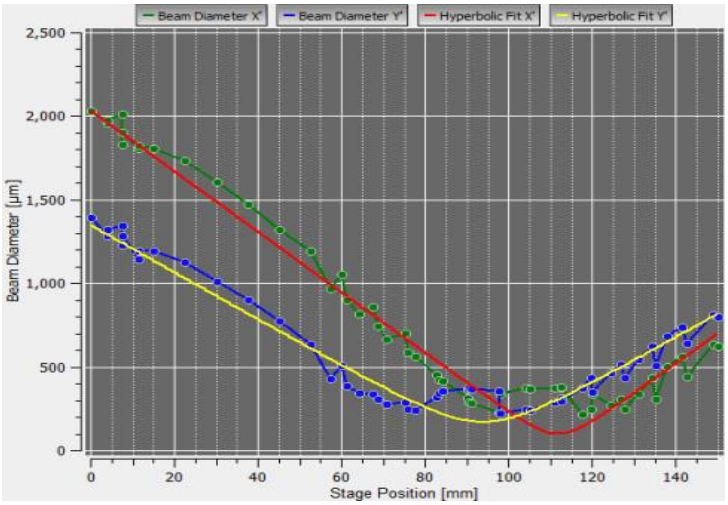

Figure 5.25 M^2 analysis for 54 MHz cavity.

5.7 100 MHz Cavity

The cavity configuration needed to get a 54 MHz repetition frequency required the addition of four extra mirrors to the main cavity. Because with this configuration it was possible to vary the repetition frequency as needed, a study of the cavity was made using only two extra mirrors instead of four. One spherical mirror of -1000 mm RoC was removed from the cavity, and the GTI mirror of -1300 fs^2 dispersion was replaced with the output coupler (Figure 5.26), so that the total GDD of the system was reduced to -21200 fs^2. The rest of the cavity was kept the same as in the 54 MHz design.

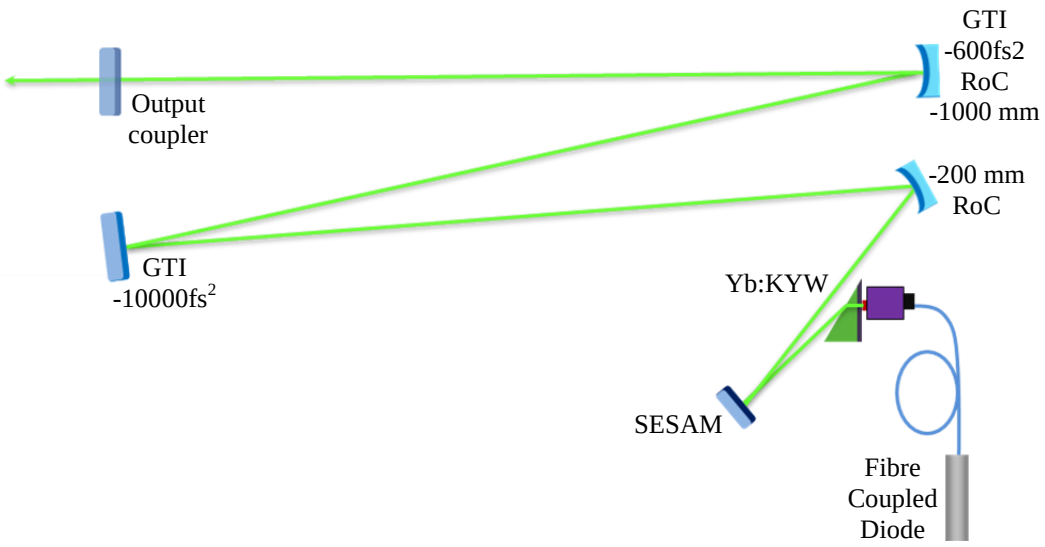

Figure 5.26 Layout of the 100 MHz cavity.

In this case the beam sizes in each element increased to 113.8 µm in the crystal, 526.7 µm in the SESAM and 1.242 mm in the output coupler as shown in Figure 5.27.

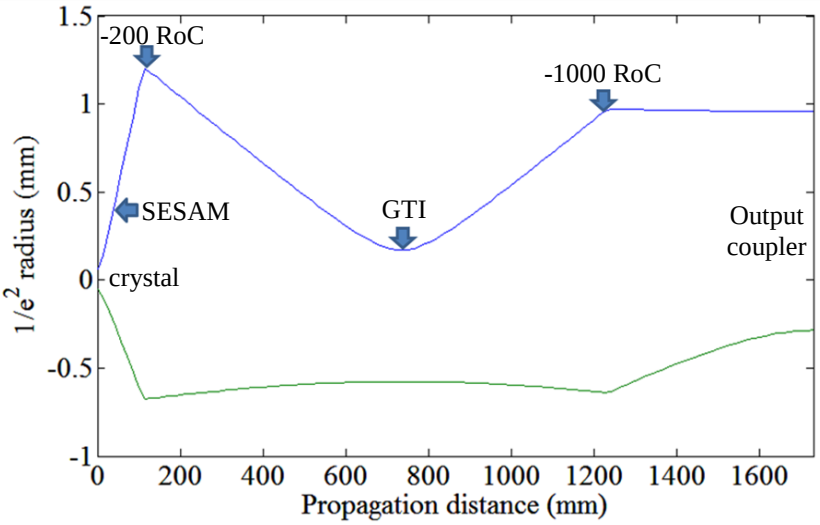

Figure 5.27 Beam propagation through the 100 MHz cavity showing the tangential beam radius in blue and the saggital beam radius in green.

This cavity had a repetition frequency of ~100 MHz. The output power of the cavity was 2.53 W at 1032 nm with a 56% average slope efficiency (Figure 5.28).

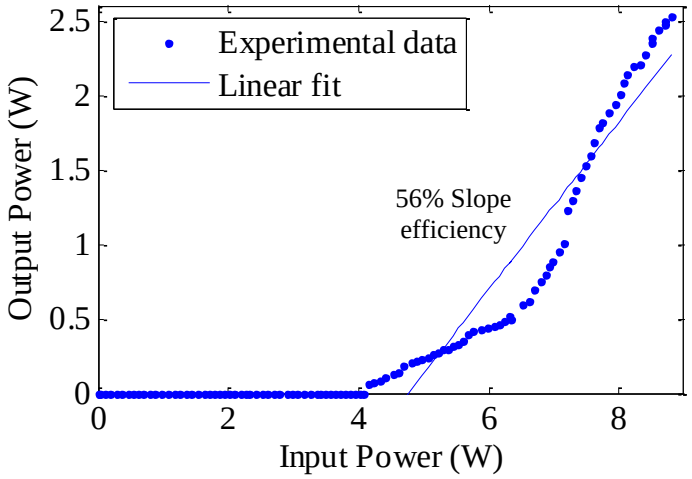

Figure 5.28 Output power of the 100 MHz cavity.

SESAMs are commonly used for achieving CW modelocking in solid state lasers [5,8-11]. Nevertheless, if the parameters for a SESAM are not chosen correctly to obtain stable modelocking, then some instabilities can be generated. In such cases, multipulsing of the system or Q-switched modelocking can be observed [12,13].

In the case of the cavity described before (54 MHz repetition-frequency), because it was the one that was required to be as close to the characteristics of the oscillator built previously, the correct parameters of the system and the SESAM were investigated to get stable CW modelocking. CW modelocking is observed when the instantaneous

power shows a train of modelocking pulses with amplitude stability [12]. For this cavity the instantaneous power as a function of time is shown in Figure 5.29. Compensating the GDD and having the correct beam size on the SESAM for the pulse energy generated, allowed stable CW modelocking behaviour of the system.

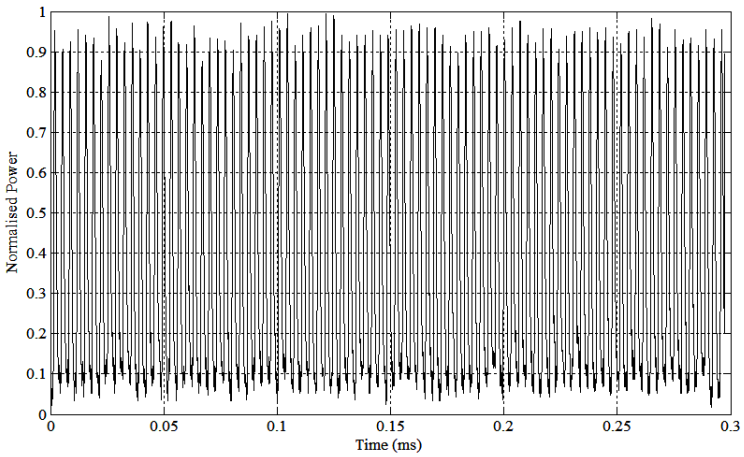

Figure 5.29 CW Modelocking of the 54 MHz cavity.

However, by modifying the cavity repetition rate from 54 MHz to 100 MHz, The parameters for stable CW modelocking changed; in that case the system oscillations became unstable and the system shifted from CW modelocking to Q-switched modelocking. When Q-switching occurs the power from the laser is modulated periodically over many round trips of the cavity [14]. Figure 5.30 shows Q-switching mode of the 100 MHz cavity.

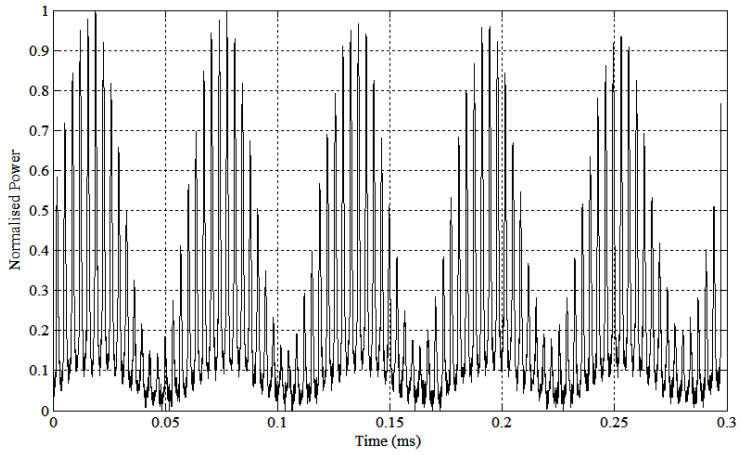

Figure 5.30 Q-switched modelocking of the 100 MHz cavity.

5.8 Conclusions

In this chapter, a new oscillator has been described which had a different geometry design than the one described in Chapter 2. This configuration used a 5 at.% Yb:KYW crystal with a plane-Brewster cut. The crystal was HR coated on its plane surface to act as an end mirror of the cavity. The cavity was pumped by a fibre-coupled diode laser which gave 9 W at 980 nm. Four GTI mirrors were used to compensate for GDD. Two of those mirrors were plane mirrors with a negative dispersion of -10000 fs^2 and -1300 fs^2, and the other two were spherical mirrors with -1000 mm radius of curvature and -600fs^2 GDD. Those two spherical mirrors with a -200 mm RoC were used to control the beam size through the cavity. The best efficiency of the system was found using a 1.5% absorbance anti-resonant SESAM and a 10% output coupler. The SESAM was placed 30 mm away from the gain material which resulted in a 260-μm spot diameter being formed on it. The first spherical mirror with -200 mm RoC was 80 mm from the SESAM at a 10 degree folding angle. A first GTI mirror was placed at 620 mm from the spherical mirrors. The rest of the elements were collocated at 500 mm from each other.

The final configuration was modified so that the total repetition frequency was 54 MHz. This cavity had an average output power of 2.42 W at 1032 nm. Modelocking was achieved by introducing a total GDD of -25000 fs^2 into the cavity. Pulses of 521 fs were achieved for a bandwidth of 2.08 nm and a duration bandwidth product of 0.31, making an improvement from the value of 0.39 obtained with the first configuration (Chapter 2). Beam quality parameters for this system were measured to be M^2_x = 1.46 and M^2_y = 1.93. The final configuration proved to be more convenient than the oscillator described in Chapter 2 due to its compactness and the way it was pumped.

It was also shown that the cavity could be modified to operate at different repetition frequencies. The parameters needed to achieve CW modelocking with the same SESAM were different. CW modelocking was obtained for a 54 MHz configuration, whilst Q-switched modelocking was achieved for a 100 MHz cavity.

Due to the improvements of this system over the first oscillator built, this configuration was used for an application different from the MOPA. In this case it was the implementation of the oscillator as a pump for an optical parametric oscillator.

5.9 References

[1] N. V. Kuleshov, A. A. Lagatsky, V. G. Shcherbitsky, V. P. Mikhailov, E. Heumann, T. Jensen, A. Diening, and G. Huber, "CW laser performance of Yb and Er,Yb doped tungstates," Applied Physics B: Lasers and Optics **64**, 409–413 (1997).

[2] G. P. Agrawal, *Nonlinear fiber optics* (Academic Press, 2001).

[3] R. Ulrich and A. Simon, "Polarization optics of twisted single-mode fibers.," Applied Optics **18**, 2241–2251 (1979).

[4] G. H. Kim, J. Yang, E. Sall, S. Chizhov, A. Kulik, D. Lee, U. Kang, and V. Yashin, "Development of Compact Femtosecond Yb : KYW Oscillators : Simulation and Experiment," Journal of the Korean Physical Society **61**, 365–370 (2012).

[5] S. A. Meyer, J. A. Squier, and S. A. Diddams, "Diode-pumped Yb:KYW femtosecond laser frequency comb with stabilized carrier-envelope offset frequency," The European Physical Journal D **48**, 19–26 (2008).

[6] W. W. Rigrod, "Homogeneously Broadened C W Lasers with Uniform Distributed Loss," IEEE Journal of Quantum Electronics **29**, 377–381 (1978).

[7] A. A. Lagatsky, N. V Kuleshov, and V. P. Mikhailov, "Diode-pumped CW lasing of Yb : KYW and Yb : KGW," Optics Communications **165**, 71–75 (1999).

[8] G. R. Holtom, "Mode-locked Yb:KGW laser longitudinally pumped by polarization-coupled diode bars.," Optics letters **31**, 2719–2721 (2006).

[9] A. A. Lagatsky, E. U. Rafailov, A. R. Sarmani, C. T. A. Brown, W. Sibbett, L. Ming, and P. G. R. Smith, "Efficient femtosecond green-light source with a diode-pumped mode-locked Yb^{3+}:$KY(WO_4)_2$ laser.," Optics Letters **30**, 1144–1146 (2005).

[10] M. Siegel, J. Aus-der-Au, and A. Guandalini, "High Repetition Rate Cavity-Dumped Yb:KYW Femtosecond Oscillator," Conference on Lasers and Electro-Optics 2010 CTuV4 (2010).

[11] A. A. Lagatsky, E. U. Rafailov, C. G. Leburn, C. T. A. Brown, N. Xiang, O. G. Okhotnikov, and W. Sibbett, "Highly efficient femtosecond Yb:KYW laser pumped by single narrow-stripe laser diode," Electronics Letters **39**, 1108–1110 (2003).

[12] C. Hönninger, "Q -switching stability limits of continuous-wave passive mode locking," Journal of the Optical Society of America B **16**, 46–56 (1999).

[13] U. Keller, K. J. Weingarten, X. K. Franz, D. Kopf, B. Braun, I. D. Jung, R. Fluck, H. Clemens, N. Matuschek, and J. A. Der Au, "Semiconductor Saturable Absorber Mirrors (SESAM ' s) for Femtosecond to Nanosecond Pulse Generation in Solid-State Lasers," IEEE Journal of Quantum Electronics **2**, 435–453 (1996).

[14] F. X. Kärtner, L. R. Brovelli, and U. Keller, "Control of solid state laser dynamics by semiconductor devices," Optical Engineering **34**, 2024–2036 (1995).

Chapter 6

Femtosecond Yb:YAG oscillator and comparative analysis with Yb:KYW oscillator

6.1 Introduction

The amplifier used in this project (Chapters 3 and 4) was based on an Yb:YAG planar waveguide. For this reason we investigated the possibility of also basing our oscillator on Yb:YAG gain material. This would ensure that the wavelength of the seed pulses was always well matched to the gain profile of the amplifier, in turn guaranteeing the optimum efficiency from the complete system.

6.2 Yb:YAG

6.2.1 Properties and femtosecond pulse generation

Yb:YAG crystals provide advantages as a gain material in high power oscillators, due to their low quantum defect of a fraction of 0.11 which reduces the thermal effects. As shown in Figure 3.1 its energy level transitions involve only the $^2F_{5/2}$ and the $^2F_{7/2}$ manifolds making it suitable for near-infrared applications at 1030 and 1050 nm. The broad gain bandwidth in these materials allows for the tunability of the oscillators and the generation of ultrashort pulses [1]. Also its pump transition wavelength at 941 nm makes it suitable for pumping with commercially available diodes as is also the case for Yb:KYW.

6.2.2 Review of previous Yb:YAG laser oscillators

In the past, different configurations of Yb:YAG lasers have been developed for a number of applications, producing output powers up to 4 kW for an amplifier configuration in CW operation [2], and ~900 W for amplified pulses [3]. Some of these configurations achieved femtosecond pulses [3-5], with a pump wavelength of 940 nm and doping of ~10 at % of the crystal. In those cases, pulses at 1030 nm were obtained with a bandwidth of ~4 nm and a repetition frequency between 50-91 MHz, although the output power achieved in some oscillators was much lower than the pump power, indicating poor conversion efficiency.

Table 6.1Properties of Yb:YAG lasers built

Ref.	Year	Pump Laser	Pump power (W)	Output power (W)	Yb^{3+} at%	Pump λ (nm)	Laser λ (nm)	Slope eff. (%)	τ_p (fs)	Δλ (nm)	Rep. rate (Hz)
[2]	2009	25 Diode bars	-	4000	1.4	940	1030	-	6 ns	-	1
[3]	2010	Limo Fibre Coupled LD	1871	963	10	940	1029	-	12.4ps	3.2	50×10^{6}
[4]	1991	InGaAs Diode laser	0.9	.073	6.5	968	1030	31	-	-	-
[5]	2009	Fibre	26.6	0.25	9.8	940	1033.3	-	417	3.02	91×10^{6}
[6]	2010	Fibre Coupled LD	26.6	0.008	9.8	940	1033.6	-	380	4.5	91×10^{6}
[7]	2009	Fibre Coupled HP	120	40	5	968	1050	72	-	-	-
[8]	2010	Fibre Coupled LD	21	8.9	20	940	1030	52	-	-	10
[9]	2010	Fibre Coupled LD	53	12	10	936.5	1030	~38	1 ms	-	100
[10]	2010	Ti:Sapphire	1.2	0.8	-	940	1030	75	-	-	-
[11]	2008	Fibre	55	3	0.7	940	1031	33	17 ns	-	5×10^{3}
[12]	2010	Nd:YAG Laser	0.45	0.033	25	946	1029	91.9	-	-	
[13]	2007	Fibre Coupled LD	30	1.32	10	941	1031	12.8	-	-	-

Table 6.1 summarises the state-of-the-art in relevant Yb:YAG lasers. The best Yb:YAG results are comparable with the ones achieved so far with our Yb:KYW crystal. Based on this information, an experimental comparison between both crystals was carried out to establish a good understanding of their relative performance using a similar pump and cavity configuration for both systems. This comparison is presented in Section 6.5 of this chapter. Guided by the information in Table 6.1, a fibre-coupled diode pump laser of 940 nm was chosen for the oscillator configuration using the YAG crystal. This is due to the absorption cross section for Yb:YAG having its peak at 940 nm (Figure 3.5).

6.3 The Yb:YAG oscillator

The oscillator (Figure 1) was pumped using a fibre-coupled diode laser pump array. The Yb:YAG crystal and the fibre diode were water cooled to 10° C. The pump beam was placed directly into the crystal using an angled-cleaved fibre spliced to the fibre connected to the pump diode, which had the same core diameter. This was to use the core diameter of the fibre as a spot radius of 105 μm which matched the intracavity

mode in the gain crystal. The angled fibre was also used to avoid the reflections from the fibre cleave returning into the pump diode. The Yb:YAG crystal was plane-Brewster cut with a HR coating at 1040 nm at the plane surface to act as one end of the cavity. The oscillator consisted of a modified asymmetric, astigmatically compensating V-fold cavity.

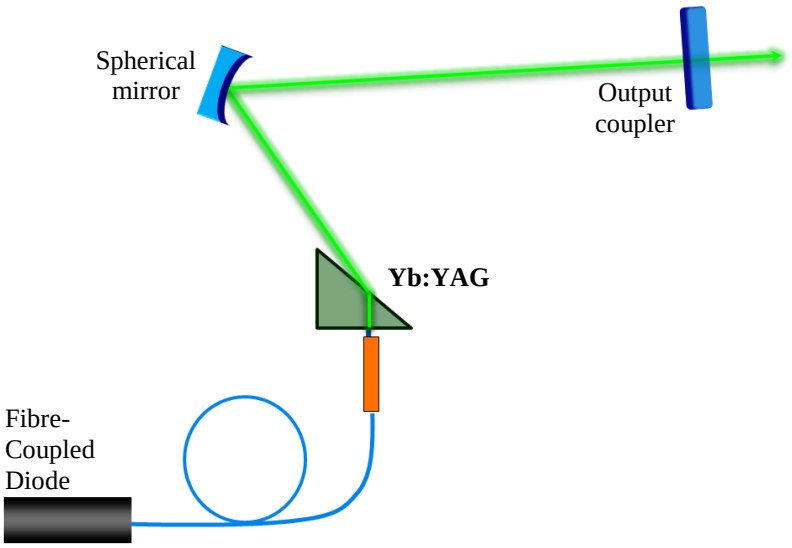

Figure 6.1 Layout of the Yb:YAG oscillator

One curved mirror was used to compensate for astigmatism generated by the Brewster-cut crystal. Three different mirror curvatures were evaluated in this cavity. At the end of the arm of the cavity an output coupler was inserted. A range of output couplers was used to optimize the power which could be extracted from the cavity.

6.4 940 nm Fibre-Coupled Diode Laser Characteristics

The pump laser used for this configuration was a fibre-coupled diode (*JDSU L4-9894010-100C*), as shown in Figure 6.2, which worked at 940 nm (corresponding to the biggest absorption peak wavelength for Yb:YAG, as discussed in Section 3.3.1). The fibre attached to it was a multimode fibre which had a 105 μm core diameter with 125 μm cladding; its numerical aperture was 0.15. The diode was operated using a THORLABS ITC4020 laser diode/temperature controller.

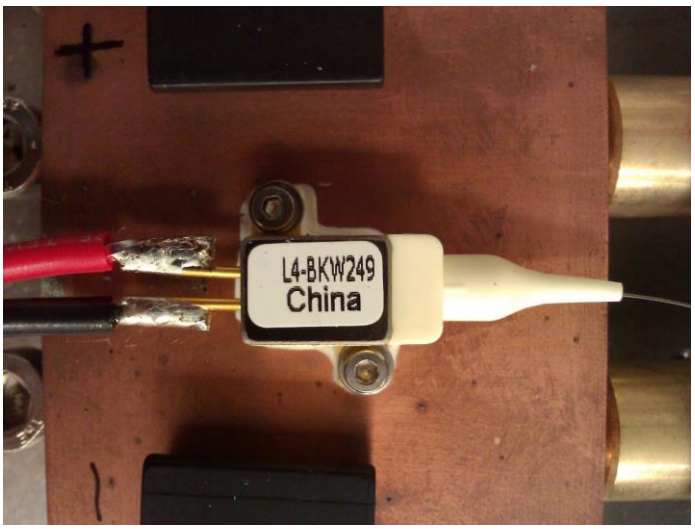

Figure 6.2 Fibre-coupled diode pump device mounted on a cooper base that was water-cooled for heat removal.

This diode was able to be driven at up to 12 A of current, but during the experiments, it was operated only up to 11.5 A which corresponded to 11.29 W of input power into the system. Figure 6.3 shows the output power of the diode for a given current of the driver. The threshold for this diode was 0.6 A of current, and it had a slope efficiency of 0.90 W/A.

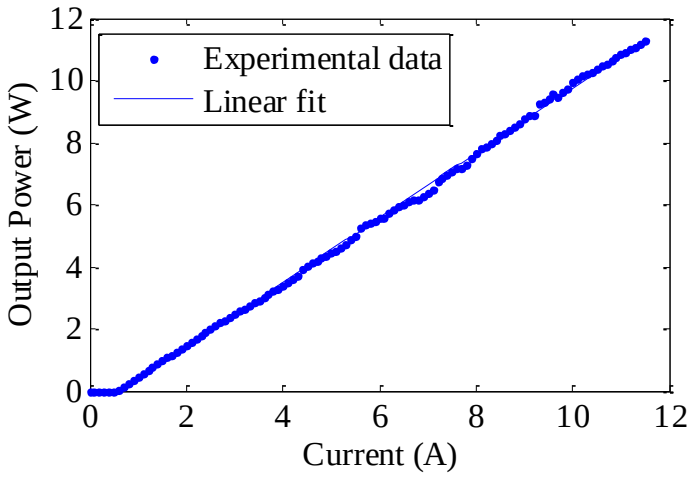

Figure 6.3 Output power from the 940 nm diode.

6.4.1 Yb:YAG Crystal Design

The crystal of Yb:YAG used as gain material had a 10 at.% doping concentration, based on the data from Table 6.1, and it was cut in a triangular geometry in order to allow us to optimize its effective thickness. The maximum thickness was 5.22 mm, its width was 9.39 mm, and its cut angle was 29.07°, as shown in Figure 6.4. The crystal had 3 mm height to make the alignment easier. Because Yb:YAG has an isotropic cubic unit cell,

the alignment was not sensitive to the polarization of the pump laser as in the case of Yb:KYW. The plane surface of the crystal was 99% HR coated for 1040 nm, to be used as an end mirror of the cavity and make the system design simple. The geometry of the Yb:KYW crystal used in the previous chapter was similar to this one.

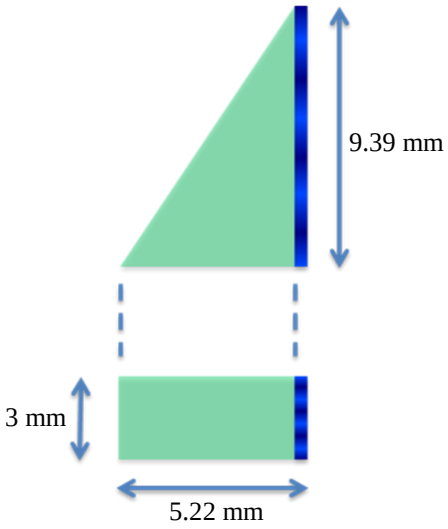

Figure 6.4 Yb:YAG crystal geometry

6.4.2 Cavity Design

Using the same approach as in the case of the Yb:KYW oscillator discussed in Chapter 5, some configurations designed with astigmatism-compensation for different cavity lengths were investigated. For the short cavity three mirrors were again used, the plane surface of the crystal, a spherical mirror and an output coupler at the other end of the cavity as shown in Figure 6.5. For this cavity three cases were considered: using a -100 mm, a -150 mm and a -200 mm radius of curvature spherical mirror. An analysis of a long cavity was also made in the same configuration as the final oscillator configuration built using Yb:KYW.

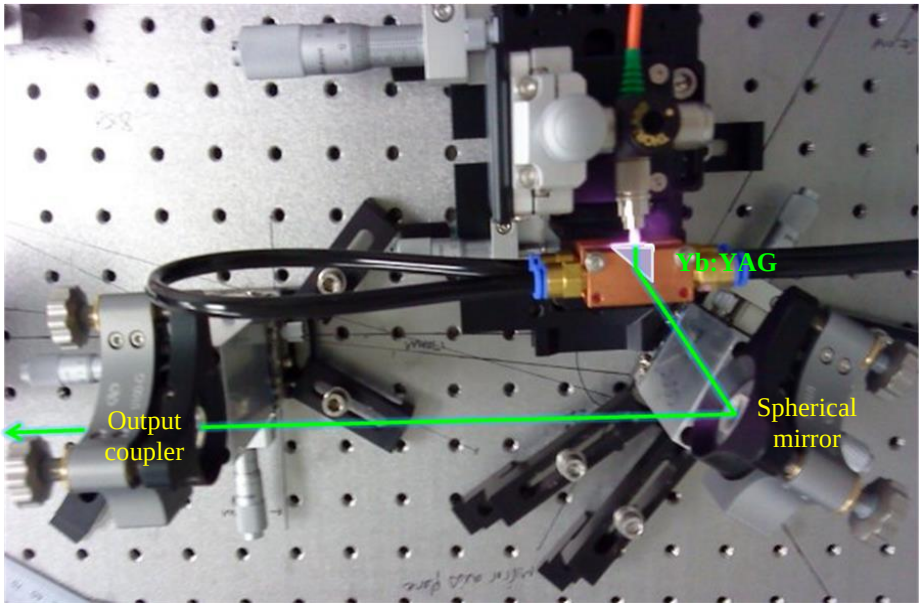

Figure 6.5 Short cavity configuration for Yb:YAG.

Thickness optimization

First an analysis of the efficiency of the system depending on the inserted crystal thickness was carried out. Figure 6.6 shows the output power obtained at different positions of the input beam through the crystal. The test was made from the thinnest side to the thickest using a 25% output coupler at 9.31 W of input power and 1030 nm wavelength. The best results were obtained for a 2.84 mm thickness which was the one used for this cavity.

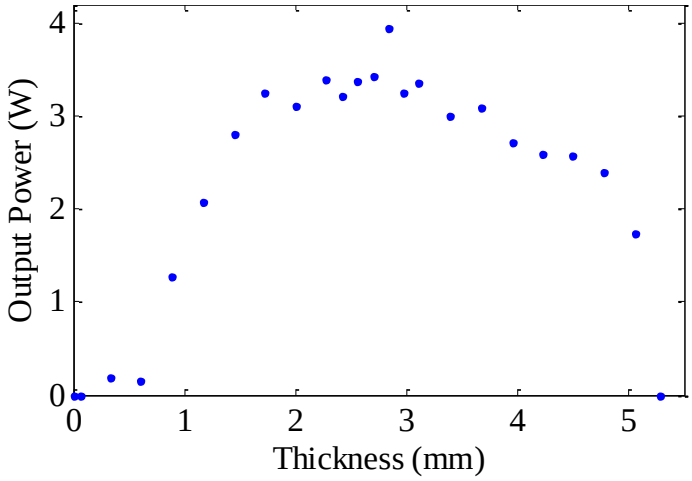

Figure 6.6 Output power efficiency of the Yb:YAG 3-mirror configuration for different crystal thicknesses at 1030 nm.

6.4.3 CW operation with a -100 RoC mirror cavity

Using the short cavity configuration the first evaluation was carried out using a -100 mm radius of curvature spherical mirror (Figure 6.7a). In this configuration, in a

procedure similar to that discussed in Chapter 5, the distances between the crystal and the two mirrors were preserved. The distance from the Brewster surface of the crystal to the spherical mirror was 58.8 mm, and from the spherical mirror to the output coupler was 165 mm. The angle of incidence on the spherical mirror was 56°. The beam size of the intracavity beam is shown in Figure 6.7b for the tangential and sagittal direction, where in the tangential direction the beam diameter was 150 µm in the crystal, 1.03 mm at the spherical mirror and 215 µm in the output coupler. And for the sagittal direction the diameter was 109 µm in the crystal, 726 µm at the spherical mirror and 646 µm in the output coupler.

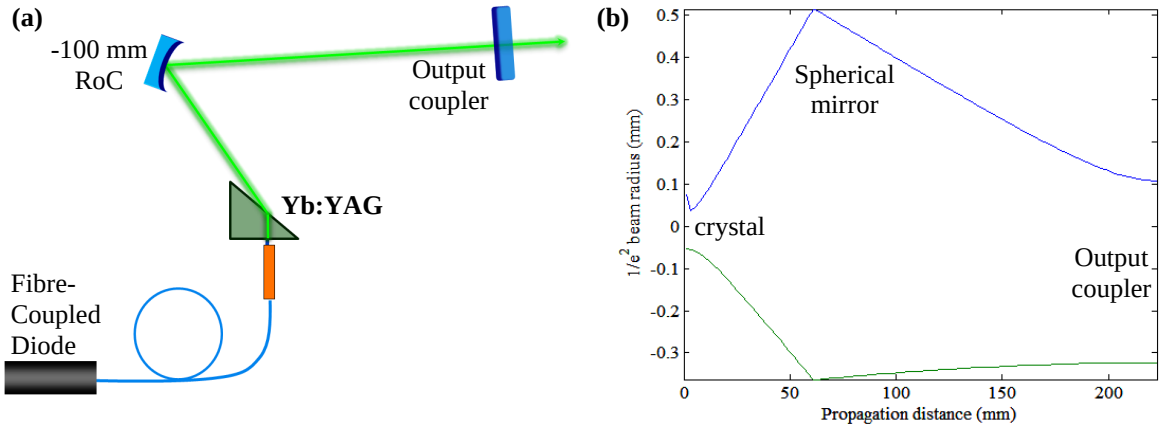

Figure 6.7 (a) Configuration using a -100 mm RoC mirror and (b) Beam size through the cavity using LCAV software, the blue line corresponds to the tangential plane and the green line to the sagittal plane.

In this configuration a Rigrod analysis was made [14] which is shown in Figure 6.8. A selection of output couplers was used, in which the transmission ranged between 0.8% and 50%. This case, contrary to the case of Yb:KYW the experiment gave two local maxima for the best option for output coupler. This is because, according to the emission cross section shown in Section 3.3.1 (Figure 3.5), the main peak emission cross section is at a wavelength of 1030 nm, but it also has a second peak not so pronounced at 1050 nm, implying that the system will be able to work at both wavelengths, giving a best efficiency for each one of them. Figure 6.8 shows that for a wavelength of 1030 nm the best output coupler is the one with 25% transmission, and for 1050 nm the best output coupler is 10% transmission.

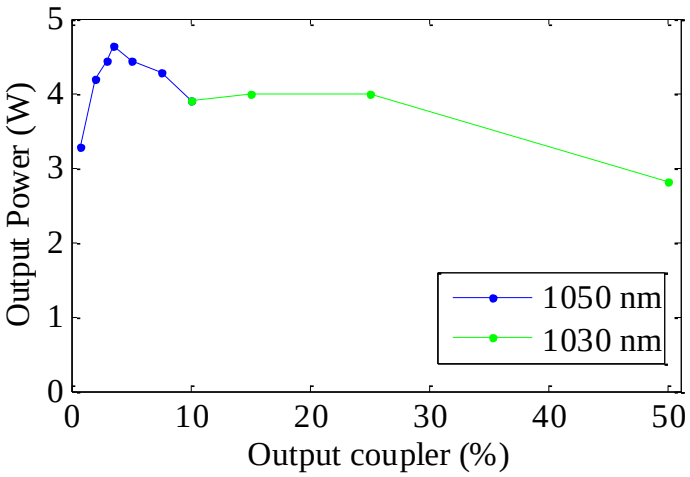

Figure 6.8 Rigrod analysis for the -100 mm mirror cavity showing results for 1050nm and 1030 nm wavelengths [14].

From this analysis, taking the best power efficiency for the configuration, a 3.5% output coupler was used. With this output coupler the output power was obtained as a function of the input power. Figure 6.9 shows that for this cavity a 43% slope efficiency was obtained and the threshold was at 1.08 W of input power. A maximum average output power of 4.63 W was found. The slope efficiency was comparable to the 45% obtained with the Yb:KYW oscillator, but in this case the threshold was lower than the 2.61 W of the Yb:KYW oscillator. Also the average output power was higher than the 3.01 W obtained with the previous oscillator.

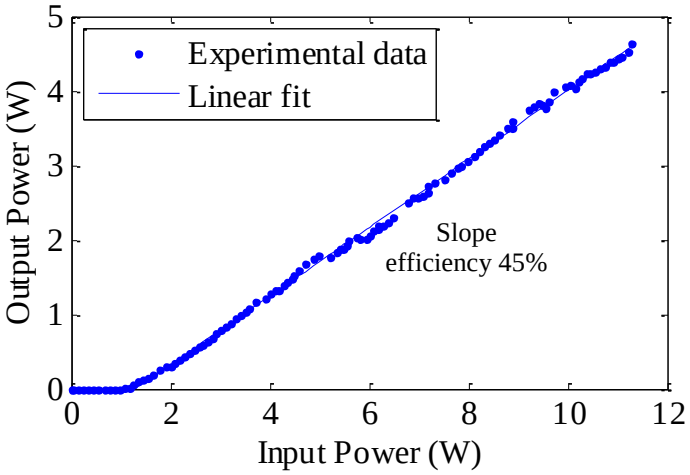

Figure 6.9 Output power variation with input power showing the slope efficiency of the -100 mm mirror cavity.

6.4.4 CW operation with a -150 RoC mirror cavity

In the second case a -150 mm radius of curvature mirror was used in the cavity, as shown in Figure 6.10a. In this configuration the distance from the crystal to the spherical mirror was 84.5 mm, from the spherical mirror to the output coupler was 343 mm, and the angle of incidence on the spherical mirror was 48°. For the intracavity

beam, the beam diameter was 87 µm and 106 µm at the crystal, 1.56 mm and 1.06 mm on the spherical mirror, and 291 µm and 945 µm at the output coupler for the tangential and sagittal directions respectively, as shown in Figure 6.10b. This case gives smaller values in the crystal and on the spherical mirror than the oscillator made with Yb:KYW for the same cavity; nevertheless the output beam diameter is the same size as in the Yb:KYW case.

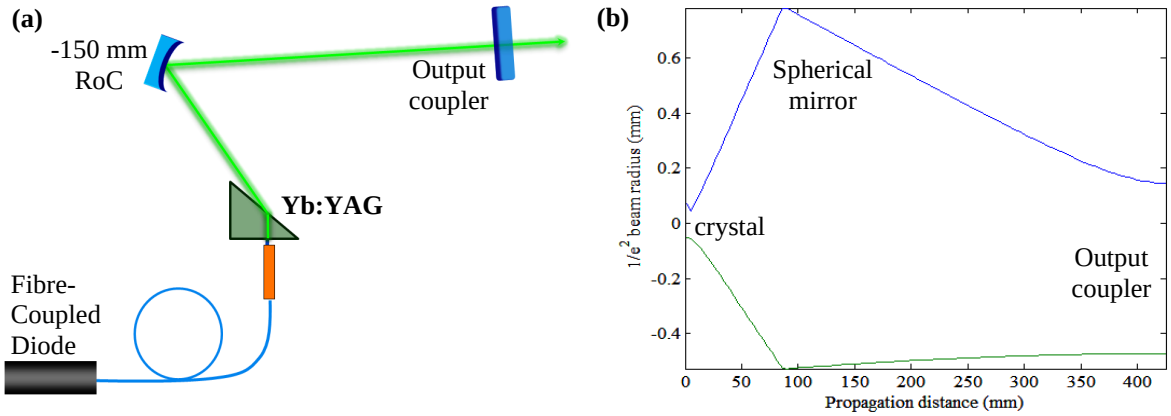

Figure 6.10 (a) Configuration for a -150 mm RoC mirror and (b) Tangential (blue) and sagittal (green) beam size inside the cavity calculated with LCAV software.

This configuration showed a maximum average output power of 5.08 W using a 3.5% output coupler as in the previous case. Figure 6.11 shows the output power as a function of the input power for this cavity, which gave a slope efficiency of 51%, and a thereshold of 1.08 W of input power, identical to the -100mm RoC mirror cavity. Compared with the Yb:KYW oscillator this cavity gave a higher average output power and a lower threshold.

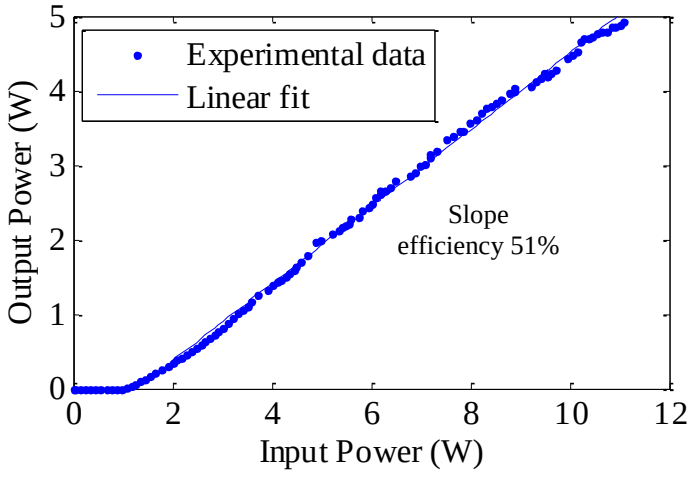

Figure 6.11 Output power from the -150 mm cavity.

6.4.5 CW operation with a -200 RoC mirror cavity

For the case using a -200 mm radius of curvature spherical mirror, the configuration shown in Figure 6.12a had the following specifications: the distance between the crystal and the spherical mirror was 110 mm, from the spherical mirror to the output coupler was 620 mm, and a 40° angle of incidence at the spherical mirror. This will be known as the short cavity for the rest of this chapter. The beam diameter in this case was 124 µm in the tangential direction and 108 µm in the sagittal direction at the crystal, 2.32 mm tangential and 1.35 mm sagittal at the spherical mirror and 353 µm and 1.15 mm respectively at the output coupler. In this case the beam sizes are almost the same as the ones from the equivalent cavity built using Yb:KYW.

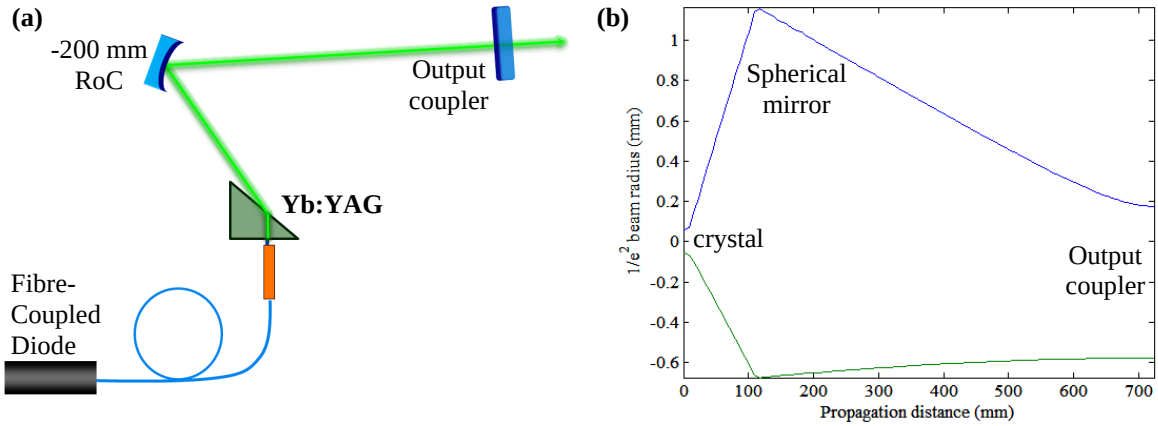

Figure 6.12 (a) Configuration for the -200 mm RoC mirror and (b) Beam size along the cavity (Showing the tangential beam in blue and the sagittal beam in green). LCAV software calculation.

After building this cavity another Rigrod analysis was performed [14], because the high powers obtained from this system meant that it would be used as the basis of the final cavity configuration. Because there are two different results for the 1030 nm and the 1050 nm wavelengths, there are therefore different values of the output power for each output coupler used but also for different input powers into the system. Figure 6.13 shows the output power obtained using the same range of output couplers (0.8%-50% transmission) as before. This results comes from the two peaks on the emission cross section of Yb:YAG as shown in Figure 3.5.

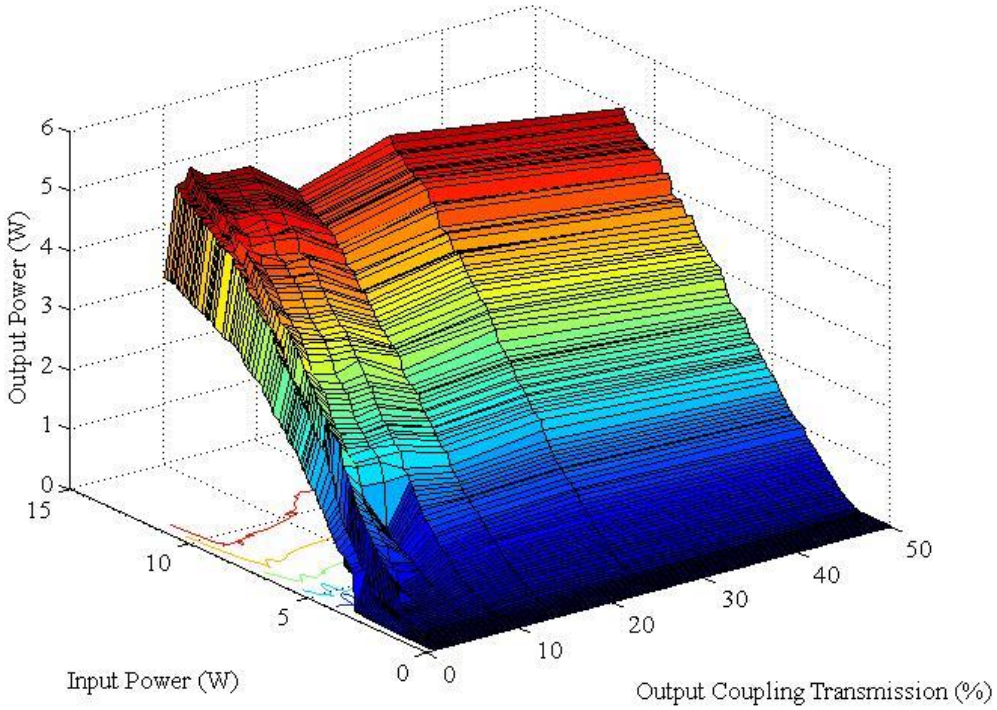

Figure 6.13 Output power for different output couplers varying the input power for the oscillator.

In this plot the dark-blue area (5 W of input power or less), and all the results obtained for the output couplers between 15% and 50% were obtained for a wavelength of 1030 nm. The results obtained for the output couplers smaller than 15% and above 5 W of input power corresponded to a wavelength of 1050 nm.

For this case, the best output coupler for the 1030 nm wavelength was found to be 25% transmission, and for the 1050 nm wavelength was 3.5% transmission. Therefore, a measurement of the output power was made for these two output couplers, which is shown in Figure 6.14. This shows a slope efficiency of 65% for the 3.5% output coupler (1050 nm), and 58% for the 25% output coupler (1030 nm).

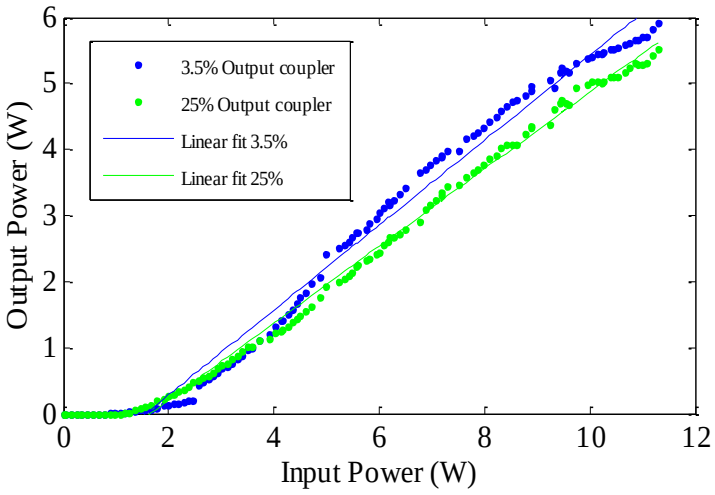

Figure 6.14 Output power variation with input power for the -200 mm mirror cavity. The slope efficiency is 65% for the 3.5% output coupler and 58% for the 25% output coupler.

6.4.6 Extension to a Modelocked Yb:YAG Laser

Using the same process as we used with the Yb:KYW oscillator, the short cavity was adopted as a base cavity that was extended using a relay system, into what will be referred to as the long cavity. The results shown in this section were obtained by Dr. David Birkin at ROFIN-SINAR UK where the laser was built and it is still in use. Figure 6.15 shows the final cavity built for the Yb:YAG oscillator.

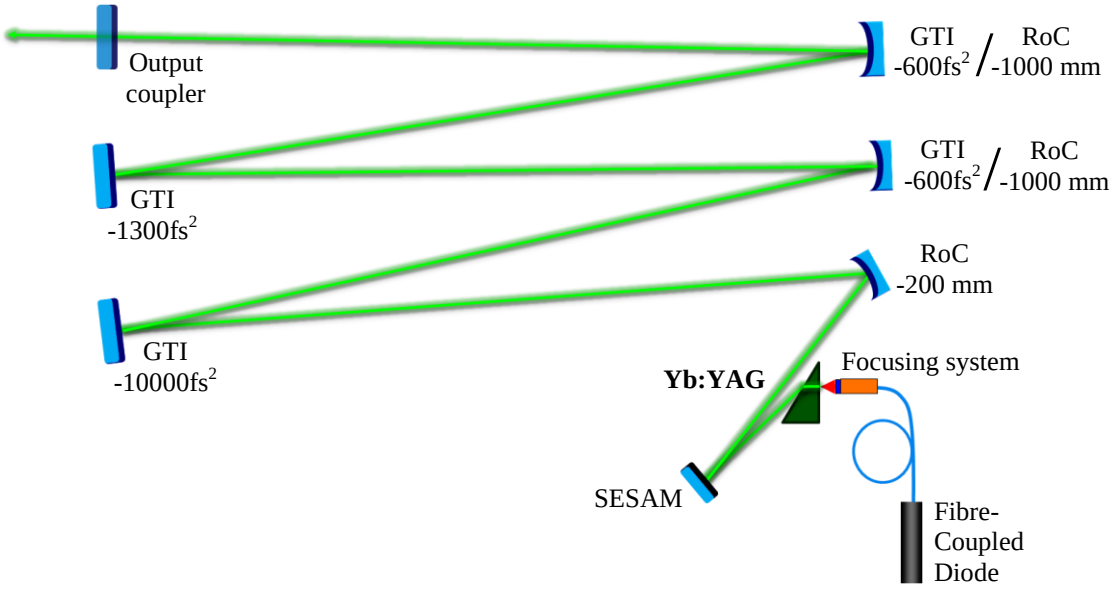

Figure 6.15 Final cavity configuration for modelocked Yb:YAG oscillator.

To make a better comparison between the Yb:KYW and Yb:YAG cavities, the same elements were used to modify the CW oscillator into a modelocked design. This means that the output coupler was replaced by a GTI mirror which had -10000 fs^2 GDD. Then, after this, a spherical mirror with -1000 mm radius of curvature was placed at 500 mm

from the GTI mirror. The next mirror was another GTI mirror with -1300 fs^2 GDD placed at 500 mm from the spherical mirror. A second spherical mirror with -1000 mm radius of curvature was placed at a further distance of 500 mm. At the end of the cavity the output coupler was placed at 500 mm from the second spherical mirror. Both spherical mirrors were also GTI mirrors with -600 fs^2 GDD, and both had an angle of incidence of 10°.

Compared to the Yb:KYW modelocked oscillator, the only difference was that a focusing system was added to the end of the fibre coupled to the pump diode. This system consisted of a collimator at the output of the fibre and a 50 mm focal lens placed at 327 mm from the collimator and 51.5 mm from the crystal as shown in Figure 6.16. This focused the input beam into the crystal to obtain a better mode match between the input beam and the intracavity beam with a beam diameter in the crystal of 260 μm in the horizontal direction and 266 μm in the vertical direction.

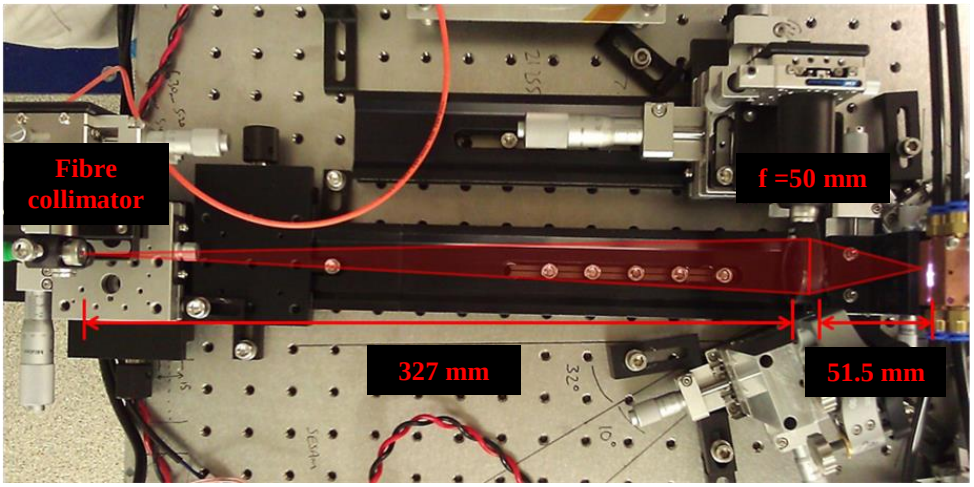

Figure 6.16 Focusing system for the Yb:YAG oscillator (system built by Dr. David Birkin).

Figure 6.17 shows the beam diameter along the complete cavity. This configuration, closely resembled the previous Yb:KYW oscillator and had a beam that started from a minimum diameter of 117 μm at the crystal in the tangential direction and 107 μm in the sagittal direction. The beam diverged until the first spherical mirror of -200 mm radius of curvature, reaching a diameter of 2.42 mm and 1.35 mm in the tangential and saggital direction respectively. From there it converged from the spherical mirror to the first GTI mirror, where it had a diameter of 333 μm and 1.16 mm. At the second spherical mirror the beam reached a diameter of 1.95 mm and 1.28 mm. At the second GTI mirror the beam diameter narrowed to 1.96 mm and 568 μm. The beam then broadened to 2 mm

and 1.29 mm at the third spherical mirror, and at the output coupler had a diameter of 336 μm and 1.16 mm respectively. The total cavity had a length of 2730 mm.

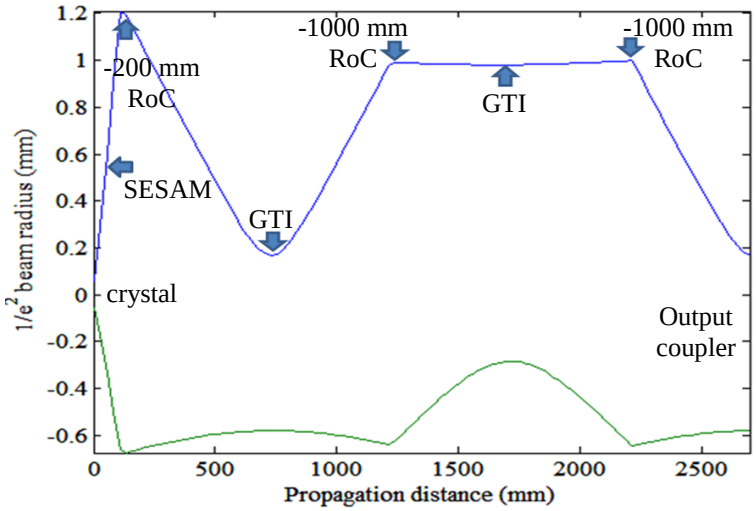

Figure 6.17 Beam radius divergence as a function of position though the cavity, Tangential diameter shown in blue and sagittal diameter in green.

An analysis of the output beam was made, which is shown in Figure 6.18. The M^2 measurement on the horizontal and vertical direction gave a result of M^2_x = 1.033 and M^2_y =1.064 respectively.

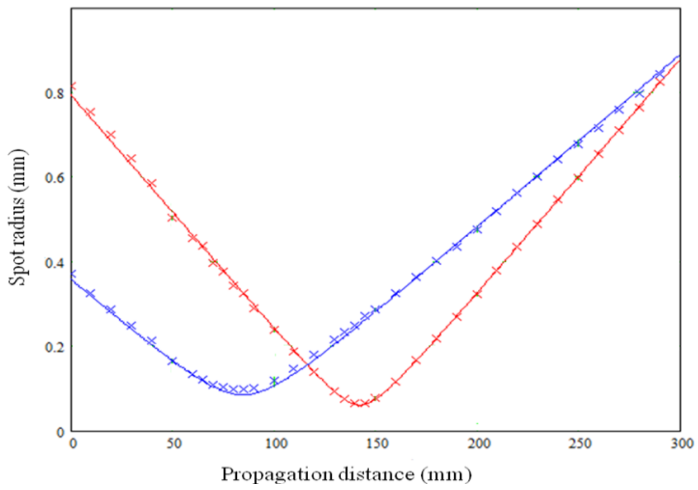

Figure 6.18 M^2 measurement for the final CW cavity configuration. The red line shows the horizontal beam spot radius and the blue line the vertical spot radius.

As in the Yb:KYW cavity, a 1.5% absorbance SESAM was again used to obtain modelocking (BATOP model SAM-1040-1.5-x-1ps). The average output power obtained was then measured and compared in Figure 6.19 for the short cavity, the long cavity, and the modelocked long cavity (SESAM cavity). For the long cavity an average output power of 5.1 W was obtained with a 58% slope efficiency and a threshold of 2 W

for CW operation. When the cavity was modelocked the maximum average output power obtained was of 2.88 W with a 47% slope efficiency and 2.5 W threshold.

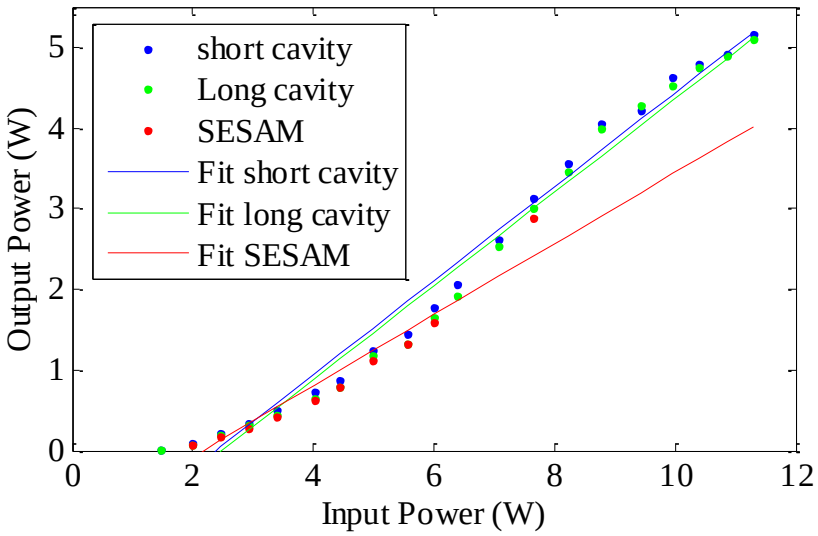

Figure 6.19 Output vs input power for the modelocked Yb:YAG cavity, The slope efficiency is 58% for the short and long cavities and 47% using the SESAM.

This reduced power in the modelocked system was because of the number of elements added to the configuration. Besides, when the SESAM is added into the cavity, it becomes possible to use the 3.5% output coupler at the required wavelength of 1031 nm, but stable modelocking is not possible above 7.65 W of input power, limiting the maximum output power to 2.88 W.

6.5 Comparative discussion of Yb:KYW and Yb:YAG performance

From the results obtained in Chapter 5 for the Yb:KYW oscillator and the ones in previous sections of this chapter for the Yb:YAG oscillator it was possible to compare both configurations. Table 6.2 summarises all of the data obtained for the short cavity in its three different configurations and the long cavity. This table gives the output powers slope efficiencies, threshold and intracavity beam diameters in the crystal (Crys. Diam.) and on the output coupler (O/C Diam.) for each case, showing also the respective output coupler used. To make this comparison, the same configurations with the same kind of elements were used. The only two differences were the doping concentration (5 at% for Yb:KYW and 10 at% for Yb:YAG), and the pumping scheme for the long cavity (a pump fibre next to the Yb:KYW crystal and a focusing system from the pump fibre to the Yb:YAG crystal).

Table 6.2 Short and long cavity characteristics for Yb:KYW and Yb:YAG

Cavity	Pump Power (W)	Output power (W)	Pump λ (nm)	Laser λ (nm)	Slope eff. (%)	Threshold (W)	Out. Coupl. (%)	Crys. Diam. (µm)	O/C. Diam. (µm)
-100mm Yb:KYW	9.5	3.01	980	1032	45	2.61	10	130	429
-100mm Yb:YAG	11.29 9.5	4.63 3.88	940	1050	43	1.08	3.5	129	430
-150mm Yb:KYW	9.5	2.87	980	1032	49	2.71	10	124	616
-150mm Yb:YAG	11.29 9.5	5.08 4.16	940	1050	51	1.08	3.5	96	618
-200mm Yb:KYW	9.5	2.79	980	1032	48	3.27	10	116	751
-200mm Yb:YAG	11.29 /9.5	5.53/4.7 5.91/5.2	940	1030 1050	58 65	1.17 0.88	25 3.5	116	754
Long Yb:KYW	9.5	2.94	980	1032	62	4	10	112	743
Long Yb:YAG	11.29 9.5	5.1 4.27	940	1031.6	58	1.46	3.5	112	748

First, for the three different configurations of the short cavity and the long cavity all the values obtained for the slope efficiency and intracavity beam diameter ($1/e^2$) are comparable for the two gain materials. Nevertheless the output power extracted from the system was much higher for Yb:YAG than for Yb:KYW. Because the Yb:YAG fibre coupled diode gives more input power to the system than the Yb:KYW fibre coupled diode, the value at the same input power for Yb:YAG is also shown in Table 6.2, proving that the output power was higher for that case.

When the long cavity configuration was modelocked the maximum average output power obtained was 2.88 W for Yb:YAG and 2.42 W for Yb:KYW with an average slope efficiency of 47 % and 56 % and threshold of 2 W and 4 W respectively (Figure 6.20). In this case the slope efficiency for Yb:KYW is higher, but the output power is higher and the threshold lower for Yb:YAG, making Yb:YAG the better choice for the available pump power.

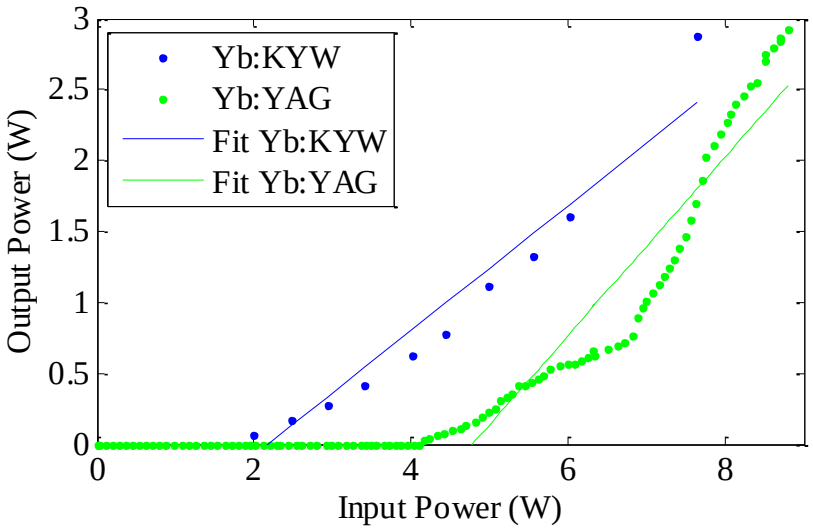

Figure 6.20 Output power for the moddelocked cavity using Yb:KYW and Yb:YAG. The slope efficiency is 47% for Yb:KYW and 56% for Yb:YAG.

For the modelocked cavity, it was shown in Chapter 5 that, for Yb:KYW pulses of 522 fs duration were obtained for a cavity of 54.8 MHz repetition rate. Figure 6.21 shows the pulses obtained with the Yb:YAG oscillator, in which pulses of 705 fs for $sech^2$ shape were inferred from an intensity autocorrelation. In this case the repetition rate was 53 MHz.

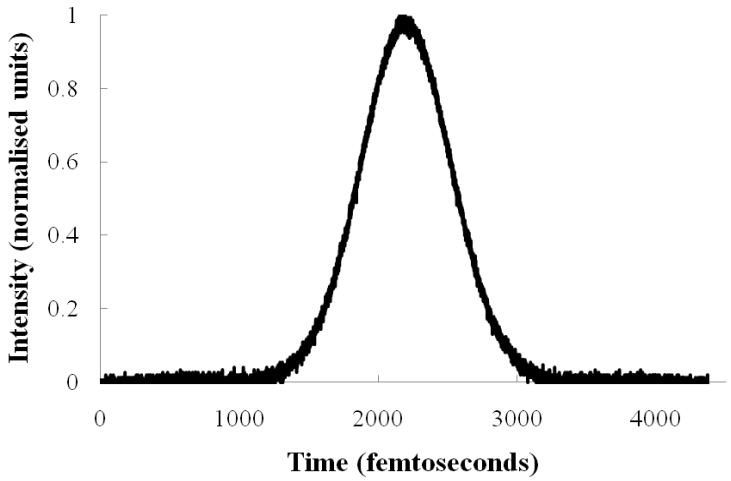

Figure 6.21 Autocorrelation of Yb:YAG cavity, showing pulses of 1.54×705 fs .

The Yb:KYW pulses had a bandwidth of 2.08 nm and a duration-bandwidth product of 0.31, where as for ideal $sech^2$-shaped pulses this is 0.315. For the Yb:YAG pulses the spectrum obtained is shown in Figure 6.22. For these pulses a bandwidth of 1.89 nm

and a duration-bandwidth product of 0.38 was obtained, which means that these pulses had a small amount of chirp.

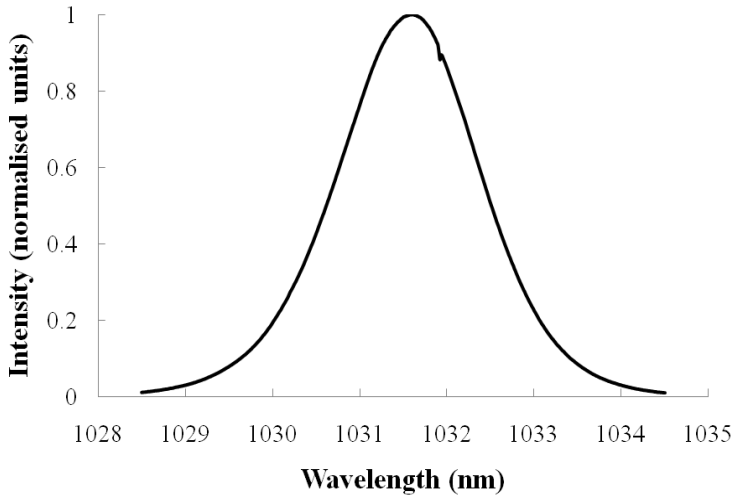

Figure 6.22 Yb:YAG cavity spectrum.

From this point of view the pulses obtained with the Yb:KYW oscillator gave shorter and less chirped pulses than the ones obtained from the Yb:YAG oscillator. Table 6.3 summarises the modelocked results obtained with both oscillators.

Table 6.3 Modelocking data obtained from the Yb:KYW and Yb:YAG laser oscillators.

Cavity	Pump Power (W)	Output power (W)	Pump λ (nm)	Laser λ (nm)	Slope eff. (%)	Threshold (W)	Out. Coupl. (%)	τ_p (fs)	Δλ (nm)	Rep. rate (MHz)	ΔνΔτ
ML YbKYW	9.5	2.42	980	1032	56	4.16	10	521.8	2.08	54	0.31
ML YbYAG	7.65	2.88	940	1031.6	47	2	3.5	705	1.89	53	0.38

Another advantage that Yb:YAG has over Yb:KYW is that its crystal cell, which is an isotropic cubic array, allows the system to be aligned more easily, and is not susceptible to polarization changes in the pump. In the case of Yb:KYW its monoclinic structure adds another characteristic which has to be considered to be able to align the system, which is obtaining the correct polarization of the pump beam relative to the crystal optic axis.

6.6 Conclusions

In this chapter, the construction and characterization of a modelocked Yb:YAG laser oscillator was described. Using a 10 at% doped crystal a maximum average output power of 2.88 W was obtained at a 53 MHz repetition rate. The output beam had an M^2 of ~1.03. The pulses obtained were of 705 fs duration with a bandwidth of 1.89 nm and a duration-bandwidth product of 0.38, implying that the pulses were slightly chirped. This configuration gave higher efficiency of 47% than some of the previously published work reported of ~30% [4, 9 and 11]. For a 10% doping concentration this oscillator gave pulses longer than the ones reported in [5] and [6] for cavities with higher repetition rates than this one, but it gave pulses shorter than in some other work where the pulses were >> 1 ps for cavities with repetition rates similar or lower.

Using the same configuration with the two different gain materials of Yb:KYW and Yb:YAG it was possible to compare the two material's efficiencies and general performance. This comparison showed that the choice between each of these materials depends on the application required. If the application requires higher power efficiency and a simpler alignment process then Yb:YAG material should be used as the gain material. On the other hand, if shorter, better quality pulses are what is required, then Yb:KYW is the better option.

In any case from Chapter 5 and 6 it is observed that this cavity configuration with this crystal geometry is the preferred option to get the best efficiency. This is because it allows one to obtain the best performance from a gain material of almost any doping concentration, unless the user already knows the best thickness for that particular doping concentration.

6.7 References

[1] W. F. Krupke, "Ytterbium solid-state lasers. The first decade," IEEE Journal of Selected Topics in Quantum Electronics **6**, 1287–1296 (2000).

[2] M. Siebold, M. Loeser, U. Schramm, J. Koerner, M. Wolf, M. Hellwing, J. Hein, and K. Ertel, "High-efficiency, room-temperature nanosecond Yb : YAG laser," Optics Express **17**, 431–437 (2009).

[3] D. C. Brown, J. M. Singley, K. Kowalewski, J. Guelzow, and V. Vitali, "High sustained average power cw and ultrafast Yb:YAG near-diffraction-limited cryogenic solid-state laser.," Optics Express **18**, 24770–92 (2010).

[4] P. Lacovara, H. K. Choi, C. A. Wang, R. L. Aggarwal and T. Y. Fan, "Room-temperature diode-pumped Yb:YAG laser," Optics Letters **16**, 1089–1091 (1991).

[5] H. Yoshioka, S. Nakamura, T. Ogawa, and S. Wada, "Diode-pumped mode-locked Yb : YAG ceramic laser," Optics Express **17**, 8919–8925 (2009).

[6] H. Yoshioka, S. Nakamura, T. Ogawa, and S. Wada, "Dual-wavelength mode-locked Yb:YAG ceramic laser in single cavity.," Optics Express **18**, 1479–86 (2010).

[7] Q. Hao, W. Li, H. Pan, X. Zhang, B. Jiang, Y. Pan, and H. Zeng, "Laser-diode pumped 40-W Yb:YAG ceramic laser.," Optics Express **17**, 17734–17738 (2009).

[8] A. Pirri, G. Toci, D. Alderighi, and M. Vannini, "Effects of the excitation density on the laser output of two differently doped Yb:YAG ceramics.," Optics Express **18**, 17262–17272 (2010).

[9] G. a Newburgh, A. Michael, and M. Dubinskii, "Composite Yb:YAG/SiC-prism thin disk laser.," Optics Express **18**, 17066–17074 (2010).

[10] J. Siebenmorgen, T. Calmano, O. Hellmig, K. Petermann, and G. Huber, "Nd:YAG waveguide laser with 1.3 W output power, fabricated by direct femtosecond laser writing," Applied Physics B **100**, 131–135 (2010).

[11] D. Sangla, N. Aubry, J. Didierjean, D. Perrodin, F. Balembois, K. Lebbou, a. Brenier, P. Georges, O. Tillement, and J.-M. Fourmigué, "Diode-pumped laser with Yb:YAG single-crystal fiber grown by the micro-pulling down technique," Applied Physics B **94**, 203–207 (2008).

[12] D. C. Brown, T. M. Bruno, and J. M. Singley, "Heat-fraction-limited CW Yb:YAG cryogenic solid-state laser with 100% photon slope efficiency.," Optics Express **18**, 16573–9 (2010).

[13] Y. Kalisky, O. Kalisky, U. Rachum, G. Boulon, and A. Brenier, "Comparative Performance of Passively Q-Switched Diode-Pumped Yb^{3+}-Doped Tungstate and Garnet Lasers Using Cr^{4+} : YAG Saturable Absorber," IEEE Journal of Quantum Electronics **13**, 502–510 (2007).

[14] W. W. Rigrod, "Homogeneously Broadened C W Lasers with Uniform Distributed Loss," IEEE Journal of Quantum Electronics **29**, 377–381 (1978).

Chapter 7

Conclusions

7.1 Summary

This thesis has described the construction and characterization of three Yb^{3+} doped KYW and YAG based laser oscillators and one master oscillator power amplifier. In Chapter 1, the motivation of the work was given, placing it in the context of the previous work in the field of Yb:doped oscillators and MOPA systems. The first chapter also described the methods and techniques used to characterize ultrafast laser pulses as well as the means of generating and controlling such pulses through different modelocking and dispersion compensation techniques.

Chapter 2 described the first Yb:KYW oscillator built in this project which was a Z-fold cavity with a 1.5 at% doping of Yb:KYW crystal used as the gain material and which had a Brewster-Brewster cut. Modelocking in this laser was obtained using a SESAM, dispersion compensation provided by multiple bounces on two GTI mirrors. This cavity produced pulses of 500 fs duration at a 53-MHz repetition rate centred at a wavelength of 1032 nm. The average output power of this laser was 4 W with a beam quality of M^2 of 1.2.

Chapters 3 and 4 presented details of the performance and construction of a MOPA using the laser described in Chapter 2 as a master oscillator and a Yb:YAG planar waveguide as the gain material for the amplifier. The amplifier was built first with a configuration based on single sided pumping with a six-bar diode stack while making five passes through the gain material with the signal from the oscillator from the front of the waveguide. This configuration gave an output power of 50 W in the form of broadened pulses of 700 fs durations at 53 MHz repetition rate and 1032 nm wavelength. After modifying the amplifier to a two-sided pumping configuration and increasing the number of passes of the signal through the gain material from five to seven plus modifying the way the signal was aligned into waveguide and changing the cylindrical mirror to make the bounces to toroidal mirrors the results improved to an output of 255 W with longer pulses of 780 fs. The repetition rate and the wavelength were kept the same as the earlier design.

The last part of this thesis, described in Chapters 5 and 6, presented a new configuration of a Yb:KYW oscillator and the use of this model to build a similar one with Yb:YAG as a gain material and make a comparison between both of them. This new configuration for both systems used a plane-Brewster cut crystal and employed a V-fold cavity which could be modified for different cavity lengths using the main cavity as a base and adding a relay imaging system to obtain the required length. The oscillator using Yb:KYW had a 5 at% doping concentration and was built using a SESAM for modelocking and a single high-value GDD GTI mirror for dispersion compensation. This oscillator gave pulses of 500 fs durations for a repetition rate of 54 MHz. The output was centred at a wavelength of 1032 nm and had an average output power of 2.42 W, and a M^2 of 1.46 in the horizontal direction, and 1.96 in the vertical direction. In the case of the cavity built with Yb:YAG, the doping concentration was 10 at% and it had the same elements included in the cavity for generating the pulses and compensating for dispersion, except for the pumping arrangement which had a focusing system added to the input of the cavity. This cavity gave pulses of 705 fs for a repetition rate of 53 MHz. The total average output power was 2.88 W at the same wavelength of 1032 nm.

As listed on page xiv, this research described above led to one journal publication and one conference paper. At the request of the project sponsor, Rofin-Sinar UK, the results relating to the highest power amplification described in Chapter 4 and the Yb:KYW/YAG oscillators presented in Chapter 5 and 6 were embargoed for publication. These results are however very competitive with other international research in a similar area.

7.2 Conclusions

The main objective of this research, namely to build a Yb:KYW laser oscillator and demonstrate high-power amplification, was accomplished successfully. The results obtained demonstrated that the combination of Yb-doped materials (Yb:KYW and Yb:YAG used for the first time together to the best of my knowledge) in a master oscillator power amplifier configuration resulted in a high quality high-power sub-picosecond output suitable for industrial applications. The use of new toroidal mirrors which involved having different curvatures in the vertical direction and horizontal directions improved the system so that it could produce more power through more

passes of the material without having oscillation along the beam path of the signal. This result was enabled by the development of a new technique for aligning the toroidal mirrors, which needed to be oriented with high precision to centre the beam on each stripe.

The aim of producing a Yb:KYW laser for pumping the MOPA led to an improvement of the configuration when the first one was finished and to testing Yb:YAG as a competitive gain medium. The first Yb:KYW oscillator built showed high output power and stable pulses over a long period, nevertheless it required some modifications to make it work that way, such as housing it in a temperature controlled box and selecting the output coupler to get the correct wavelength. For this reason the second oscillator which was built offered a great improvement to the system. This new oscillator configuration proved to be better in many aspects. The main body of the laser was more compact and did not need water cooling for the material and the pump laser. The cavity could be configured to different lengths by using a simple relay system of optical elements, that allowed the modification of the repetition rate and peak power of the output pulses. The crystal geometry provided another advantage of this cavity due to the capacity of the user to be able to obtain the best efficiency of the system by varying of the crystal thickness. Because with this configuration the dispersion compensation was done by the use of a single high-GDD GTI mirror, it made the entire system less sensitive to mechanical perturbations and thus it did not need to be temperature controlled.

The analysis of the two materials (Yb:KYW and Yb:YAG) demonstrated that both are suitable for high power modelocked oscillator applications in an end-pumped configuration (in contrast to other thin-disk research). Yb:KYW proved a better host material for applications in which shorter pulses and better pulse quality is required. If what is required is high power and low threshold then Yb:YAG is the most suitable option. This is due to the higher gain efficiency that Yb:YAG has compared with Yb:KYW which is related to the emission cross section and upper-state lifetime of these materials. Nevertheless for Yb:YAG the pulses would be broader than for Yb:KYW.

7.3 Future work

There remains room for improvements in the MOPA system described in this thesis. As mentioned before, it was the first time that Yb:KYW and Yb:YAG were used together in a MOPA design, so further analysis of this configuration could be carried out by studying some properties. First, the improved laser described in Chapter 5 could be used to seed the amplifier. To do this a higher power pump for the oscillator would provide higher output powers that, coupled to the amplifier would produce higher gain with the same number of passes through the waveguide. A second case would be to increase the number of passes though the material to nine or even eleven, which could be done by modifying the beam size of the seed signal from the Yb:KYW oscillator at the input of the waveguide. This would also require a further refinement to the alignment procedure into the waveguide and for the toroidal mirrors due to accuracy with which the mirrors have to be positioned. Because in this research we already identified the best radius of curvature in each direction, then, instead of working with several stripes new toroidal mirrors could be used which only have the correct radius for each direction. Alternativeley, more stripes with different curvatures to the ones mentioned before could be analysed in order to further improve the efficiency of the amplifier. A separate problem is the heating of the mounts of the amplifier which makes it difficult to maintain high power for long periods. A water cooled microchanel design similar to the one used for the waveguide mount could be used for the rest of the mounts in the amplifier to allow the system to run for longer times.

A comparison between Yb:KYW and Yb:YAG was described in this thesis, there are still some features to be studied in these configurations. A comparison between the exact doping concentrations could be carried out to know exactly the relationship between the two materials but also the optimum connection between the doping concentration and the crystal thickness, making it possible choose the appropriate crystal for a specific design before buying it. Another case that should be studied is the implementation of the focusing system in the Yb:KYW oscillator to try to improve the mode-matching inside the crystal. It was already proven that these cavities can be used to generate pulses by modelocking or Q-switching, but the case of Q-switching has yet to be characterized, as well as the pulsed operation for cavity lengths different to the ones described in this thesis. This analysis would also need to address the choice of dispersion compensation for different cavity lengths. Another improvement to the system would be to modify the crystal mount to allow it to tilt in vertical and horizontal

directions to achieve a better alignment of the cavity like in the case of the first cavity oscillator described in Chapter 2.

Due to the good performance achieved with the oscillator systems described in this thesis, they are going to be used for different applications. The first laser constructed is now to be used in a frequency doubled configuration for a Raman scattering project at Heriot-Watt University. The oscillator described in Chapter 5 was also used to pump an OPO system that worked in the region between 1400 nm and 1700 nm, and later on a second OPO which worked in the 1-micron region. A complete characterization of this system was not possible to be finished before, therefore it was not published. More work has to be done with this system to obtain complete results. The last oscillator described in Chapter 6 was built at Rofin-Sinar UK where it is planned to be used as a seed for other types of applications. Therefore the work described in this thesis has resulted in a useful template for Yb-doped oscillators suitable for use in high power amplifier applications. Besides this, because of the wavelength region and the pulse durations obtained, such oscillators could be used in a wide range of other applications.